NOTE TO USERS

University of Alberta

Synthesis and Hierarchical Self-Assembly Studies of Self-Complementary Motifs

by

Martins Sunday Oderinde

A thesis submitted to the Faculty of Graduate Studies and Research
in partial fulfillment of the requirements for the degree of

Master of Science

Department of Chemistry

Edmonton, Alberta
Spring, 2008

Your file Votre référence
ISBN: 978-0-494-45864-8
Our file Notre référence
ISBN: 978-0-494-45864-8

ABSTRACT

Self-assembly represents an efficient means of generating one-dimensional nano-structured material with the use of non-covalent interactions. When designed properly, a functional group can be expressed on the resulting self-assembled nano-structure, conferring specific physical properties.

Synthetically designed self-complementary compounds were self-assembled and studied in solution and in the solid state. Our focus was the synthetic design of G^C motifs tuned with different functionalities. The G^C motifs formed supramacrocycles with their moderate directional hydrogen bond information alone. The π-π stacking of these supramacrocycles resulted in complex hierarchical assembly states which were characterized by tapping mode atomic force microscopy (TM-AFM), scanning electron microscopy (SEM), transmission electron microscopy (TEM), ultra-violet/visible (UV-Vis), dynamic light scattering (DLS) and molecular modeling.

DEDICATION

Dedicated to Grigory Tikhomirov for his commitment to my research work.

ACKNOWLEDGEMENTS

I would like to first thank the Almighty God for his grace upon my life without whom I would have achieved nothing. I would to thank Professor Hicham Fenniri for serving as my research director and for believing in me. I would like to thank my grandmother, Mrs Ayodabo, my mother, Ruth Omokayode Oderinde, my brother, Lawrence Rotimi Oderinde and my sister, Comfort Bukuola Oderinde for standing behind him and for their continuous prayers for me.

I would like to thank my committee members Professors John C. Vederas, West Frederick G., Jonathan G. C. Veinot, and Shaw John for taking the time to serve on my committee. I thank the Department of Chemistry, University of Alberta for admitting me into their graduate program as well as making my transition to Edmonton from Nigeria successful. Many thanks to Grigory Tikhomirov, Dr. Rachel Beingessner, Dr. Andrew Myles, Dr. Jae-Young Cho, Dr. Fenton, Dr. Baker Al-Hourani, Dr. Darren Makeiff, Dr. Christophe Danumah, Dr. Mounir El Bakkari, Gabor Borzsonyi, Ross Johnson, Mustapha St. Jules, Usha Devi Hemraz and all other Supramolecular Nanoscale Assembly Group (SNAG) members for being my friends and colleagues, and for their many academic contributions as well as their scientific discussions during my graduate studies.

Finally, I would like to thank the University of Alberta and the National Institute for Nanotechnology and the Government of Canada for their funding and assistance during my thesis.

TABLE OF CONTENTS

LIST OF TABLES

LIST OF FIGURES

LIST OF SCHEMES

LIST OF ABBREVIATIONS

AFM	Atomic force microscopy
aq	Aqueous
Boc	*T*-Butyloxy carbonyl
$(Boc)_2O$	Di-*t*-Butyl dicarbonate
C	Carbon or Celsius
$CHCl_3$	Chloroform
CH_2Cl_2	Methylene Chloride
CH_3CN	Acetonitrile
d	Day(s)
DCE	1,2-Dichloroethane
DCM	Dichloromethane
dH_2O	Deionized water
DIPEA	Diisopropylethylamine
DLS	Dynamic light scattering
DMAP	4-N,N-Dimethylaminepyridine
DMF	Dimethyl formamide
DMSO	Dimethylsulfoxide
EA	Ethyl acetate
ESI	Electrospray ionization
Et_3N	Triethylamine
G^C	Guanine-Cytosine
H	Hydrogen

H-bond	Hydrogen bond
h	Hour
HCl	Hydrochloric acid
Hex	Hexane
LHMDS	Lithium hexamethyldisilazide
MeOH	Methanol
MS	Mass spectrometry
$NaHCO_3$	Sodium bicarbonate
$NaIO_4$	Sodium periodate
NaOMe	Sodium methoxide
Na_2SO_4	Sodium sulfate
NMO	N-methyl morpholine-N-oxide
NMR	Nuclear magnetic resonance
OsO_4	Osmium tetroxide
$POCl_3$	Phosphorous oxychloride
RNT	Rosette nanotubes
RNTs	Rosette nanotubes
SEM	Scanning electron microscopy
TEM	Transmission electron microscopy
TFA	Trifluoroacetic acid
TFAA	Trifluoroacetic anhydride
THF	Tetrahydrofuran
TM-AFM	Tapping mode Atomic force microscopy

3-D	Three-Dimensional

CHAPTER 1

SUPRAMOLECULAR CHEMISTRY, SELF-ORGANIZATION AND ROSETTE NANOTUBES FORMATION

1.1. Introduction to Supramolecular Chemistry

From divided to condensed and on to organized, living, and thinking matter, the path is toward an increase in complexity through self-organization.[1] Thus emerges the prime question set to science, in particular to chemistry, the science of the structure and transformation of matter: how does matter become complex? What are the steps and the processes that lead from the elementary particle to the thinking organism, the entity of highest complexity? These questions made scientists think beyond covalent bonds in order to understand and achieve complexity through self-organization.[1]

Molecular chemistry has created a wide range of ever more sophisticated molecules and materials and has developed a very powerful arsenal of procedures for the construction of ever more complex molecular structures by the making or breaking of covalent bonds between atoms in a controlled and precise fashion.[2] The approach has proved to be extremely fruitful for the synthesis of molecules with molecular weights in the range of 100-3000 Da.[3] However, the investment of time and effort necessary to construct monodisperse functional nanoscale structures of 10-100 kDa using this approach has to be viewed as prohibitive.[4] Thus the idea of non-covalently joining small molecules to form very complex molecules became very attractive.

In 1987, professors Jean Marie Lehn, Donald Cram and Charles Pedersen received the Nobel Prize in chemistry for their contributions in defining supramolecular chemistry.[5] The term supramolecular refers to ordered molecular aggregates that are held together by noncovalent binding interactions, such as metal-ligand bonds, hydrogen bonds, van der Waals' forces, π-π stacking and hydrophobic effect.[1,6] Due to the weakness of such binding interactions, the formation of such supramolecular assemblies is often thermodynamically dictated, they are commonly generated by spontaneous self-assembly rather than through sequential bond-forming synthetic strategies.[6] One major advantage over covalent synthesis is noncovalent assembly formation is often reversible, meaning the assembled structures are self-correcting.[5]

1.2. From Molecular Synthesis to Self-Organization and Programmed Systems

Supramolecular chemistry relies first on molecular synthesis, which is the construction of molecular entities with covalent bonds capable of molecular recognition.[5] Molecular recognition involves specific interaction between one molecule and another.[7] Beyond molecular synthesis lies the design of systems undergoing self-organization, that is systems capable of spontaneously generating well defined, organized, and functional supramolecular architectures by self-assembly from their components, thus behaving as programmed systems.[7] Chemical programming requires the incorporation into molecular components of suitable information for the generation of a well-defined supramolecular entity. The program is molecular, which is the information being contained in the covalent structural framework but its operation is supramolecular, making use of recognition algorithms

based on specific interaction patterns.[7] Understanding, inducing, and directing self-processes is key to unravelling the progressive emergence of complex matter. Self-organization is the driving force that led to the evolution of the biological world from inanimate matter.[8]

The general term self-assembly has been defined as, the autonomous organization of components into patterns or structures without human intervention. Self-assembly is of vital importance in biological processes such as, the transfer and storage of genetic information in nucleic acids and the organization of proteins into efficient molecular machines.[8] Whereas self-assembly may be taken as simple collection and aggregation of components into a confined entity, we shall here consider self-organization as the spontaneous, but also information-directed generation of organized functional structures in equilibrium conditions. A relevant biological example is the formation of a virus particle from its components, genomic nucleic acid and coat proteins.[9] The inclusion of dissipative, nonequilibrium processes, as present in the living world, constitutes a major goal and challenge for the future.[9]

A self-organization process may be considered to involve three main stages: (i) molecular recognition for the selective binding of the basic components; (ii) growth through sequential and eventually hierarchical binding of multiple components in the correct relative disposition, it may present cooperativity and nonlinear behaviour; and (iii) termination of the process, requiring a built-in feature, a stop signal, that specifies the end point and signifies that the process has reached completion.[1,7]

1.3. Supramolecular Self-assembly Induced by Molecular Recognition Between Complementary Hydrogen Bonding Sites

The self-assembly of well-defined supramolecular architectures rests on the design of molecular components containing the appropriate information and interacting through the correct recognition algorithm.[10,11] Hydrogen bonds, with their moderate directional characteristics and predictable patterns, are especially useful instructions, and their incorporation in molecules has resulted in a spectacular array of assemblies. Molecular ribbons,[12] tapes,[13] sheets,[14] cages,[15] rosettes,[16] cubes,[17] and capsules[18] have all been designed, synthesized, and characterized, both in solution and in the solid state (Figures 1.1 and 1.2). Although hydrogen bonds (energies in the range 0.1 to 5 kcal/mol) are weaker than covalent bonds (energies in the range of 50-100 kcal/mol), they are collectively strong in a self-organized system.[19] Hydrogen bonds are ubiquitous in organic crystals and because they are often stronger than other intermolecular forces, they frequently control the molecular packing arrangement.[20]

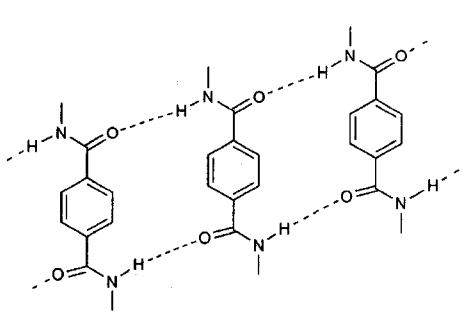

Supramolecular sheet

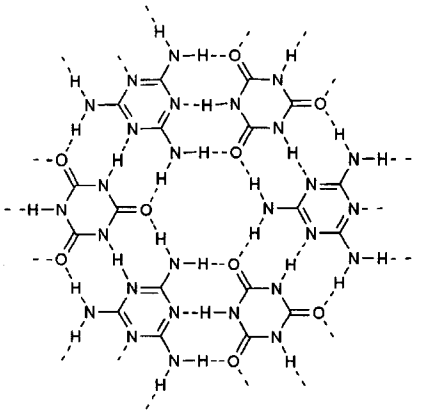

Supramolecular rosette

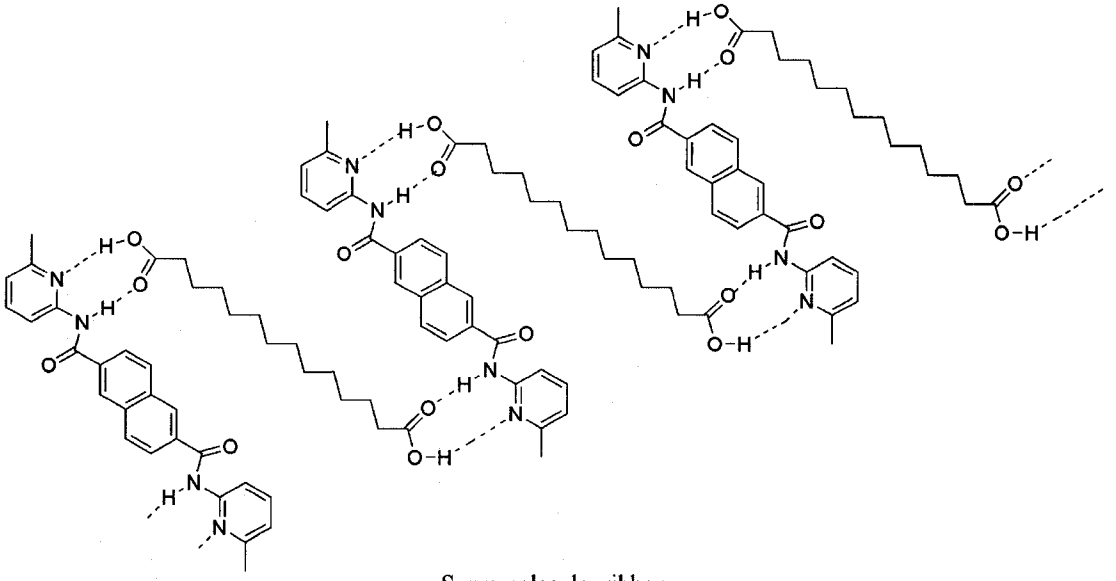

Supramolecular ribbon

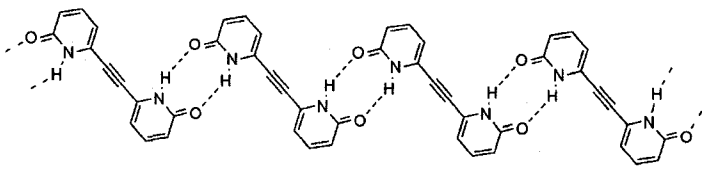

Supramolecular tape

Figure 1.1. Different arrays of assemblies induced by H-bonding sites.

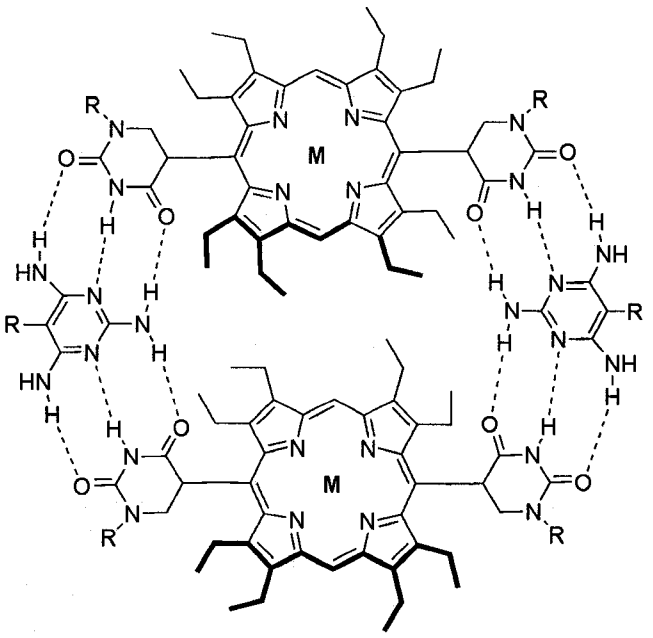

Supramolecular cage

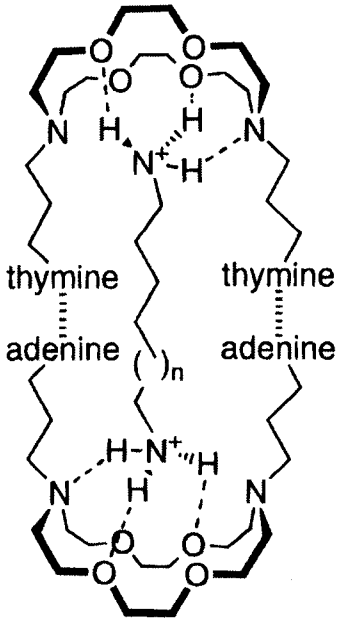

Supramolecular capsule

Figure 1.2. Hydrogen bond mediated supramolecular cage and capsule.

It is evident from the different assemblies shown in Figures 1.1 and 1.2 that information plays a key role in supramolecular chemistry.[2,7]

Artificial cylinder and tubular aggregates of specifically programmed molecules are of interest for sensing, transport, and bioactive systems and a number of supramolecular macrocycles designed have been obtained for these purposes.[21]

1.4. From Rosettes to Nanotubes

H-bonding and π-π stacking interactions play important role in the construction of rosettes and columnar supramolecular architectures.[22] Rosettes are supramolecular macrocyclic arrangement of molecules (modules) or groups of molecules induced by H-bonding interactions. The moiety bearing the hydrogen is referred to as the proton donor 'D', while the complementary electronegative group is referred to as the proton acceptor 'A'. The key to rosettes formation is the H-bond, therefore, it is important to first understand the stabilities of assemblies based on H-bonds information patterns.

π-π stacking interactions, as well as other factors such as, metal coordination, electrostatic and hydrophobic interactions that orchestrate the formation of tubular supramolecular architectures from supramacrocycles both in the solid and liquid-states have been briefly reviewed in this section.

1.4.1. Hydrogen Bonds Patterns and Their Stabilities

A hydrogen bond can be considered to represent a special type of electrostatic interaction. Although it is difficult to give a generally acceptable definition of a hydrogen bond, a simple working description is an attractive interaction between a proton donor and a proton acceptor.[19a] There are various ways of arranging hydrogen bond donors and acceptors in molecules that are capable of molecular recognition, some examples are illustrated in Figure 1.3.

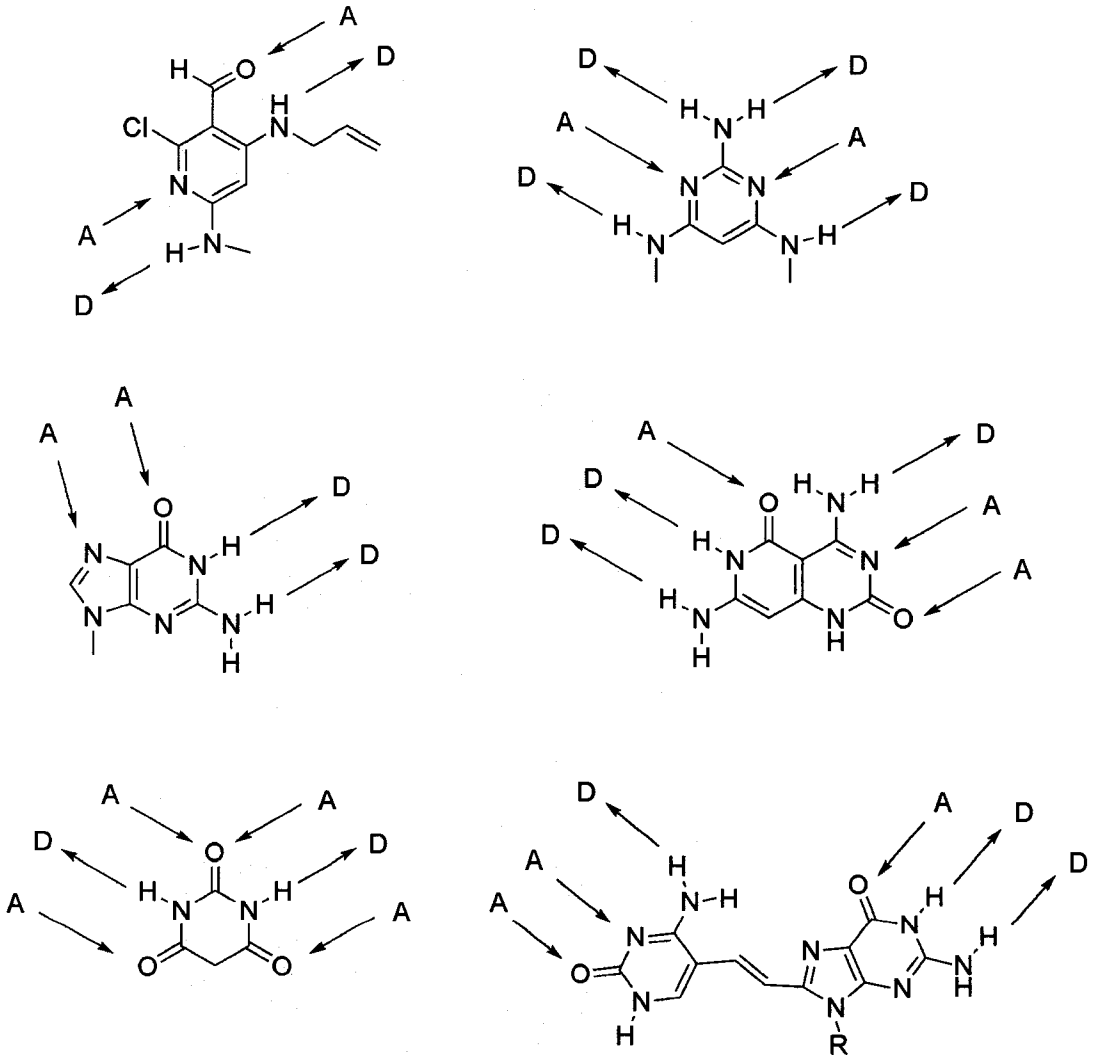

Figure 1.3. Molecules capable of molecular recognition and their intermolecular hydrogen bond patterns.

The particular arrangement of donor and acceptor group in an array of hydrogen bonds has a strong influence on the stability of the assembly. About two decades ago, Jorgensen and co-workers showed that these differences in stability can be largely attributed to attractive and repulsive *secondary* interactions.[23] Stabilization arises from the electrostatic attraction between positively and negatively polarized atoms in adjacent H-bonds, whereas destabilization is likewise the result of electrostatic repulsion between two positively or negatively polarized atoms (Figure 1.4 and 1.5).

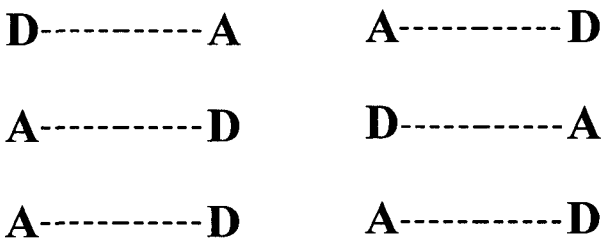

Figure 1.4. Intermolecular Hydrogen bonding (primary interaction) in **DAA-ADD** and **ADA-DAD** systems.

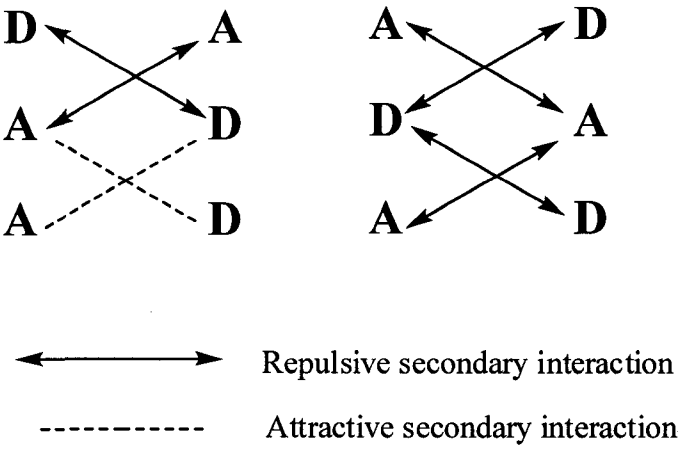

Figure 1.5. Attractive and repulsive secondary interactions in DAA-ADD, ADA-DAD systems.

As shown in Figure 1.5, there are two repulsive secondary interactions in the DAA-ADD system and four in the ADA-DAD system, this result indicates that the former is more stable than the later system. Zimmerman and co-workers studied the difference in thermodynamic stabilities of a series of dimeric complexes with ADA-DAD, DAA-AAD, and AAA-DDD arrays with 0, 2, and 4 favourable secondary interactions, respectively, in order to test Jorgenson's hypothesis on secondary interactions.[24] The stability constants were found to be of the order of 10^2, 10^3-10^4, and $>10^5$ M^{-1}, respectively, in $CHCl_3$, which are fully in line with Jorgenson's model. It has been reported that for acceptor and donor groups involved in hydrogen bonds, there is a destabilising effect of approximately 7kJ/mol per secondary interaction and if the groups responsible for the secondary interaction are not involved in hydrogen bonding (Figure 1.6), this value is estimated to be approximately 11kJ/mol.[25] These effects can be used as general guidelines for interpreting differences in stability measured for different rosettes as well as for those that form rosette nanotubes.

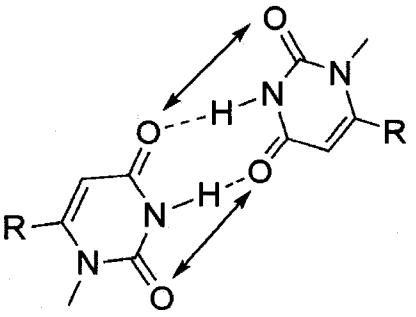

Figure 1.6. Destabilizing effect of non-bonding secondary interaction.

1.4.2. π-π Stacking Interaction: Hunter and Sanders Model

Stacking in supramolecular chemistry refers to columnar arrangement of aromatic molecules, which interact through aromatic interactions (π-π interaction and electrostatic interaction). Intermolecular overlapping of p-orbitals in π-conjugated systems causes π-π interactions. In 1990, Hunter and Sanders proposed a conceptually simple model for treating such interactions, which is based upon electrostatic and van der Waals forces.[26] Their approach enables analysis of the 'off-set', face-to-face and T-geometry arrangements for both neutral and polarized π-systems.

The main feature of the model is it considers the σ-framework and the π-electrons separately. It concludes that apparently net favorable π-π interactions are not due, in fact, to attractive electronic interactions between the two π-systems, but rather occur when the attractive interactions between π-electrons and the σ-framework (namely, π-σ attractions) outweigh unfavorable contributions such as π-electron repulsion (Figure 1.7).[26]

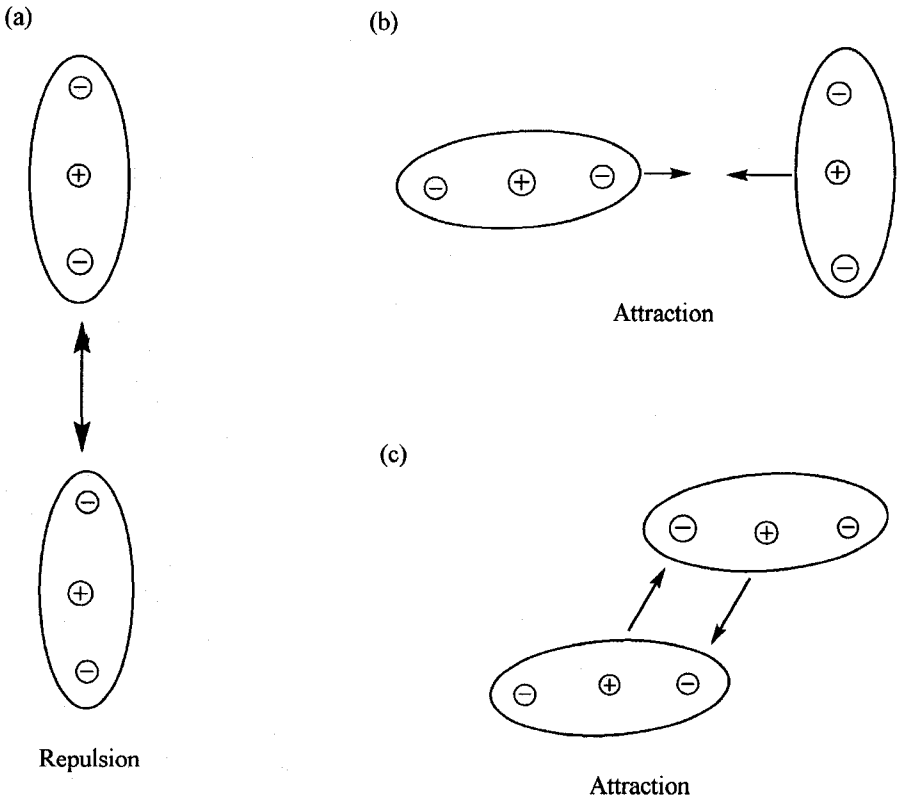

Figure 1.7. Hunter and Sanders' model of interactions between idealized π-atoms: (a) in a face-to-face interaction π-atom repulsion dominates; (b) whereas π-σ attraction dominates in a T interaction; (c) as well as in an offset π-stacked geometry.

The π-π stacking interactions play an important role in a large number of biological and chemical systems, including in DNA,[27] molecular recognition,[28] aromatic crystal packing,[29] and biomolecular self-aggregation.[30] In DNA, π-π stacking occurs between adjacent nucleotides and adds to the stability of the molecular structure. The base-base stacking interactions are usually associated with an offset rather than a face-to-face geometry,[31a] and this offset is complementary to the twist of the helix. In interactions between π-systems polarized by heteroatoms, the face-to-face stacked geometry is always favored by van der Waals interactions and solvophobic effects, but is generally disfavored by π-π repulsion. Highly polarized π-deficient molecules

such as tetranitrofluorenone form stable π-stacked complexes with a range of π-systems in offset geometries due to the reduced π-electron density at the site of π-overlap and favorable charge-charge interactions.[31c] Conversely, an electron-rich atom on π-systems would destabilize the π-π stacking interactions. The donor-acceptor stacks in Stoddart's systems for instance, clearly show offset and cross-interaction.[31d]

1.4.3. Self-Assembly of Guanosine

The G-quartet (Figure 1.8) fits particularly well with contemporary studies in rosettes and self-assembly. The G-quartet, an H-bonded complex formed by cation-templated assembly of guanosine was first identified in 1962.[32] A G-quadruplex is a structure built from the vertical stacking of multiple G-quartets. Anion H-bonding to the amino groups projecting from the G-quartets have also been used to further stabilize the G-quadruplex (Figure 1.8).[33] The G-quadruplex formation can be dissected into three organizational levels. First, four molecules of G (**1**) use self-complementary hydrogen bonds to form a planar G-quartet in level I. In level II, G-quartets stack with a separation of 3.3 Å between individual layers. Here, an octacoordination cation, which forms cation-dipole interactions with eight molecules of G (**1**) and located between two G-quartets, stabilizes hydrogen-bonded quartets and enhances base-stacking interactions to give a $G_8 \cdot M^+$. Finally, in level III, nucleobase-anion hydrogen bonds link two inner G-quartets in the D_4-symmetric hexadecamer $[\mathbf{1}]_{16} \cdot 4M^+ \cdot pic^-$, a quadruplex that is stable in the solid state and solution.[33]

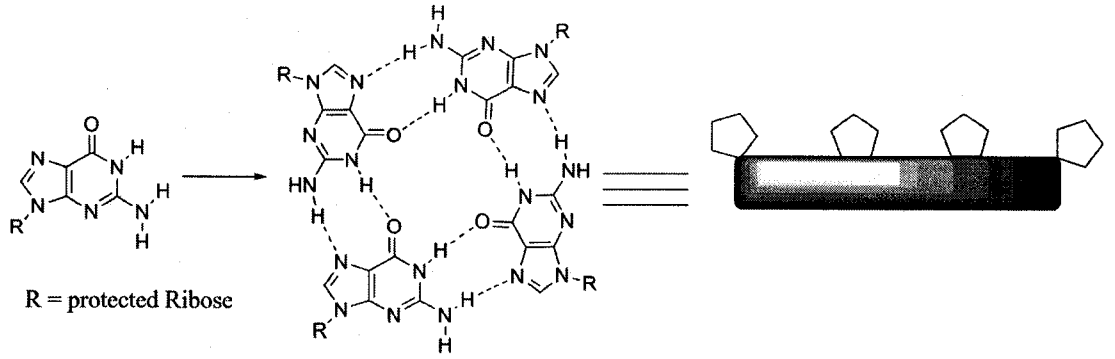

Level I. Hydrogen-Bonded G-Quartet

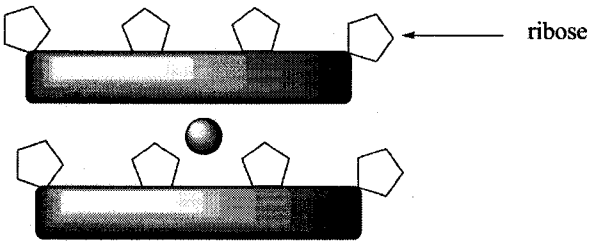

$[\mathbf{1}]_8\,M^+$

Level II. $G{\cdot}M^+$ Octamer Formed by Cation-Dipole interaction and pi-Stacking

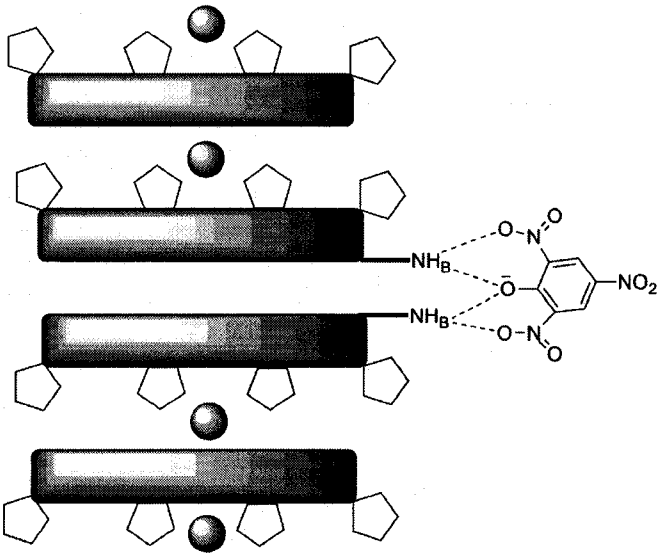

$[\mathbf{1}]_{16}{\cdot}\,4M^+{\cdot}\,pic^-$

Level III. Hexadecameric G-quadruplex with Anion-Nucleobase H-bonds

Figure 1.8. Schematic representation of the hierarchical self-assembly to give G-quadruplex $[\mathbf{1}]_{16}{\cdot}4M^+{\cdot}pic^-$.

1.4.4. Controlling the Self-Assembly Through the Nucleobase Structure and the Cation Template

Small differences in the building block have been shown to dramatically alter supramolecular structures. For instance, G and isoG (Figure 1.9) are two isomers that differ only in the location of an oxygen and nitrogen atom, yet they self-assemble much differently.[34] While G gives G_4-quartet in the presence of cation, isoG gives $isoG_5$-pentamer with 90° and 67° van der Waals angles, respectively (Figure 1.9). The identity of the cation is also critical in controlling the self-assembly of isoG. The same sequences that form pentaplexes with Cs^+ ions assemble into four-stranded structures with the smaller (and more charge dense) K^+ and Na^+ ions.[34]

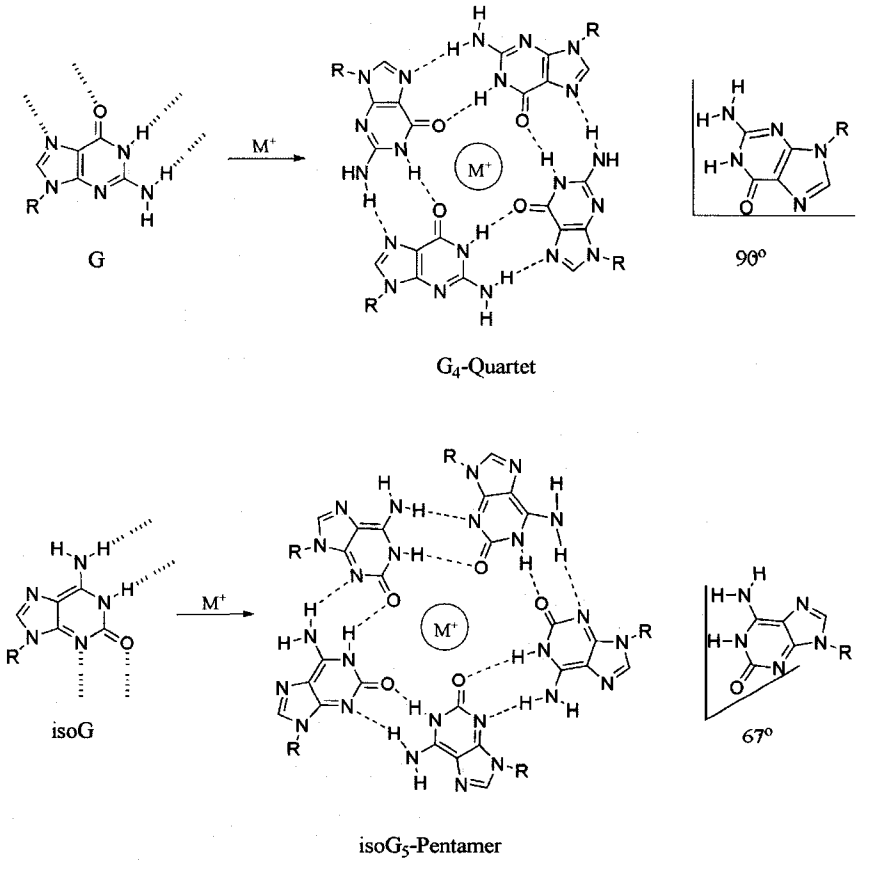

Figure 1.9. Self-association of G and isoG in the presence of cations to give hydrogen-bonded G_4-quartets and $isoG_5$-pentamers, respectively.

1.4.5. Induction of Supramolecular Chirality by Hierarchical Chiral Structures: Self-Assembly of Folic Acid Derivatives.

The self-assembly of folic acid and its derivatives through intermolecular hydrogen bonds of the pterin rings result in formation of self-organized tetrameric structures.[35] Folic acid is a useful candidate for a chiral building block, because of its self-assembling nature and the molecular chirality in its amino acid component. Takashi Kato and co-workers reported the induction and tuning of supramolecular chirality in the self-assembled folic acids **2a-c** in polar and apolar solution and in bulk state (Figure 1.10).[36] They reported that the tetramers formed by compounds **2a-c** stacked to form hexagonal columnar structures (Figure 1.11).

The circular dichroism (CD) spectra of pure **2a-c** measured in hexagonal columnar states in chloroform are inactive, indicating that the columnar structures formed do not have chiral order. In contrast, the addition of sodium triflate to **2a** and **2b** gave positive and negative CD spectra, respectively. For **2c**, less active CD spectrum is seen in the presence of sodium ions (Figure 1.12). Application of an apolar solvent (dodecane) drives the folic acid derivatives to form chiral assemblies in the absence of ions. In this case, it was thought that the lipophilic interactions promote nanophase segregation, which enhances the formation of chiral columns.[36]

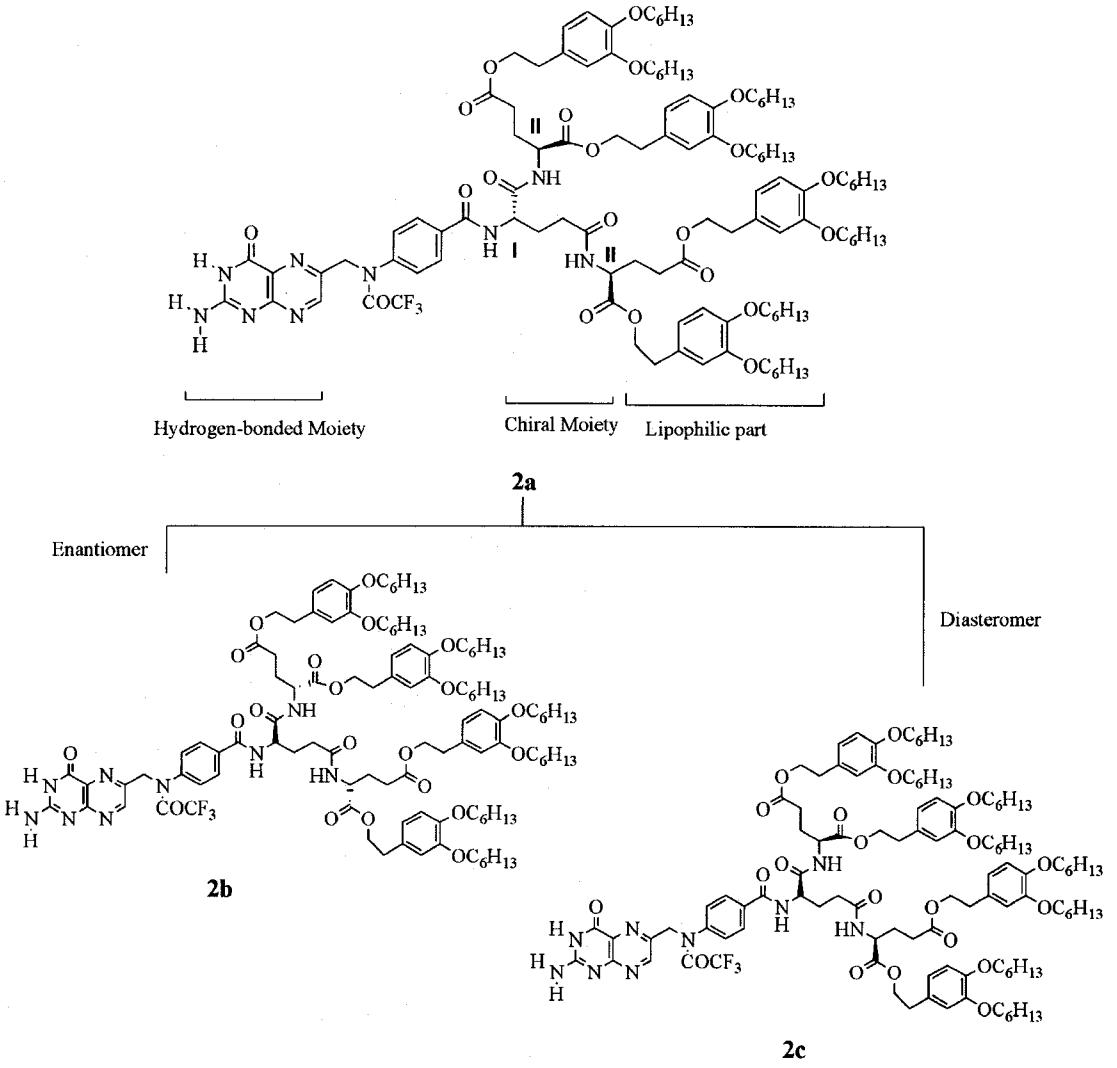

Figure 1.10. Structures of folic acid derivatives **2a-c**.

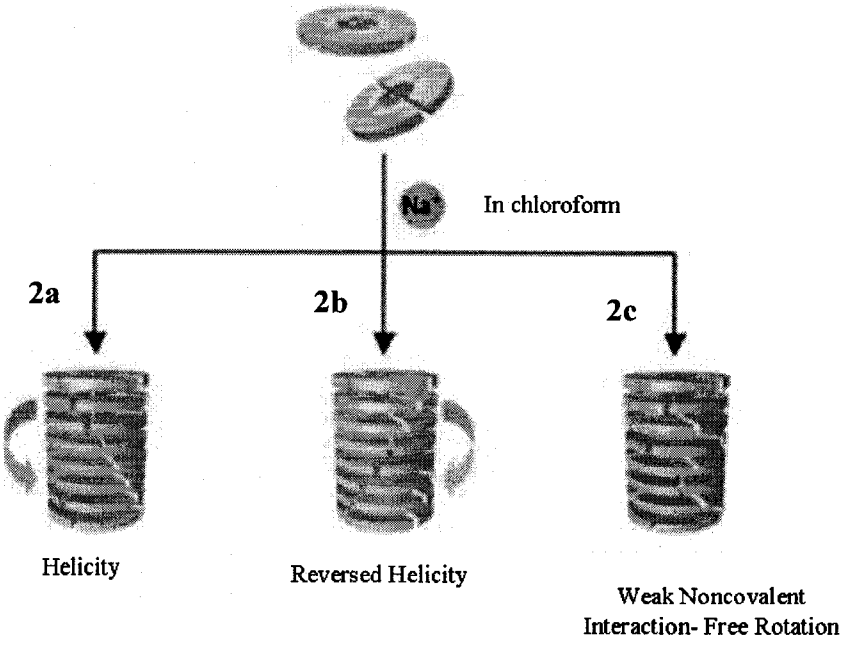

Figure 1.11. Schematic representation of the formation of chiral columnar assemblies in chloroform.

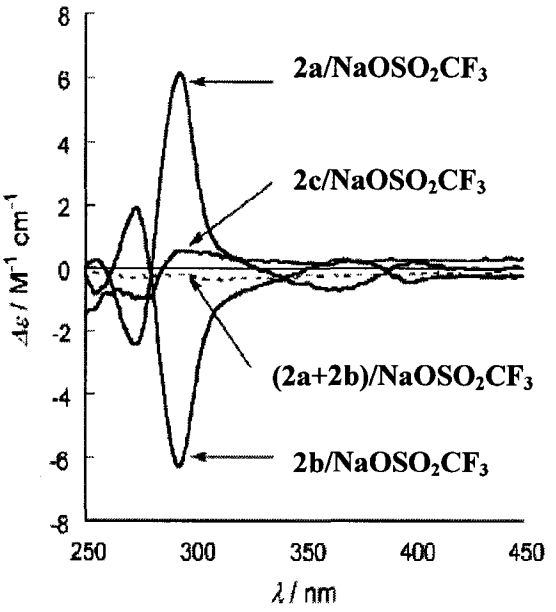

Figure 1.12. CD spectra **2a-c** in the presence of $NaOSO_2CF_3$.

These results suggest that **2** self-assembles in chloroform to form disk-like tetramers, which stack to form columnar assemblies through ion-dipolar interactions between sodium ions and the carbonyl groups of the pterin rings (Figure 1.13).[36]

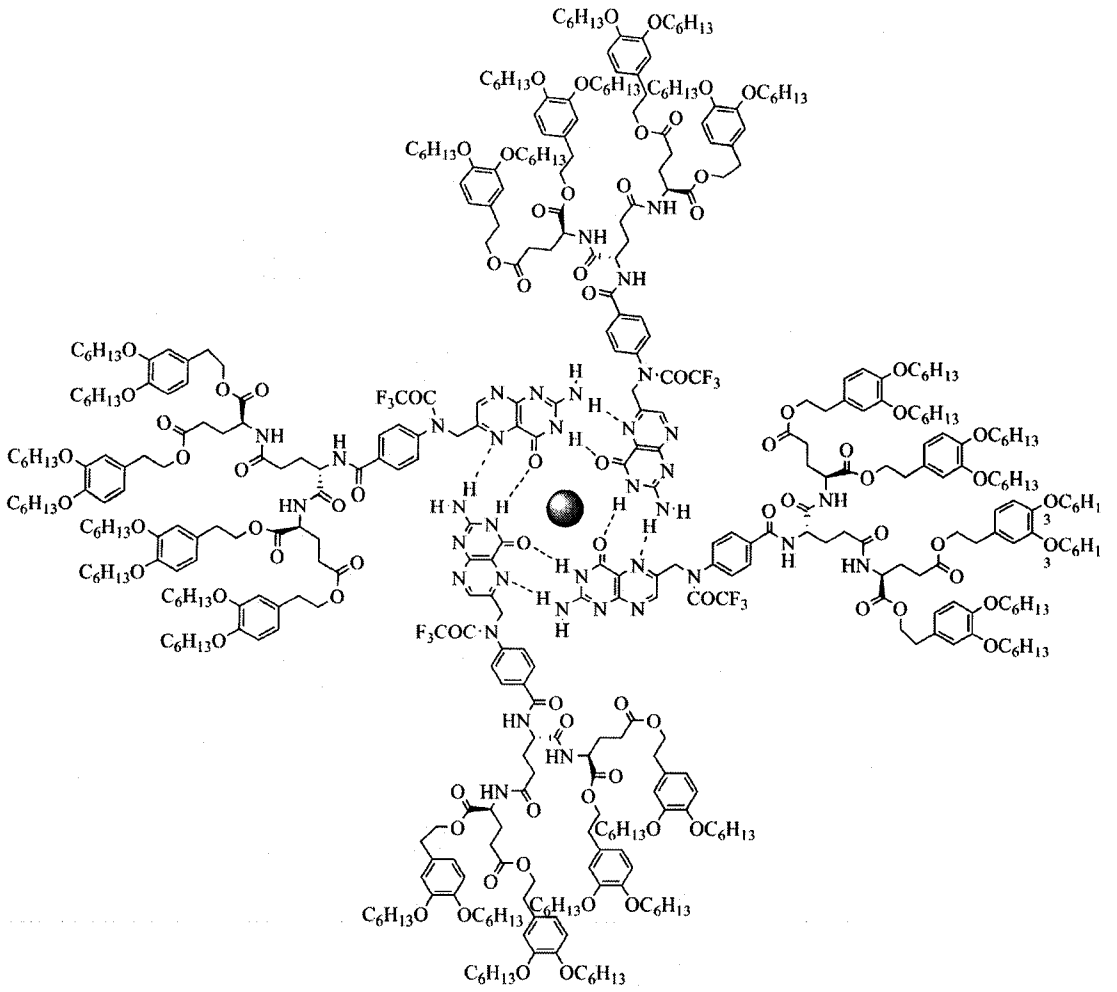

Figure 1.13. Schematic representation of self-assembled **2a**/$NaOSO_2CF_3$ in chloroform solution.

1.4.6. Hexameric Rosettes

Hexameric rosettes can either be homomodular or heteromodular. A homomodular rosette is composed of a single molecule that is self-complimentary through its H-bonding faces.[37] Such molecules contain two faces that could either be bicyclic or tricyclic. These molecules are sometimes referred to as "Janus-type" molecules.[38] Heteromodular systems, on the other hand contain at least two molecules, each having a H-bonding pattern that is complementary to one another.[39]

1.4.7. Self-Assembly of Melamine-Cyanuric/Barbituric Acid Derivatives

The H-bond directed self-assembly of cyanurate or barbiturate and melamine derivatives can in principle give rise to three different types of aggregates: rosettes,[39] linear tapes,[40] and crinkled tapes (Figure 1.14a).[41] Whitesides and co-workers have shown two general concepts for preferential formation of a rosette.[42] The first is the concept of *covalent preorganization* (Figure 1.14b), in which a Hub-spacer (C_3 symmetry) is used to preorganize the individual melamine units in a cyclic fashion. The second is the concept of *peripheral crowding,* which is based on the fact that melamines with sterically bulky substituents promote single rosette formation through the introduction of unfavourable steric interactions in the corresponding tape-like structures.

Timmerman and co-workers later re-evaluated the concept of peripheral crowding using theoretical calculations obtained from developed models that describe the self-assembly of melamine and cyanuric acid derivatives into rosettes and tapes.[43] The results do not support the concept of peripheral crowding as put forward by

Whitesides, but clearly show that steric interactions play a minor role in this self-assembly process.[44-45]

(a)

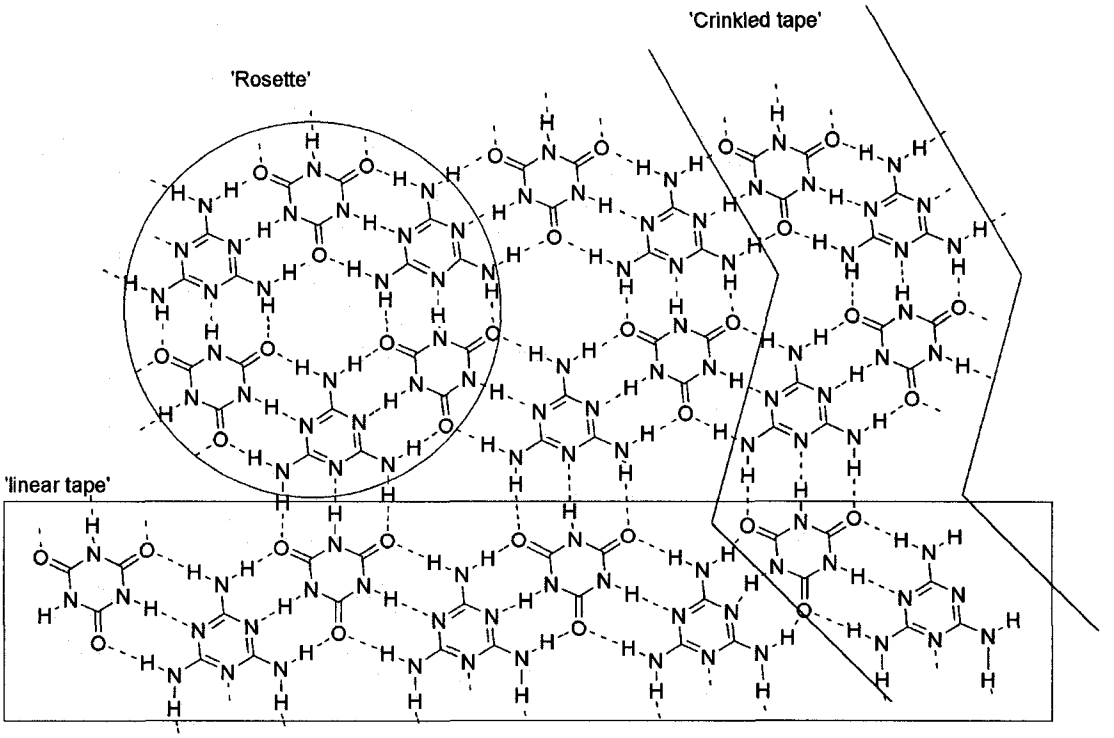

(b)

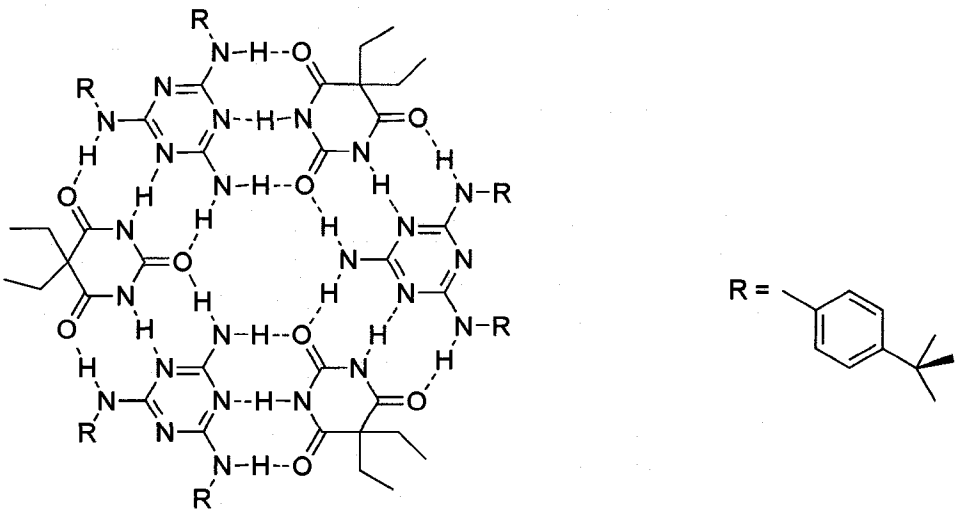

Figure 1.14. (a) Assembly motif: melamine·cyanuric acid (b) selective formation of the rosette motif using the concepts of covalent preorganization.

1.4.8. Self-Assembly of a Multi-Porphyrin Supramolecular Macrocycle

Lehn and co-workers, in an attempt to preferentially form a discrete cyclic structure rather than linear assemblies (tapes), found that three triaminotriazine units bearing two appended tetraphenylprophyrins (diPT) or their zinc complexes (diZnPT) undergo self-assembly through multiple H-bonding with three complementary dialkylbarbituric acids (diBBA) yielding a supramolecular macrocycle containing six porphyrins.[46] This is another example where peripheral crowding (steric) has been used to enforce the formation of a cyclic structure. They reported that incorporation of the photochemically rich porphyrin into these assemblies also allowed further characterization in solution. The results obtained from both the absorption and the fluorescence spectra on addition of diBBA to a solution of diZnPT, agree with the formation of a discrete cyclic structure rather than with linear assemblies of varying lengths (Figure 1.15).

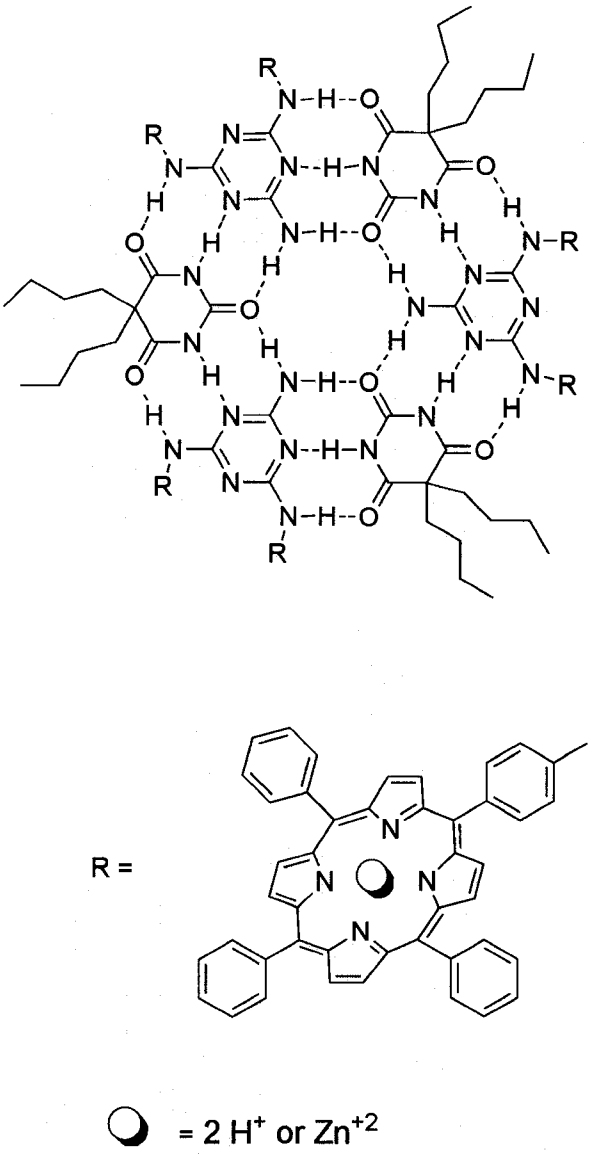

Figure 1.15. A supramolecular multiporphyrin macrocycle.

1.4.9. Self-Assembly of DNA Base Derivatives: Guanine (G) and Cytosine (C): G^C Base

So far, the formation of a cyclic array rested on additional factors, such as metal ion binding or steric effects, the H-bond pattern itself being not sufficient to univocally determine the outcome of the assembly. Such is the case for the species obtained from the interaction of melamine with cyanuric acid or barbituric acid derivatives, which may generate either linear (tape, crinkled tape) or cyclic rosette arrays. In order to generate a macrocyclic supramolecular architecture on the basis of the H-bond information alone, Lehn and co-workers set out to design a molecular entity that is H-bond programmed to self-assemble uniquely into a supramolecular cyclic array.[47] They designed compounds **3** and **4** (Figure 1.16), which incorporate the complementary H-bonding codes of both cytosine (AAD) and guanine (DDA) in the same molecule. These self-complementary G^C DNA hybrid bases self-assembled into hexameric rosettes **M** held together by 18 H-bonds. The group was unable to recrystallize **M** for X-ray crystallographic studies but instead supported the assembly by ^{1}H NMR studies.

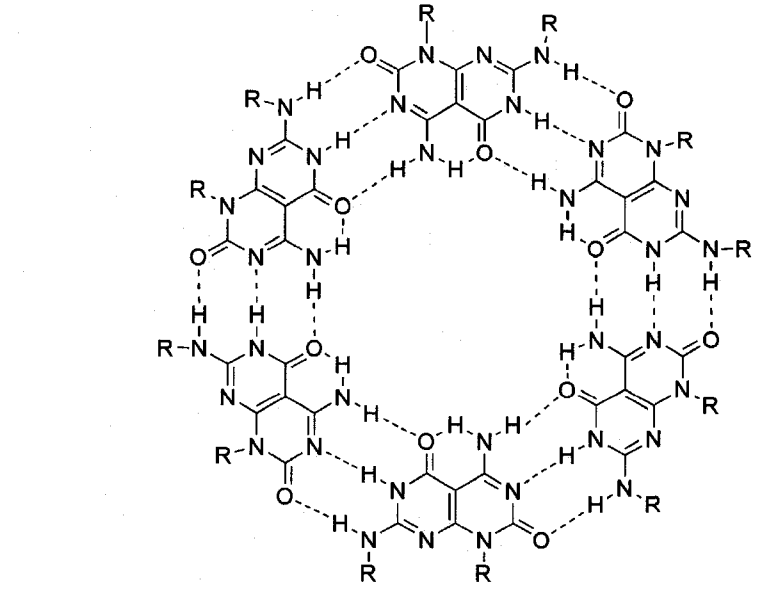

M

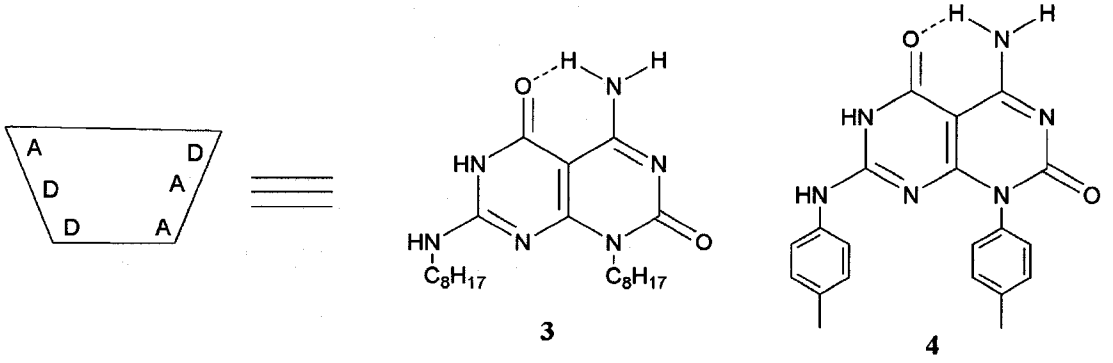

3 **4**

Figure 1.16. Lehn's proposed self-assembly of G^C bases **3** and **4** into rosette **M**.

1.4.10. Mascal's G^C Motif

At the same time Lehn and co-workers reported the synthesis and the supramolecular macrocyclic properties of the G^C DNA hybrid base moiety, Mascal and co-workers reported a shorter synthetic route for making the G^C DNA hybrid base.[48-50] Their short synthetic design resulted in the replacement of the non-bonding N-atom in the G-ring with a sp^2 C-atom (Figure 1.17). They were able to get an X-ray structure of the self-assembled G^C base, which confirmed the formation of a supramolecular macrocycle (rosette) in the solid state.

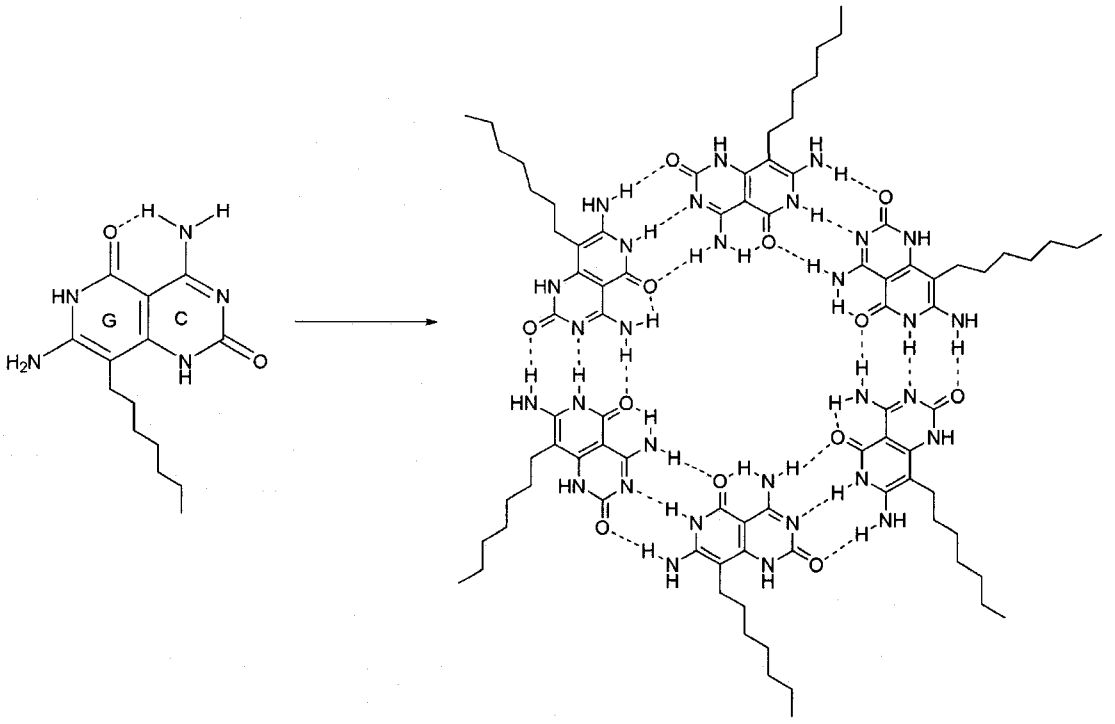

Figure 1.17. Self-assembly of six molecules of G^C into a hexameric rosette.

1.4.11. Hierarchical Self-Assembly of G^C Base into Rosette Nanotubes

Hierarchical self-assembly is a process by which natural systems converge small components into complex functional architectures.[52] Fenniri and co-workers have established that nanotubular architectures can be constructed from the self-assembly of G^C base motifs.[22,51-55] They have demonstrated by variable temperature UV-Visible studies, dynamic light scattering (DLS), small angle X-ray scattering (SAXS), transmission electron microscopy (TEM), atomic force microscopy (AFM), scanning electron microscopy (SEM), nuclear magnetic resonance (NMR) and high resolution mass-spectroscopy (MS) that G^C-based rosettes serve as very stable, non-covalent, scaffolds for supramolecular synthesis of tubular assemblies.[51-55] They have since designed and synthesized different G^C base moieties all modeled after Lehn's G^C base motifs.[47]

Fenniri and co-workers reported that the self-assembly process of the G^C base is entropically driven similar to the self-assembly process of natural systems such as the polymerization of the coat protein of the tobacco mosaic virus.[52] To demonstrate this, they synthesized **5** (Figure 1.18a) and studied its self-assembly properties in water. The G^C motif undergoes a hierarchical self-assembly process fueled by hydrophobic effects in water to form a six-membered supramacrocycles maintained by 18 H-bonds. The resulting and substantially more hydrophobic aggregate self-organizes into a linear stack defining an open central channel 1.1 nm across and several micrometers long (Figure 1.18b).

(a)

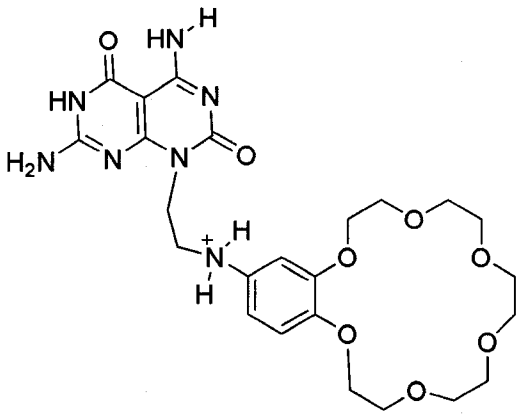

(b)

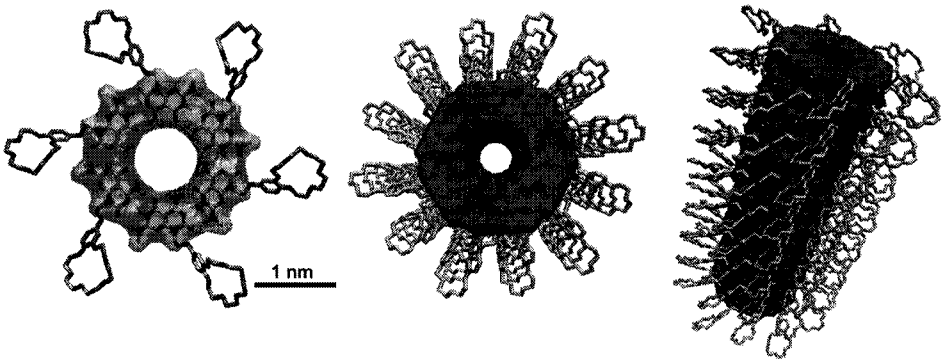

Figure 1.18. (a) G^C motif **5**, (b) self-assembly of **5** into a six-membered supramacrocycle and RNT.

It was observed that as the temperature increases, there was an increase and controlled level of aggregation of the supramacrocycles. This is a hallmark of the hydrophobic effect as release of ordered water on the surface of the hydrophobic surfaces of the bases to the bulk solvent as the temperature increases, contributes to the solute's self-association.

1.4.12. Hierarchical Self-Assembly of Twin G^C Base

In order to enhance the thermal stability of the nanotubes by better preorganization, increased amphiphilic character, and greater number of H-bonds per module (12 instead of 6), Fenniri and co-workers designed **6**, which has two G^C bases linked together (twin bases) (Figure 1.19).[53] The syn comformer of the twin bases self-assemble into a double rosette maintained by 36 H-bonds instead of the 18 H-bonds in the single base. Modeling and experimental results showed that the resulting RNT is sterically less congested due to better preorganization and also experiences reduced electrostatic repulsion on its surface (Figure 1.20). TEM and AFM images of the aqueous sample of **6** both showed well formed RNTs (Figure 1.21 and Figure 1.22).

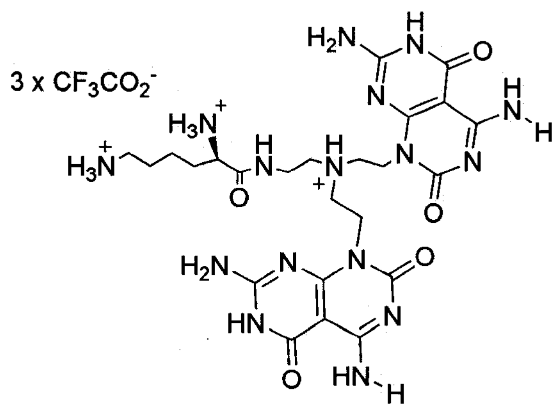

Figure 1.19. Twin G^C base **6**.

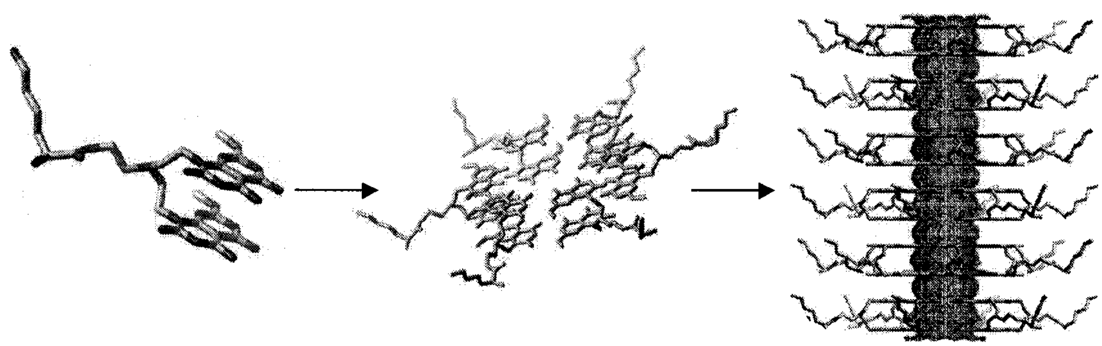

Figure 1.20. Self-assembly of twin G^C base **6** into double rosette held by 36 H-bonds and its RNT.

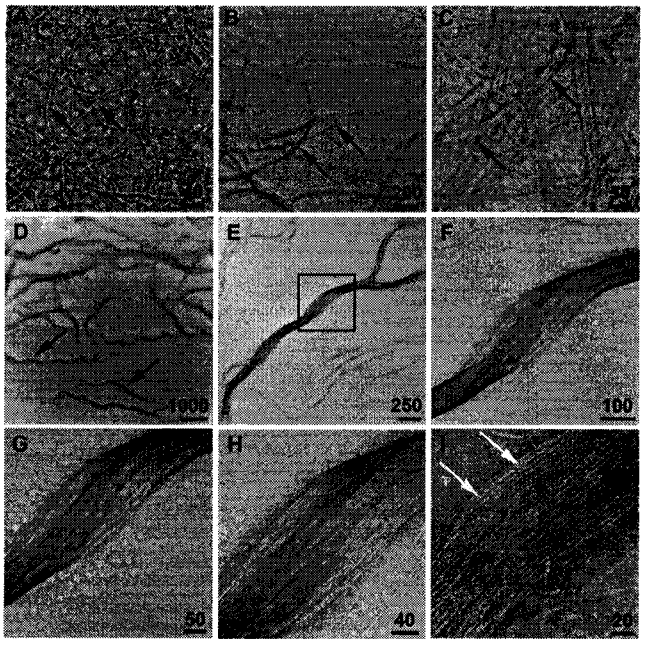

Figure 1.21. TEM micrographs of negatively stained assemblies obtained from **6** at pH 4 (A), pH 7 (B and C) and pH 11 (D-I). Pointed arrows show RNTs.

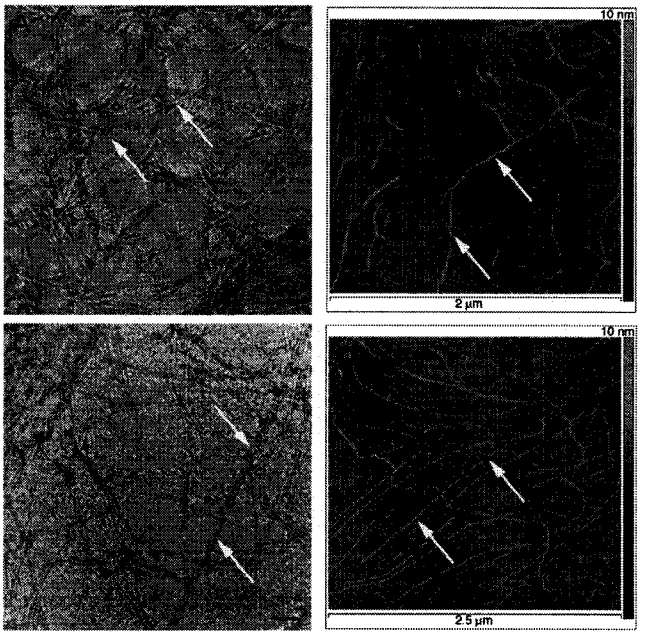

Figure 1.22. SEM micrographs of negatively stained (uranyl acetate) assemblies obtained from **6** (A and C) and TM-AFM micrographs obtained from **6** (B and D). Pointed arrows show RNTs.

1.5. Research Focus

Achieving the design of supramolecular nanostructures with hierarchical order that parallels the complexity of natural systems requires in-depth understanding of the forces that orchestrate their organization, and the characterization of the intermediate states leading to the final superstructure.[53]

Fenniri and co-workers have thus designed different hierarchical rosette nanostructures including the induction of supramolecular chirality in the self-organized nanostructures.[53,55]

My research is divided into two parts. The first part (Chapter 2) is the synthesis and self-assembly of amphiphilic RNTs whose G^C base is modeled after Lehn's G^C base motif. The second part (Chapter 3) is the synthesis and self-assembly of different functional G^C bases modeled after Mascal's G^C motif.

1.6. References

1. Lehn, J.-M. *Proc. Natl. Acad. Sci. USA.* **2002**, *99*, 4763.
2. Lehn, J.-M. *Science,* **1993**, *260*, 1762.
3. Nicolaou, K. C.; Sorensen, E. J. *Classics in Total Synthesis* VCH, New York **1996**
4. Timmerman, P.; Prins, L. J. *Eur. J. Org. Chem.* **2001**, 3191.
5. Lehn, J.-M. *Supramolecular Chemistry* VCH, New York. **1995.**
6. (a) Lehn, J.-M. *Chem. Eur. J.* **2000**, *6*, 2097-2102. (b) Halpern, J. *Proc. Natl. Acad. Sci.* **2002**, *99*, 4762.
7. (a) Atwood, J. L.; Davies, J. E. D.; MacNicol, D. D.; Vögtle, F.; Lehn, J.-M. *Comprehensive Supramolecular Chemistry.* Pergamon, Oxford, **1996**. (b) Lehn, J.-M. *Angew. Chem. Int. Ed. Engl.* **1990**, *29*, 1304. (c) Lindsey, J. S. *New J. Chem.* **1991**, *15*, 153. (d) Stoddart, J. F.; Philip, O. *Synlett.*, **1991**, 445. (e) Whitesides, G. M.; Mathias, J. P.; Seto, C. T. *Science*, **1991**, *254*, 1312.
8. Brackmann, S. *Biophys. Chem.* **1997**, *66*, 133.
9. Eigen, M. *Naturwissenschaften* **1971**, *58*, 465.
10. Lehn, J.-M. *Angew. Chem. Int. Ed. Engl.* **1988**, *27*, 89.
11. Lehn, J.-M. *Angew. Chem. Int. Ed. Engl.* **1990**, *29*, 1304.
12. (a) Gallant, M.; Viet, M. T. P.; Wuest, J. D. *J. Org. Chem.* **1991**, *56*, 2284. (b) Garcia-Tellado, F.; Geib, S. J. Goswami, S.; Hamilton, A. D. *J. Am. Chem. Soc.* **1991**, *113*, 9265.
13. (a) Whitesides, G. M.; Zerkowski, J. A.; Seto, C. T.; Wierda, D. A. *J. Am. Chem. Soc.* **1990**, *112*, 9025. (b) Whitesides, G. M.; Zerkowski, J. A.; Seto, C.

T. *J. Am. Chem. Soc.* **1992**, *114*, 5473. (c) Whitesides, G. M.; Zerkowski, J. A.; MacDonald, J. C.; Seto, C. T.; Wierda, D. A. *J. Am. Chem. Soc.* **1994**, *116*, 2382.

14. (a) Schmidt, G. M. J.; Leiserowitz, L. *J. Am. Chem. Soc.* **1969**, 2372. (b) Hollinggsworth, M. D.; Harris, K. D. M. *Nature*, **1989**, *341*, 9. (c) Lauher, J. W.; Chang, Y. L.; West, M. A.; Fowler, F. W. *J. Am. Chem. Soc.* **1993**, *115*, 5991.
15. Lehn, J.-M.; Drain, C. M.; Fischer, R.; Nolen, E. G. *J. Chem. Soc. Chem. Commun.* **1993**, 243.
16. (a) Zimmerman, S. C.; Zeng, F.; Reichert, D. E. C.; Kolotuchin, S. V. *J. Chem. Soc. Chem. Commun.* **1996**, *271*, 1095. (b) Reinhoudt, D. N.; Vreekamn, R. H.; Van Duvnhoven, J. P. M.; Hubert, M.; Verboom, W. *Angew. Chem. Int. Ed. Engl.* **1996**, *35*, 1215.
17. Atwood, J. L.; MacGillivray, L. R. *Nature*, **1997**, *389*, 469.
18. Rebek Jr., J.; Conn, M. M. *Chem. Rev.* **1997**, *97*, 1647.
19. (a) Pimentel, G.C; McClellan, A. L. *The hydrogen bond*, **1960**. Freeman, San Francisco. (b) Timmerman, P.; Prins, L. J.; Reinhoudt, D. N. *Angew. Chem. Int. Ed.* **2001**, *40*, 2382.
20. Hollingsworth, M. D.; Harris, K. D. M. *Nature*, **1989**, *341*, 9.
21. Kelly, T. R.; Bridger, G. J.; Zhao, C. *J. Am. Chem. Soc.*, **1990**, *112*, 8024.
22. Fenniri, H.; Deng, B.-L.; Ribbe, A. E. *J. Am. Chem. Soc.* **2002**, *124*, 11064.
23. Jorgenson, W. L.; Pranata, J. *J. Am. Chem. Soc.* **1990**, *112*, 2008.

24. (a) Zimmerman, S. C.; Murray, T. J. *J. Am. Chem. Soc.* **1992**, *114*, 4010. (b) Sherrington, D. C.; Taskinen, K. A. *Chem Soc. Rev.* **2001**, *30*, 83.

25. Beijer, F.H.; Sijbesma, R. P.; Vekemans, J.A. J. M.; Meijer, E. W.; Koojman, H.; Spek, A. L. *J. Org. Chem.* **1996**, *61*, 6371.

26. (a) Hunter, A. C.; Sanders, J. K. M. *J. Am. Chem. Soc.* **1990**, *112*, 5525. (b) Scott, L. C.; Christopher, A. H.; Kevin, R. L.; Julie, P.; Christopher J. U.; *J. Am. Chem. Soc.* **2005**, *127*, 8594.

27. Kelley, S. O.; Barton, J. K. *Science*, **1999**, *283*, 375.

28. Lehn, J.-M.; Petitjean, A. P.; Khoury, R. G.; Kyritsakas, N. *J. Am. Chem. Soc.* **2004**, *126*, 6637.

29. Sygula, A.; Fronczek, F. R.; Sygula, R.; Rabideau, P. W.; Olmstaed, M. M. *J. Am. Chem. Soc.* **2007**, *129*, 3842.

30. (a) Alberts, B. *Molecular Biology of the cell.* **1989**, Gerland, New York, *ed. 2*, 84. (b) Saenger, W. *Principles of Nucleic Acid Structure.* **1986**, Springer-Verlag, New-York.

31. (a) Saenger, W. *Principle of Nucleic Acid Structure.* **1984**, Springer-Verlag: New York, **1984**; pp 132. (b) Morokuma, K. *Acc. Chem. Res.* **1977**, *10*, 294. (c) Zimmerman, S. C.; Mrkisch, M.; Baloga, M. *J. Am. Chem. Soc.* **1989**, *111*, 8528. (d) Ortholand, J.-Y.; Slawin, A. M. Z.; Spencer, N.; Stoddart, J. F.; Williams, D. J. *Angew. Chem. Int. Ed.* **1989**, 1394. (e) Forman, S. L.; Fettinger, J. C.; Pieraccini, S.; Gottarelli, G. *J. Am. Chem. Soc.* **2000**, *122*, 4060.

32. Gellert, M.; Lipsett, M. N.; Davies, D. R. *Proc. Natl. Acad. Sci. USA.* **1962**, *48*, 2013.

33. (a) Shi, X. D.; Fettinger, J. C.; Davis, J. T. *J. Am. Chem. Soc.* **2001**, *123*, 6738. (b) Shi, X. D.; Fettinger, J. C.; Davis, J. T. *Angew. Chem. Int. Ed.* **2001**, *113*, 2909.

34. (a) Chaput, J. C.; Switzer, C. *Proc. Natl. Acad. Sci. USA.* **1999**, *96*, 10614. (b) Chaput, J. C.; Switzer, C. *Methods.* **2001**, *23*, 141-148. (c) Seela, F.; Wei, C. F.; Melenewski, A.; Feiling, E. *Nucleosides Nucleotides.* **1998**, *17*, 2045. (d) Seela, F.; Wei, C. F. *Chem. Commun.* **1997**, 1867. (e) Seela, F.; Wei, C. F.; Melenewski, A. *Nucleic Acids Res.* **1996**, *24*, 4940.

35. (a) Ciuchi, F.; Nicola, G. D.; Franz, H.; Gottarelli, G.; Mariani, P.; Bossi, M. G. P.; Spada, G. P. *J. Am. Chem. Soc.* **1994**, *116*, 7064. (b) Bonazzi, S.; De Morais, M. M.; Gottarelli, G.; Mariani, P.; Spada, G. P. *Angew. Chem. Int. Ed.* **1993**, *105*, 251. (c) Bonazzi, S.; De Morais, M. M.; Gottarelli, G.; Mariani, P.; Spada, G. P. *Angew. Chem. Int. Ed.* **1993**, *32*, 248. (d) Shi, X.; Mullaugh, K. M.; Fettinger, J. C.; Jiang, Y.; Hofstadler, S. A.; Davis, J. T. *J. Am. Chem. Soc.* **2003**, *125*, 10830.

36. Kamikawa, Y.; Nishii, M.; Kato, T.; *Chem. Eur. J.* **2004**, *10*, 5942.

37. (a) Duchamp, D. J.; Marsh, R. E. *Acta Cryst.* **1969**, *5*, 5. (b) Lackinger, M.; Griessl, S.; Kampschulta, L.; Jamitzky, F.; Heckl, W. M. *Small.* **2005**, *1*, 532. (c) Zafar, A.; Yang, J.; Geib, S. J.; Hamilton, A. D.; *Tet. Lett.* **1999**, *37*, 2327. (d) Jonkheijm, P.; Miura, A. A.; Zdanowska, M.; Hoeben, F. J. M.; De Feyte,

S.; Schenning, H. J.; De Schryver, F. C.; Meijer, E. W.; *Angew. Chem. Int. Ed.* **2004**, *43*, 74.

38. Asadi, A.; Patrick, B. O.; Perrin, D. M. *J. Org. Chem.* **2007**, *72*, 466.

39. (a) Ranganathan, A.; Pedireddi, V. R.; Rao, C. N. R.; *J. Am. Chem. Soc.* **1999**, *121*, 1752. (b) Lehn, J.-M.; Mascal, M.; DeCian, A.; Fischer, J.; *J. Chem. Soc., Chem. Commun.* **1990**, 479. (c) Seto, C. T.; Whitesides, G. M. *J. Am. Chem. Soc.* **1990**, *112*, 6409. (d) Zerkowski, J. A.; C. T.; Whitesides, G. M. *J. Am. Chem. Soc.* **1992**, *114*, 5473. (e) Nicolaisen, F. M.; Meyland, I.; Schaumberg, K. *Acta Chem. Scand.* **1980**, *B34*, 579.

40. Zerkowski, J. A.; Seto, C. T.; Wierda, D. A.; Whitesides, G. M. *J. Am. Chem. Soc.* **1990**, *112*, 9025.

41. Zerkowski, J. A.; Whitesides, G. M. *J. Am. Chem. Soc.* **1994**, *116*, 4298.

42. (a) Whitesides, G. M.; Simanek, E. E.; Mathias, J. P.; Seto, C. T.; Chin, D. N.; Mammen, M.; Gordon, D. M. *Acc. Chem. Res.* **1995**, *28*, 37. (b) Whitesides, G. M.; Simanek, E. E.; Mathias, J. P.; Seto, C. T.; Mammen, M.; Zerkowski, J. A. *J. Am. Chem. Soc.* **1994**, *116*, 4316. (c) Whitesides, G. M.; Simanek, E. E.; Mathias, J. P. *J. Am. Chem. Soc.* **1994**, *116*, 4326.

43. Bielejewska, A. G.; Marjo, C. E.; Prins, L. J.; Timmerman, P.; De Jong, F.; Reinhoudt, D. N. *J. Am. Chem. Soc.* **2001**, *123*, 7518.

44. (a) Vreekamp, R. H.; Van Duynhoven, J. P. M.; Hubert, M.; Verboom, W.; Reinhoudt, D. N. *Angew. Chem. Int. Ed.* **1996**, *35*, 1215. (b) Timmerman, P.; Vreekamp, R. H.; Hulst, R.; Verboom, W.; Reinhoudt, D. N.; Rissanen, K.; Udachin, K. A.; Ripmeester, J. *Chem. Eur. J.* **1997**, *3*, 1823.

45. Prins, L. J.; Hulst, R.; Timmerman, P.; Reinhoudt, D. N. *Chem. Eur. J.* **2002**, *8*, 2288.

46. Drain, C. M.; Russell, K. C.; Lehn, J.-M. *Chem. Commun.* **1996**, 337.

47. Marsh, A.; Silvestri, M.; Lehn, J.-M. *Chem. Commun.* **1996**, 1527.

48. Mascal, M.; Hext, N.; Warmuth, R.; Moore, M. H.; Turkenburg, J. P. *Angew. Chem. Int. Ed. Engl.* **1996**, *35*, 2203.

49. Mascal, M.; Hext, N.; Warmuth, R.; Moore, M. H.; Turkenburg, J. P.; Arnall-Culliford, J. R. *J. Org. Chem.*, **1996**, *64*, 8479.

50. Mascal, M.; Farmer, S. C.; Arnall-Culliford, J. R. *J. Org. Chem.*, **2006**, *71*, 8146.

51. Fenniri, H.; Mathiavanan, P.; Vidale, K. L.; Sherman, D. M.; Hallenga, K.; Wood, K. V.; Stowell, J. G. *J. Am. Chem. Soc.* **2001**, *123*, 3854.

52. Fenniri, H.; Deng, B. L.; Ribbe, Hallenga, K.; Jacob, J.; Thiyagarajan, P. *Proc. Natl. Acad. Sci. USA.* **2002**, *99*, 6487.

53. Moralez, J. G.; Raez, J.; Yamazaki, T.; Motkuri, R. K.; Kovalenko, A.; Fenniri, H. *J. Am. Chem. Soc.* **2005**, *127*, 8307.

54. Raez, J.; Moralez, J. G.; Fenniri, H. *J. Am. Chem. Soc.* **2004**, *126*, 16298.

55. Johnson, R. S.; Yamzaki, T.; Kovalenko, A.; Fenniri, H. *J. Am. Chem. Soc.* **2007**, *129*, 5735.

CHAPTER 2

SYNTHESIS AND SELF-ASSEMBLY OF SELF-COMPLEMENTARY AMPHIPHILIC G^C BASE

2.1. Introduction and System Design

A wide range of synthetic and natural compounds self-organize into bulk aggregates exhibiting periodicities on the nanoscale as a consequence of their molecular shape, preorganization, degree of amphiphilic character and often, the presence of additional non-covalent interactions (H-bonding, π-π stacking interactions, hydrophobic effects and van der Waal forces). The resulting periodicity can be one-dimensional, two-dimensional, or three dimensional.[1]

Self-assembled nanostructures of amphiphiles held together by noncovalent interactions are currently the focus of interest due to their potential application in controlled release, electroactive composites, and multifunctional materials.[2] Amphiphilic molecules, of which soap is a typical example, possess antagonistic hydrophilic and hydrophobic moieties in the same molecule. Carbohydrate amphiphiles commonly referred to as glycolipids, greatly contribute to the structural stability and the function of biomembranes in living systems.[3] Lipids are well known amphiphilic molecules that form diverse aggregate morphologies in aqueous media.[4] Many amphiphilic polymers can also self-assemble to generate various morphologies including micelles, rods, and vesicular aggregates.[5] Nanotube formation is however, limited to several block copolymer systems. The reason for this limitation is that nanotube formation generally requires highly ordered molecular packing and

anisotropic intermolecular interactions, and most coil-coil block copolymers show higher chain flexibility and fewer anisotropic intermolecular interactions than low-molecular weight lipids.[6] Furthermore, many of the polymer nanotubes are generated under kinetic conditions.[7] Construction of amphiphilic hexameric rosette nanotubes under thermodynamic conditions could be a better way of generating well ordered stable aggregates with diverse morphologies in solutions.

Here we describe the design and synthesis of an amphiphilic G^C base **7** (Figure 2.1). Compound **7** was anticipated to self-assemble in apolar solvents to form RNTs (Figure 2.2), driven by H-bonding and the solvophobic effect.[8]

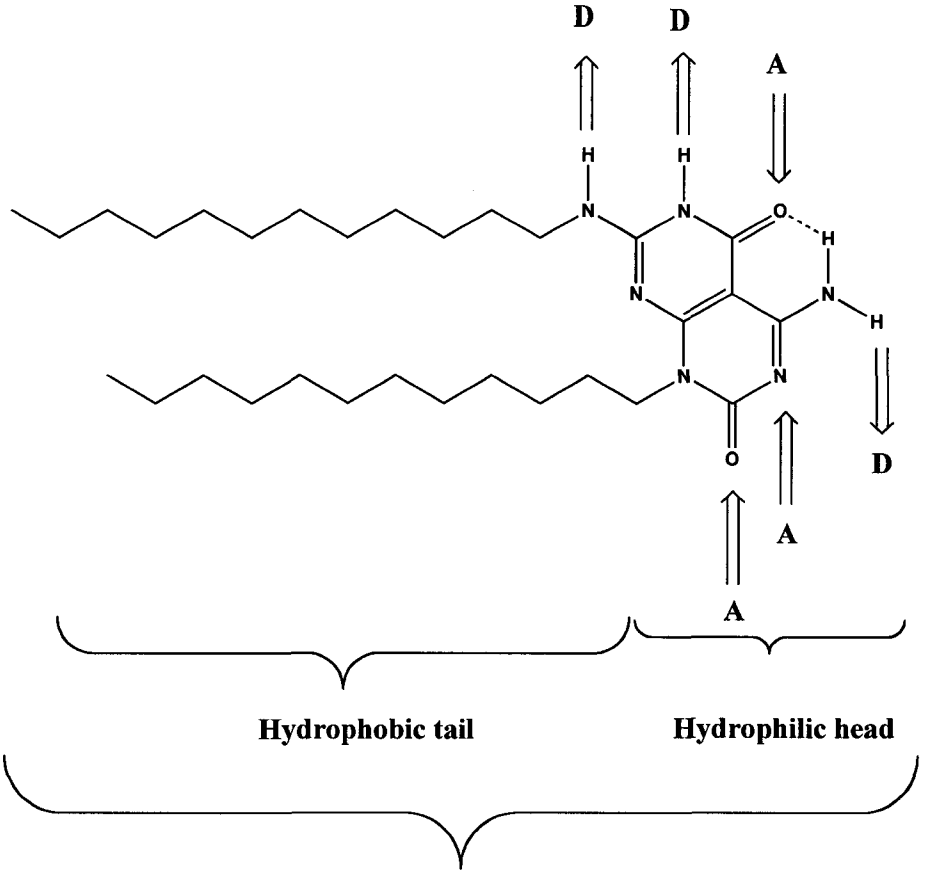

Figure 2.1. Diagram showing both the hydrophobic tail and the hydrophilic head of the amphiphilic G^C base **7**.

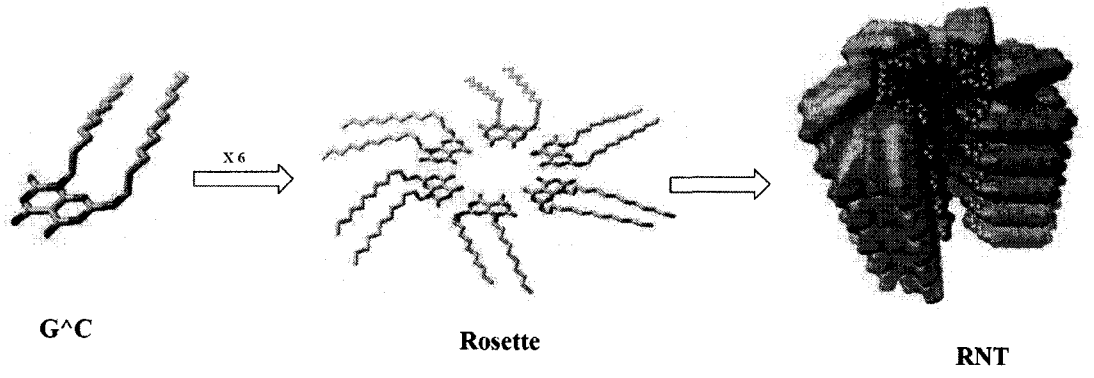

Figure 2.2. Hierarchical self-assembly of G^C base **7** in hexane.

2.2. Retrosynthesis of G^C Base 7

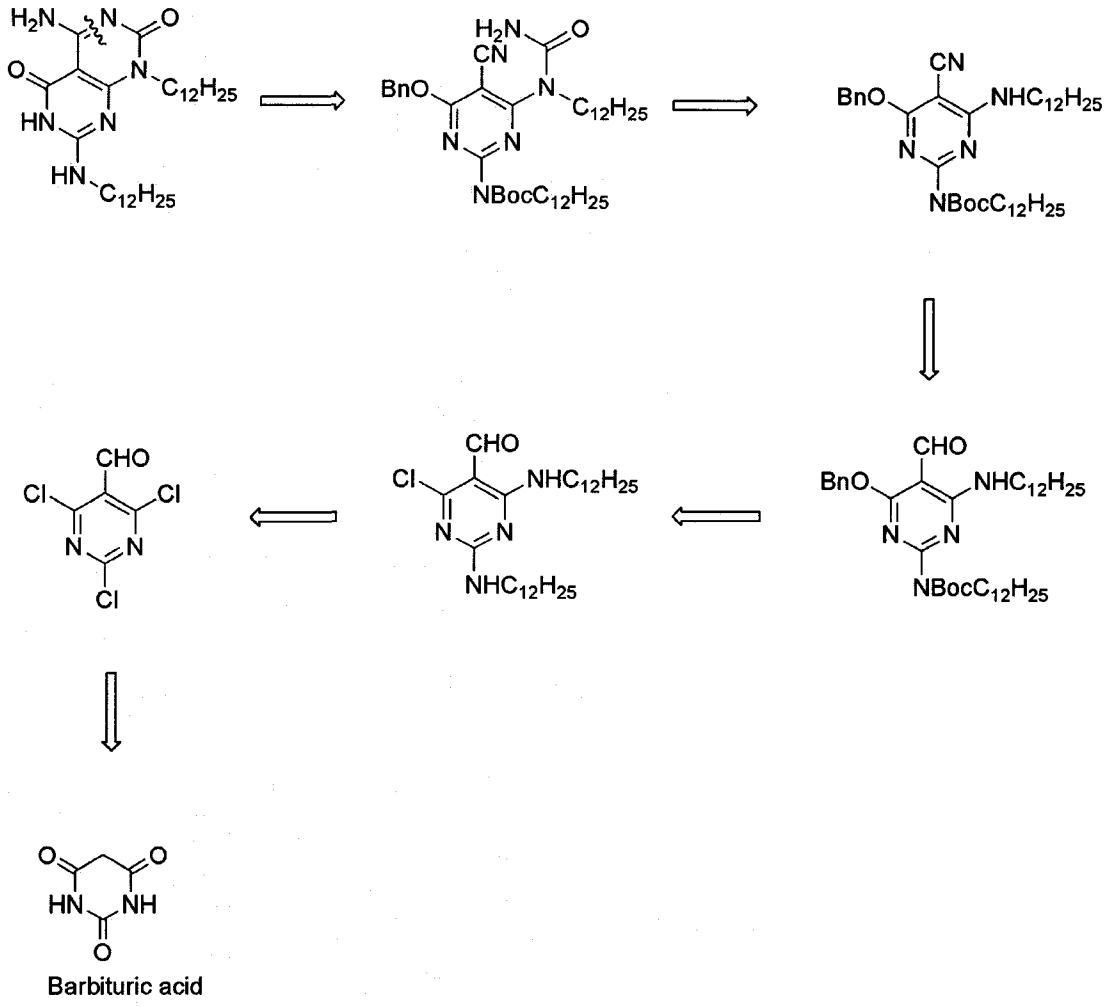

Scheme 2.1. Retrosynthesis of G^C base **7**.

The target is thought to be accessible from commercially available barbituric acid as illustrated in Scheme 2.1.[9]

2.3. Synthesis of 7: Results and Discussions

The synthesis of the amphiphilic G^C base **7** began with the reaction of the commercially available barbituric acid (**8**), with $POCl_3$ in DMF to give **9** in 55% yield (Scheme 2.2). Compound **9,** was then reacted with dodecylamine in the presence of triethylamine to give **10** in 98% yield. The last aromatic substitution on **10** with Benzylalkoxide gave **11** in 99% yield. The selective protection of the more reactive amino group of **11** with di-*tert*-butyl dicarbonate gave **12** in 98% yield. Compound **12** was then converted to oxime **13** in 95% yield by treating it with hydroxylamine in pyridine. The conversion of the oxime **13** to nitrile **14** did not go as smoothly as anticipated. Treatment of **13** with TFAA gave mixture of side products in addition to the desired product (Scheme 2.3). The separation of **14** from the side products by recrystallization and/or flash chromatography was unsuccessful. The product mixture was then carried on to the next step without purification, which also yielded mixture of products. It was then necessary to seek better reaction conditions that would eliminate the side products and to get an improved yield of the desired product. Thus oxime **13** was converted to nitrile **14** in 92% yield (Scheme 2.4) by reacting with 2,4,6-trichloro[1,3,5]triazine (TCT).[10] No side products were detected.[11] The slow addition of freshly distilled N-(chlorocarbonyl) isocyanate to a solution of **14** at $0^{o}C$ gave **15** in 94% yield. The treatment of **15** with NH_3 in methanol followed by deprotection of the resulting **16**, with HCl in dioxane gave **7** in 100% yield. The amphiphilic G^C base **7** was synthesized in 9 steps in 43% overall yield without column chromatography. The synthesis was thus optimized without any side-products

and the intermediate compounds and the final product were purified by either recrystallization or reprecipitation.

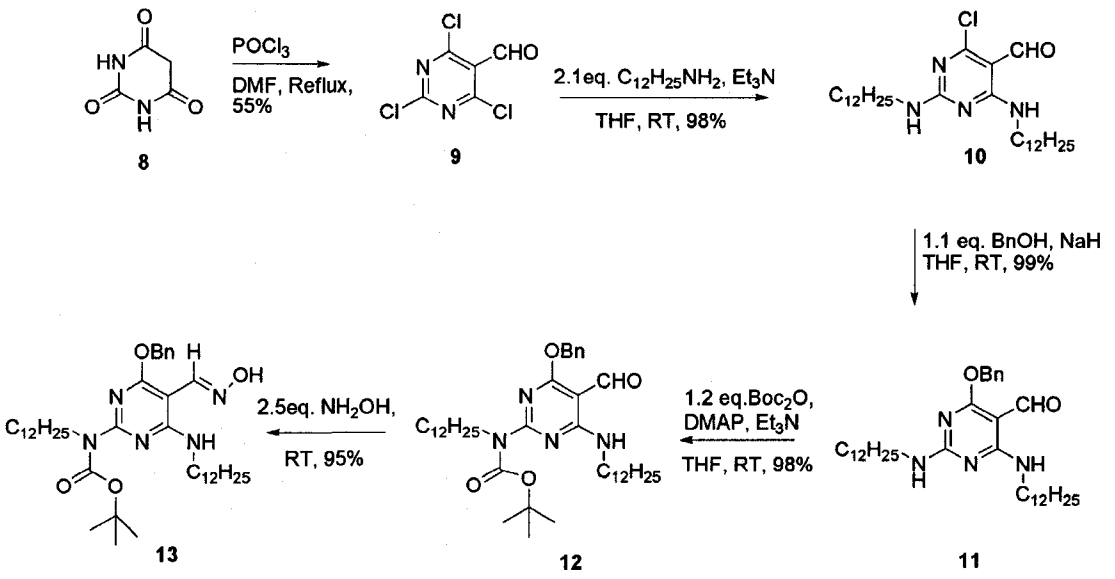

Scheme 2.2. Synthesis of oxime, **13**.

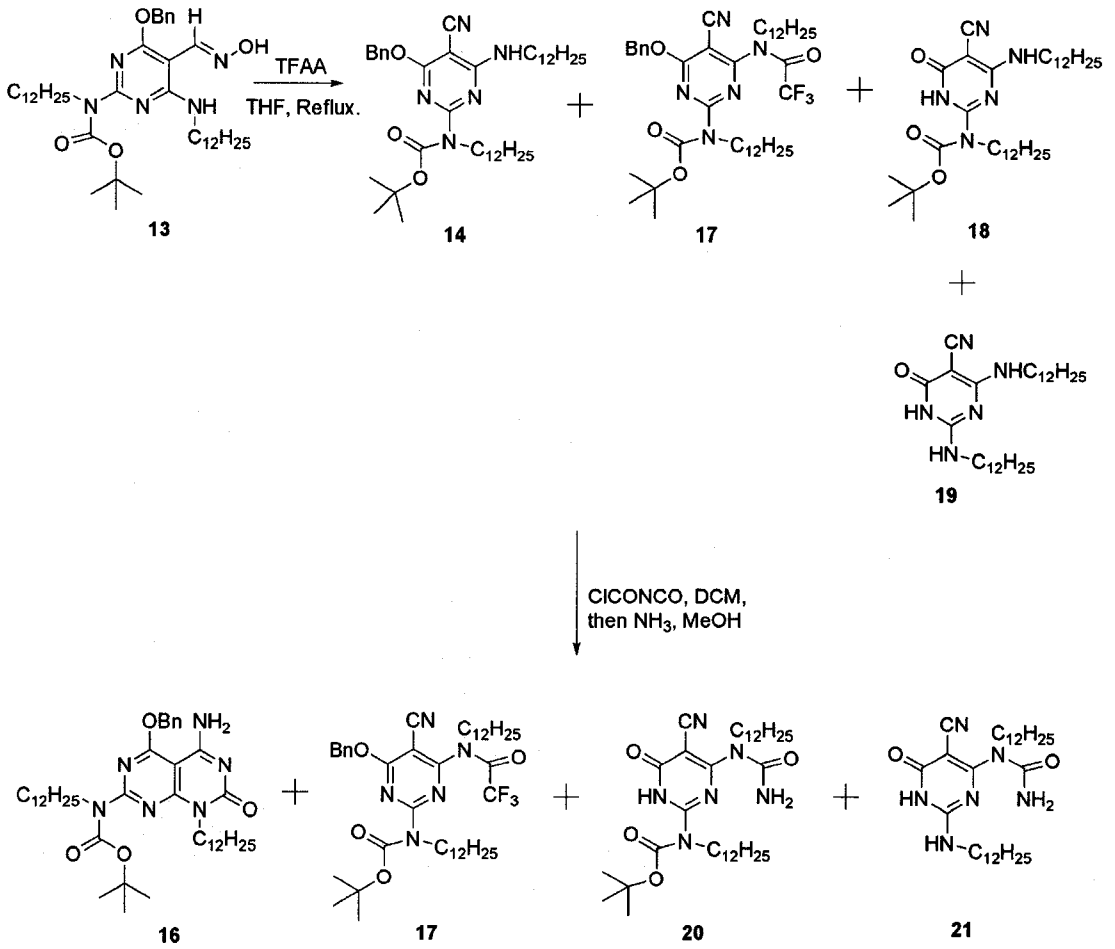

Scheme 2.3. Reaction of **13** with trifluoroacetic anhydride followed by N-(chlorocarbonyl) isocyanate.

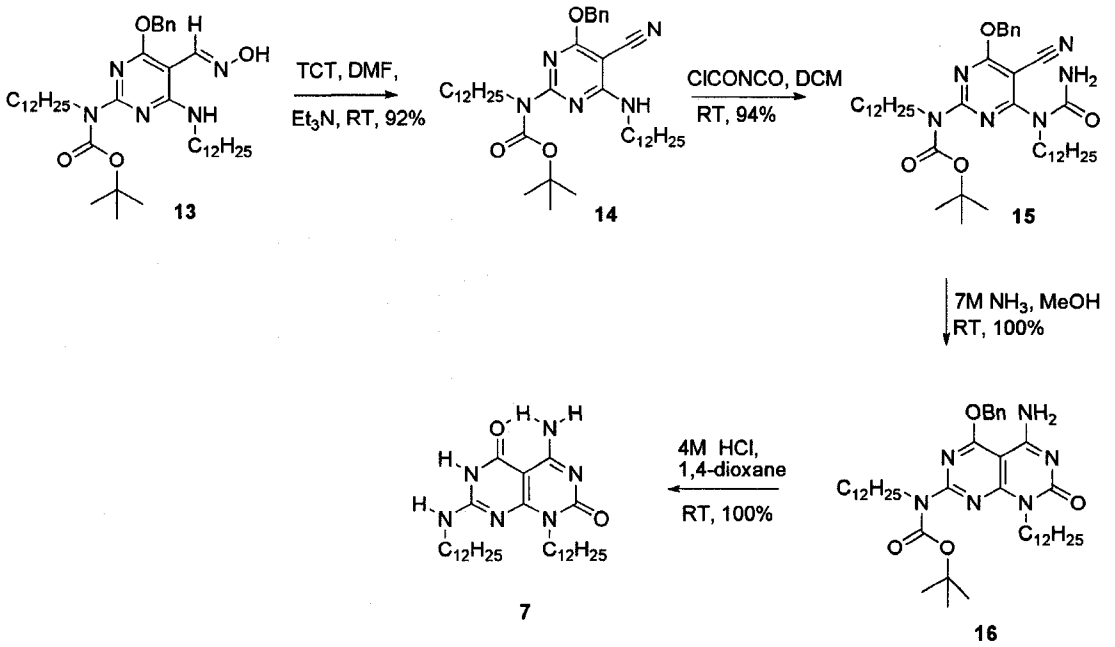

Scheme 2.4. Optimized synthesis of G^C base **7** from **13**.

2.4. Self-Assembly and Microscopy Studies of G^C base **7**

Compound **7**, was self-assembled in hexane and methanol and then characterized by TM-AFM, SEM, and DLS. Compound **7**, was soluble in hexane up to ca. 0.5 mg/mL. This concentration enabled us to self-assemble **7** into RNT in this apolar organic solvent. Tapping mode atomic force microscopy (TM-AFM) of a sample of this solution showed thick multi-layers of RNTs, from which it was difficult to resolve individual RNTs. The concentration was then reduced by half in order to get well dispersed individual RNTs. Drop casting on mica of a 0.25 mg/mL solution of **7** after an hour of self-assembly on mica resulted in networks of RNTs (Figure 2.3 and 2.4). The average height of a single RNT was measured to be 3.5 ± 0.3 nm.

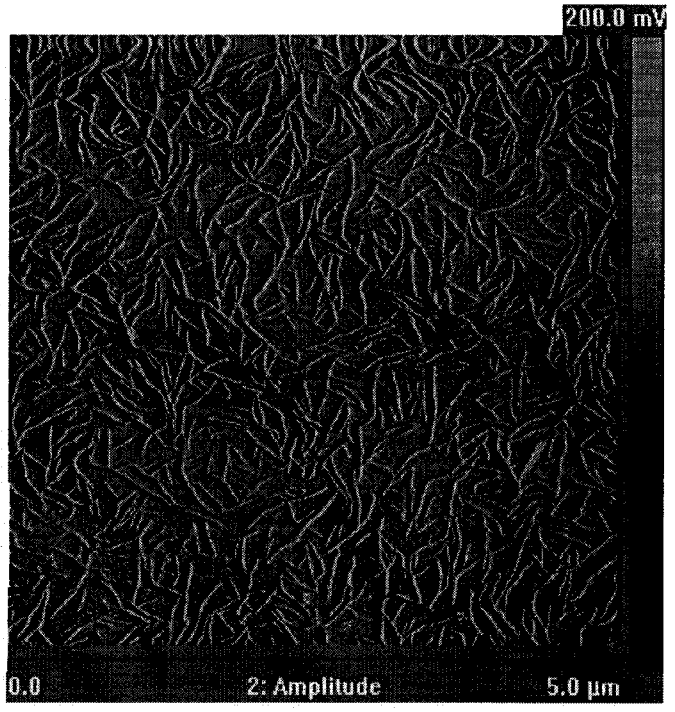

Figure 2.3. Amplitude image showing RNTs obtained by TM-AFM of G^C base **7** (0.25 mg/mL, 1 hour) cast from hexane on mica.

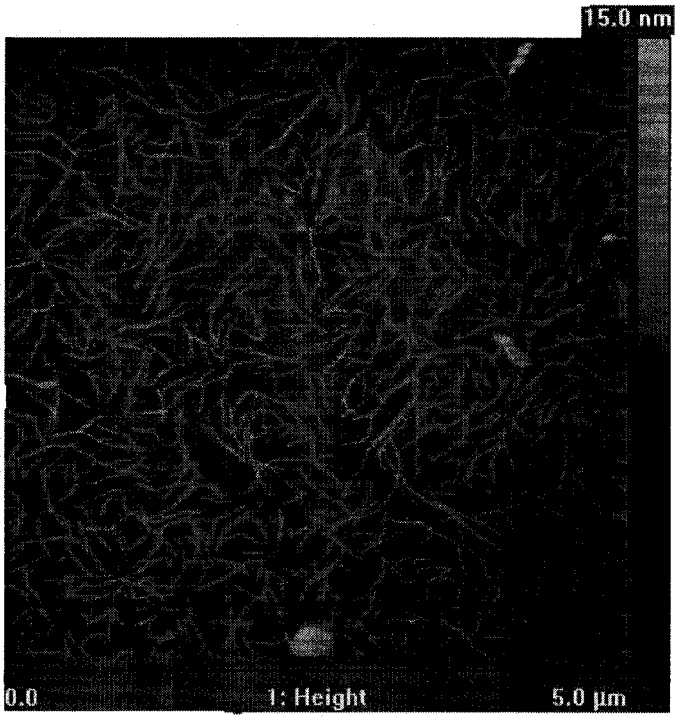

Figure 2.4. Height image showing RNTs obtained by TM-AFM of G^C base **7** (0.25 mg/mL, 1 hour) cast from hexane on mica.

TM-AFM imaging of drop-cast solution (0.25 mg/mL to 0.5 mg/mL) of Compound **7**, in methanol on mica shows no sign of RNTs (Figure 2.5).

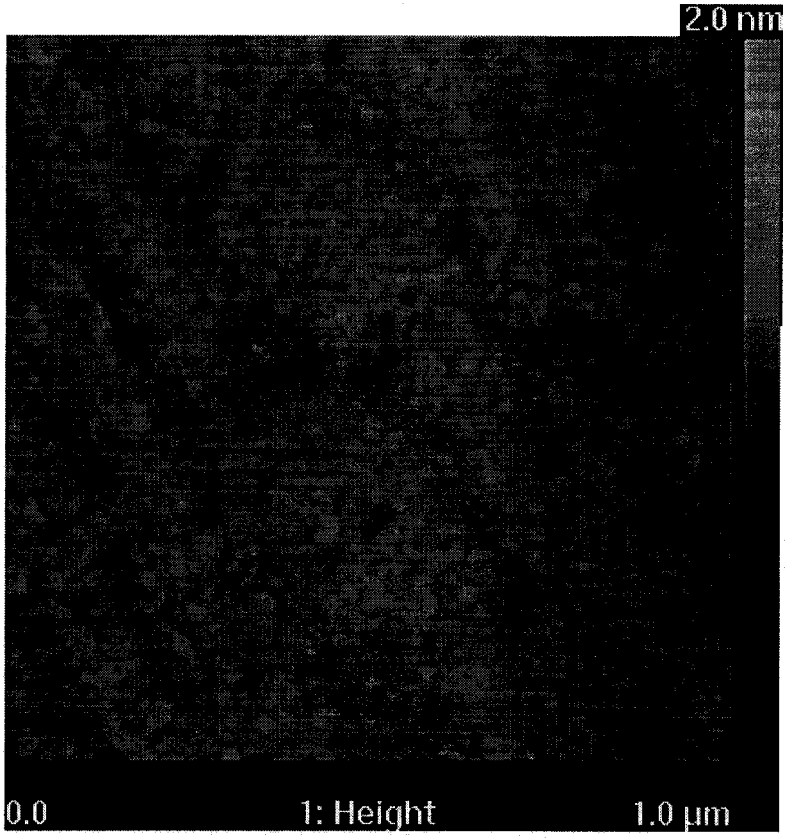

Figure 2.5. Height image showing no RNTs obtained by TM-AFM of G^C base **7** (0.25 mg/mL, 24 hour) cast from methanol on mica.

Scanning electron microscopy imaging of 0.25 mg/mL solution of G^C base **7** drop-cast from hexane on carbon coated grid after 24 hours of preparation also showed RNTs (Figure 2.6).

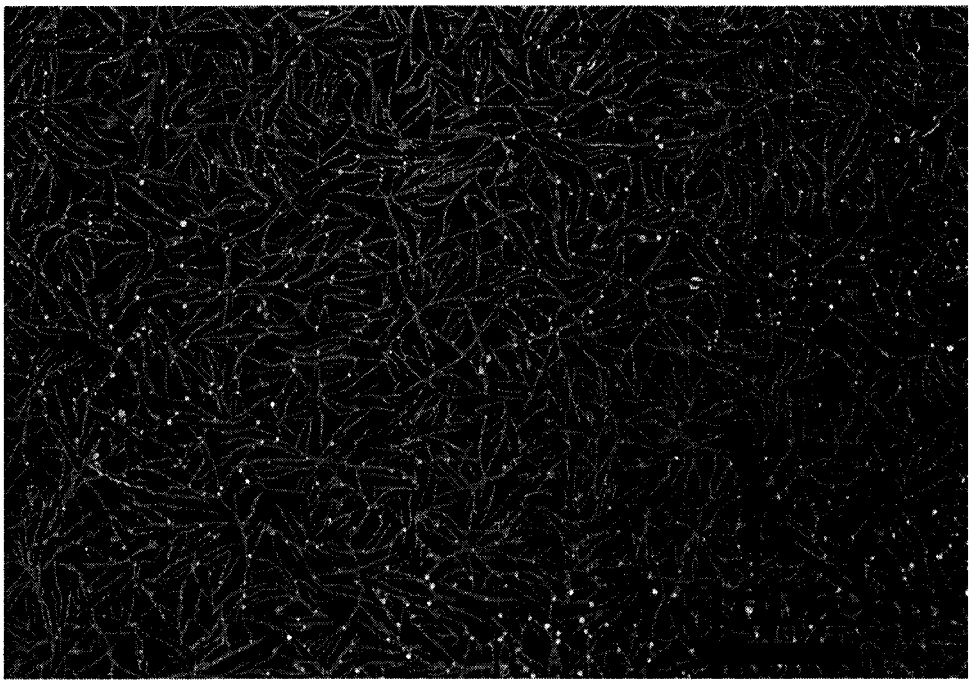

Figure 2.6. SEM image showing RNTs obtained from G^C base **7** (0.25mg/mL, 24 hours) cast from hexane on carbon coated grid.

Similar to the TM-AFM results, SEM imaging of Compound **7** in methanol shows no RNTs in this solvent (Figure 2.7).

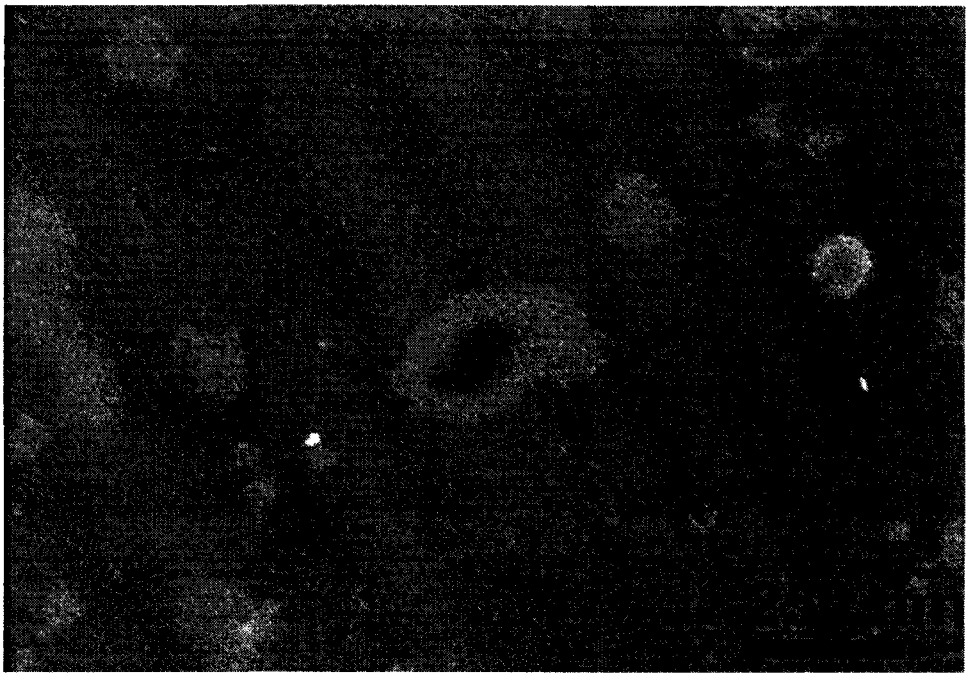

Figure 2.7. SEM image showing no RNTs obtained from G^C base **7** (0.25mg/mL, 24 hours) cast from methanol on carbon coated grid.

The results obtained from TM-AFM and SEM imaging of solutions of Compound **7** in hexane and methanol are consistent with the molecular modeling, which supports the preferential formation of RNT in an apolar solvent. Finally, to support the microscopy experiments, dynamic light scattering (DLS) experiments were carried out on 0.25 mg/mL solution of Compound **7** in hexane and methanol. The DLS experiments showed the formation of relatively large aggregates with a broad distribution centered around 700 nm in hexane and the presence of particles ~1-2 nm in methanol (Figure 2.8). This result supports the presence of RNTs only in hexane.

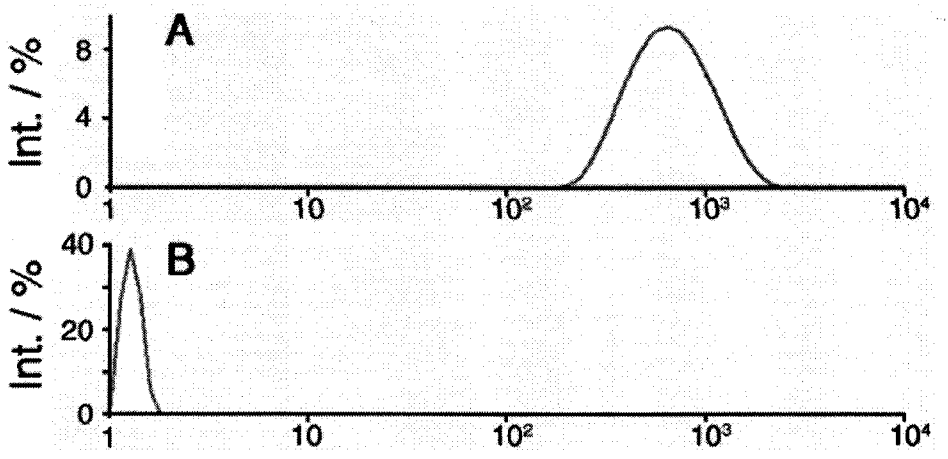

Figure 2.8. Dynamic light scattering (DLS) regularization diagram showing the hydrodynamic diameter (D_H) for G^C base **7** (0.25 mg/mL) *versus* scattering intensity in hexane (A) and methanol (B). The polydispersity indices are 1.000, and 0.017, respectively.

All freshly prepared samples were hot filtered through 0.2 μm nonsterile PVFD membranes (Whatman filters) prior to measurement. The fact that the aggregates after filtration are larger than the membrane pores used is the result of RNTs self-assembly or growth after the filtration. Blank experiments with only a solvent filtered through membrane showed no DLS signal.

2.5. Molecular Modeling and Solvation Free Energy

To investigate the thermodynamic stability of the RNT in apolar and polar solvents, we generated molecular models of 11 possible conformations of RNT of **7** in hexane and methanol, respectively and their free energy trajectories were estimated (Figure 2.9 - 2.11). It was observed that the stability of the RNT is dominated by solvent. Our theory predicted that RNT formed in hexane have the most stable conformation in which almost all the carbons of the alkyl chains are on the same plane as in **7** (Figure 2.2). It also shows that RNT conformers identified have a positive free energy of formation in methanol, thus unstable. Since the internal energy of RNT is the same in both solvents, the difference in stability came from the solvation free energy. The lower the solvation free energy of a RNT, the more stable it is, and the more surrounded is the RNT by solvent molecules and thus isolated from other RNTs in solution. Conversely, RNTs with higher solvation free energy are repelled by the solvent, and therefore prefer to stick with each other to reduce the solvent accessible surface area and hence the penalty in the solvation free energy (solvophobic attraction).

In hexane, the alkyl chains were well solvated whereas the base was not because of its relative polar character. Hence in this solvent, the rosette formation and stacking interactions are driven by polar and stacking interactions between bases and to a smaller extent via inter-chain van der Waals interactions on the periphery of the RNTs.

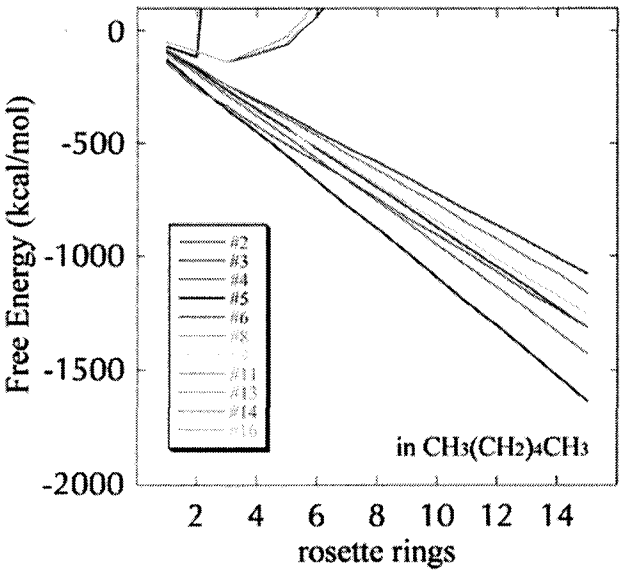

Figure 2.9. Negative free energy trajectories of 11 RNT conformers in hexane.

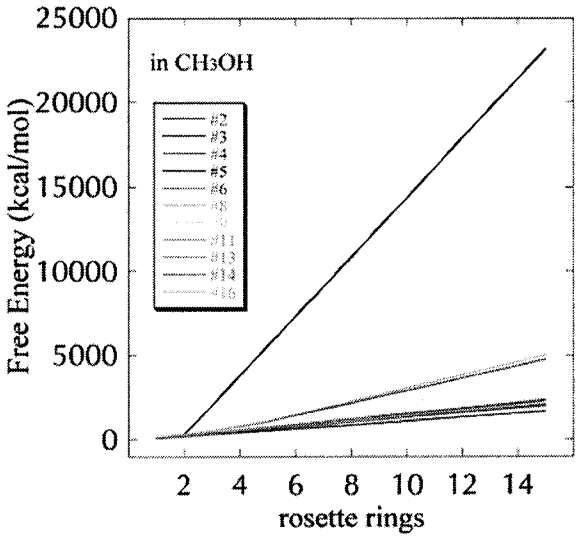

Figure 2.10. Positive free energy trajectories of 11 RNT conformers in methanol.

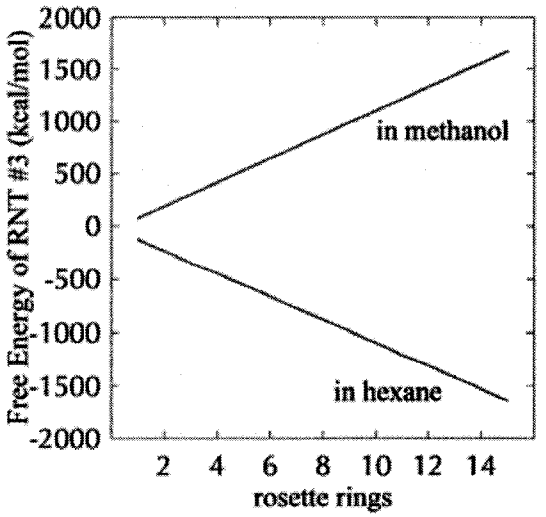

Figure 2.11. Free energy trajectories of RNT conformer number 3 in the both solvents.

2.6. Conclusion

The need to create supramolecular tubular architectures for selective separation of liquids and substrates based on their polarity difference have prompted us to design and synthesize the amphiphilic G^C base derivative **7**.

The synthesis of **7** was optimized. We have also demonstrated in this Chapter that the self-assembly of the motif is solvent-dependent. Based on theoretical and experimental results we have shown that **7** formed RNTs in apolar solvent, whereas there is no indication of RNT formation in polar solvent.

2.7. Experimental Section

2.7.1 Physical Studies

1. DLS measurements. Dynamic Light Scattering (DLS) experiments were performed on a Malvern Zetasizer Nano S working at a 90° scattering angle at 25°C. The instrument is equipped with a 40 mW He–Ne laser (λ = 633 nm) and an avalanche photodiode detector. Size distributions were calculated using an inverse Laplace transform algorithm, and the hydrodynamic radii were calculated using the Stokes–Einstein equation.

2. AFM imaging. RNT samples were prepared by dissolving **7** in methanol, or hexane, sonicating, heating to the boiling point, and then allowing the solution to age for 1 hour at room temperature. Samples for AFM imaging were prepared in a Class 10000 Clean Room spin coating 25 μL (Cookson G3-8 Desk-Top Precision Spin Coating System) on 10×10 mm^2 freshly peeled Mica grade V-4 (SPI supplies) substrates. AFM measurements were performed in tapping mode (TM–AFM) at a scan rate of 2 Hz per line using a Digital Instruments/Veeco Instruments MultiMode Nanoscope IV equipped with an E scanner. Silicon cantilevers (MikroMasch USA, Inc.) with spring constants of 40 N/m were used.

3. SEM imaging. Samples for scanning electron microscopy (SEM) were prepared by placing a carbon–coated 400–mesh copper grid on a droplet of RNT (**7**) (0.25 g/L) for 5 s. The grid was then blotted and air–dried prior to imaging.

4. Theory and Modeling. To investigate the thermodynamically stable RNT conformation, we performed a conformational search in hexane, and methanol according to the following algorithm:

Step 1. Conformational Search. Compound **7** was generated and minimized in vacuum phase using Macromodel 8.5 with the OPLS-AA force field.[12] This force field has been successfully applied to the Guanine-Cytosine base pair which is close to our compound.[13] 16 conformations were generated by varying the dihedral angles around two bonds in the alkyl chains (Figure 2.12). All other bonds in the alkyl chains were set to the trans conformation in this step, but were optimized in Step 3.

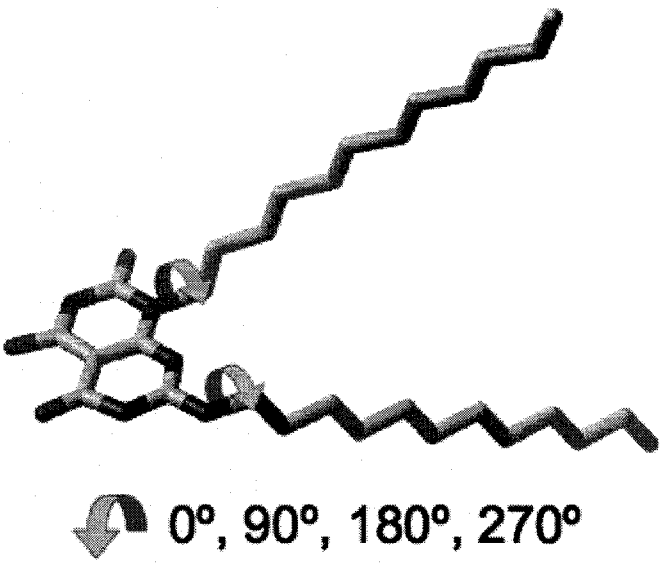

Figure 2.12. Conformers of a single motif were generated by varying the dihedral angles around two bonds as indicated by the curved arrows.

Step 2. Formation of RNTs. Each of the 16 conformers was multiplied and arranged to form a six-fold symmetry rosette maintained by 18 H-bonds. The rosettes were then stacked in a tubular fashion with an inter-plane distance of 4.5Å, and a rotation angle of 30° per rosette along the main axis. This arrangement was based on previous work done on similar systems.[14] Due to steric constraints, 11 out of 16 conformers could be assembled into RNTs.

Step 3. Geometry Optimization. Molecular models of the RNTs were generated using Macromodel 8.5. The OPLS-AA force field was employed to describe the energetics of the tube. The energy minimization in vacuum phase was applied to 11 RNTs consisting each of 15 rosette rings, with the top 3 and bottom 3 rosettes as well as all the G∧C bases fixed to reduce the end effects. After optimization, the central rosette in each of the 11 RNTs was taken to finally construct RNTs composed of N = 1–15 rosette.

Step 4. Solvation Free Energy. To obtain the thermodynamics of RNTs in liquid hexane, we employed the three-dimensional reference interaction site model (3D–RISM) integral equation theory of solvation, complemented with the Kovalenko–Hirata (KH) closure approximation.[15] The 3D–RISM/KH theory explicitly and properly accounts for the chemical specificity of RNTs as well as solvent molecules. This theoretical approach provides a detailed microscopic insight into solvation both inside and outside the RNTs and its role in nanotube formation.[16]

The 3D-RISM equation is written as

$$h_\gamma(\mathbf{r}) = \sum_\alpha \int d\mathbf{r}\, c_\alpha(\mathbf{r}-\mathbf{r}')\, \chi_{\alpha\gamma}(r') \tag{1}$$

Where $h_\gamma(\mathbf{r})$ and $c_\gamma(\mathbf{r})$ are, respectively, the 3D total and direct correlation function of solvent site γ around the solute, and $\chi_{\alpha\gamma}(r)$ is the site-site susceptibility of pure solvent. The other relation between 3D total and direct correlation function we employed to complement the 3D-RISM integral equation is the 3D-KH closure:

$$\begin{aligned} g_\gamma(\mathbf{r}) &= \begin{cases} \exp(d_\gamma(\mathbf{r})) & \text{for } d_\gamma(\mathbf{r}) \le 0 \\ 1 + d_\gamma(\mathbf{r}) & \text{for } d_\gamma(\mathbf{r}) > 0 \end{cases} \\ d_\gamma(\mathbf{r}) &= -\frac{u_\gamma(\mathbf{r})}{k_B T} + h_\gamma(\mathbf{r}) - c_\gamma(\mathbf{r}) \end{aligned} \tag{2}$$

Where $u_\gamma(\mathbf{r})$ is the 3D intermolecular interaction potential between the whole solute supramolecule and site γ of solvent molecules which is specified by the molecular force field, and $k_B T$ is the Boltzmann constant times the solution temperature.

The susceptibility of pure solvent can be decomposed into the intra- and intermolecular terms,

$$\chi_{\alpha\gamma}(r) = w_{\alpha\gamma}(r) + \rho h_{\alpha\gamma}(r) \tag{3}$$

Where, $w_{\alpha\gamma}(r)$ is site-site intramolecular correlation function specifying the geometry of solvent molecules, $h_{\alpha\gamma}(r)$ is site-site total correlation function, and ρ is the number density of solvent. The total correlation function of bulk solvent $h_{\alpha\gamma}(r)$ is obtained from RISM theory in advance to the 3D-RISM calculation, and we employed the RISM/KH theory to obtain $h_{\alpha\gamma}(r)$ in this study.

The solvation free energy of a supramolecule immersed in solution, obtained from the 3D-RISM/KH theory is given by the closed analytical expression,

$$\mu_{\text{solv}} = k_B T\rho \int d\mathbf{r}\left[\frac{1}{2}h_\gamma^2(\mathbf{r})\Theta(-h_\gamma(\mathbf{r})) - c_\gamma(\mathbf{r}) - \frac{1}{2}h_\gamma(\mathbf{r})c_\gamma(\mathbf{r})\right] \tag{4}$$

where $\Theta(x)$ is the Heaviside step function,

$$\Theta(x) = \begin{cases} 1 & \text{for } x \geq 0 \\ 0 & \text{for } x < 0 \end{cases} . \tag{5}$$

The 3D-RISM/KH theory was applied to 11 RNT conformers each composed of N rosettes (N = 1–15) in liquid hexane, and methanol. The OPLS–AA model was used for RNTs, and the OPLS–UA model was used for hexane[17] and methanol[18] solvent molecules. The force field parameter proposed by Dietz *et al.* was used for the chloroform solvent molecule.[19] The density of liquid hexane, methanol, and chloroform were 0.655 and 0.787 g/cm^3, respectively, and the temperature was set to 25 °C. The free energy of a given RNT conformer was obtained as a sum of internal energy of RNTs obtained by Macromodel 8.5 and its solvation free energy given by the 3D-RISM/KH theory. Figures 2.4–2.6 present the trajectories of the total free energy in the two solvents, and show that RNT number 3 in which almost all carbons of the alkyl chains are in the same plane as the G^C base (Figure 2.2) is the most stable in each of the two liquids examined (Figure 2.6). Our theory predicts that the relative stability of RNT conformer number 3 in hexane > in methanol.

2.7.2. Synthetic Procedures

Melting points were recorded on a Büchi capillary melting point apparatus (model B–545). ^{1}H and ^{13}C–NMR spectra were recorded on Varian Inova NMR spectrometers (400 to 600 MHz) with the solvent as internal reference. The NMR data is presented as follows: chemical shift, peak assignment, multiplicity, coupling constant, integration. Mass spectrometric analysis was performed by positive mode electrospray ionization on either a Micromass ZabSpec Hybride Sector-TOF or a PerSeptive Biosystems Mariner Biospectrometry Workstation (Mass Spectrometry Laboratory at the Department of Chemistry, University of Alberta). A suitable liquid carrier solution was infused into the electrospray source by means of syringe pump at a flow rate of 15 μL/min. A small amount of the sample, enough to produce a concentration in the low mg/μL range was dissolved in the same solution and introduced via a 1 or 2 μL-loop-injector. Prepurified nitrogen was used as a spray pneumatic aid and bath gas.

All the reagents and solvents are commercially available from Aldrich, Fluka, or Fisher Scientific, and were used without further purification. Reagent grade CH_2Cl_2, THF, and CH_3OH were purified on an MBraun solvent purification system. Silica–coated TLC plates (Merck F 60254) were used for monitoring reaction progress and visualizations were made under UV light.

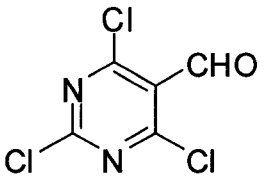

9

Synthesis of **9**.

Dimethylformamide (21.4 mL, 280 mmol) was added to $POCl_3$ (219 mL) and stirred under N_2. After the initial warmth had subsided, barbituric acid **8**, (35.0 g, 280 mmol) was added in one portion. The resulting suspension was heated refluxed for 19 h after which the mixture was cooled to ambient temperature. Excess $POCl_3$ was recovered from the reaction vessel by direct distillation under reduced pressure (105 mbar, heated water bath) and the resulting solid was carefully hydrolyzed through addition of crushed ice (~ 1 kg) and DCM, accompanied by mechanical rendering with a spatula. Extraction of the mixture with DCM (4 × 400 mL) and filtered through celite/cotton. The extract was washed with H_2O (3 × 300 mL), saturated aq. $NaHCO_3$ solution (2 × 50 mL), then saturated brine (200 mL), drying (Na_2SO_4) and finally solvent removal by rotary solvent evaporation gave a yellow solid. Hot filtration from acetone and recrystallization from the same medium gave **3** (31.9 g, 55.0% yield) of the product in two crops of pale yellow prisms.

R_f 0.43 (10% EtOAc/hexanes); mp 129-130°C; ^{1}H NMR (400 MHz, $CDCl_3$) δ 10.4 (s, 1H); ^{13}C NMR (100 MHz, $CDCl_3$) δ 185.06, 164.50, 123.44.

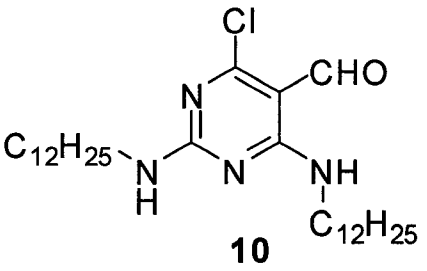

10

Synthesis of **10**.

Dodecylamine (23.2 g, 125 mmol), followed by Et_3N (16.8 mL, 121 mmol) were added at r.t. to a stirred solution of 2,4,6-trichloro-pyrimidine-5-carbaldehyde **9** (12.7 g, 60 mmol) in THF (200 mL) under N_2 atmosphere. The reaction mixture was refluxed for 18 h. The mixture was then cooled in an ice/water bath and acidified by addition of HCl solution (1.0 M, 20 mL). After the separation of the organic layer, followed by its dilution with dH_2O (300 mL), a solid precipitated. Removal of the preceding material by gravity filtration and copiously washing with water followed by drying in vacuum over P_4O_{10} afforded the crude product. Dissolution of the crude material in $CHCl_3$ to give a saturated solution, and subsequent re-precipitation by addition of CH_3OH afforded **10** (30.0 g, 98% yield). R_f 0.44 (15% EtOAc / 85% hexanes); mp 93-95°C; ^{1}H NMR (400 MHz, $CDCl_3$) δ 10.03 (s, 1H), 9.30 (br s, 1H), 5.56 (br s, 1H), 3.51 (q, J = 7.2 Hz, 2H), 3.42 (q, J = 7.2 Hz, 2H), 1.61 (m, 4H), 1.32–1.25 (m, 36H), 0.88 (t, J = 6.8 Hz, 6H); ^{13}C NMR (100 MHz, $CDCl_3$) δ 188.44, 165.72, 162.40, 160.93, 101.81, 41.57, 40.71, 31.96, 29.67, 29.64, 29.61, 29.39, 29.35, 29.28, 27.08, 26.92, 22.72, 14.14; FTIR (microscopic) 3254, 3111, 2954, 2915, 2915, 2847, 1649, 1596, 1566 cm^{-1}; HRMS (ESI) for $C_{29}H_{54}ClN_4O$ ($M+H^+$) calcd 509.3980, found 509.3981. Anal. Calcd for $C_{29}H_{53}ClN_4O$: C, 68.51; H, 10.53; N, 11.02. Found: C, 68.81; H, 10.25; N, 10.91.

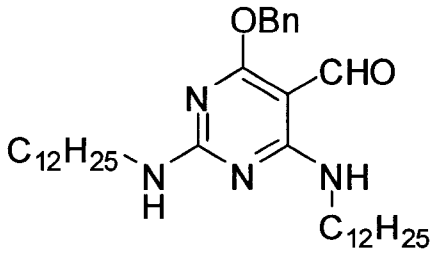

11

Synthesis of **11**.

Benzyl alcohol (1.8 ml, 18 mmol) was added to a stirred suspension of NaH (0.84 g, 35 mmol) in THF (10 ml) at r.t. under N_2 atmosphere. After 15 minutes the solution was cooled to 0°C, then a solution of **10** (7.9 g, 16 mmol) in THF (100 mL) was added. The mixture was allowed to come to r.t. then it was refluxed for 20 h. After cooling, the mixture to 0°C, the solvent was removed under reduced pressure (rotovap), and the residual solid was dissolved in Et_2O, washed with distilled H_2O (3 × 100 mL) and saturated brine (50 mL) and dried over anhydrous Na_2SO_4. The solvent was evaporated under reduced pressure (rotovap). Dissolution of the crude material in EtOAc to give a saturated solution, and subsequent precipitation by addition of CH_3OH afforded **11** (8.9 g, 99% yield). R_f 0.45 (6% MeCN / 84% PhMe); mp 92-94°C; ^{1}H NMR (400 MHz, DMSO-d_6) δ 9.82 (s, 1H), 9.03 (br s, 1H), 7.45–7.28 (m, 5H), 7.26 (br s, 1H), 5.39 (s, 1H), 3.41 (m, 2H), 3.28 (q, J = 6.4, 2H), 1.52 (m, 4H), 1.30–1.20 (m, 36H), 0.95 (t, J = 6 Hz, 6H); ^{13}C NMR (100 MHz, $CDCl_3$ δ 186.03, 185.84, 172.05, 171.57, 163.55, 162.39, 136.79, 128.51, 127.98, 127.71, 92.83, 67.38, 41.47, 40.47, 31.97, 29.69, 29.44, 29.40, 27.05, 22.73, 14.14; FTIR (microscopic) 3331, 3258, 2953, 2912, 2847, 1631, 1593, 1576, 1539, 1518, 1208,

1111 cm^{-1}; HRMS (ESI) for $C_{36}H_{61}N_4O_2$ ($M+H^+$) calcd 581.4789 found 581.47912. Anal. Calcd for $C_{36}H_{60}N_4O_2$: C, 74.48; H, 10.44; N, 9.65. Found: C, 74.08; H, 10.26; N, 9.49.

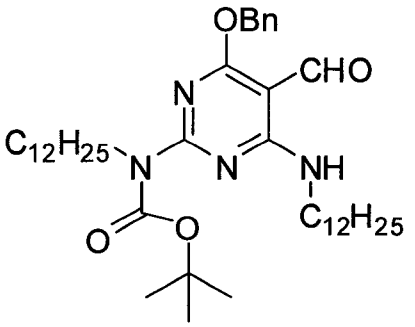

12

Synthesis of **12**.

To a stirred solution of **11** (7.10 g, 12.2 mmol) and DMAP (0.74 g, 6.1 mmol) in THF (100 mL), Et_3N (3.00 mL, 21.5 mmol) was added at room temperature under N_2 atmosphere. After stirring for 5 min, Boc_2O (3.3 g, 15 mmol) was added, and the mixture was stirred at room temperature for 24 h. The reaction was quenched with distilled H_2O (10 mL) followed by the removal of the solvent under reduced pressure (rotovap). The residual solid was dissolved in EtOAc (200 mL) and washed with distilled H_2O (3 × 50 mL), 5% aq. $NaHCO_3$ (2 × 50 mL) and saturated brine (50 mL). After drying over anhydrous Na_2SO_4, the solvent was evaporated under reduced pressure (rotovap). Dissolution of the crude material in EtOAc to give a saturated solution, and subsequent precipitation by addition of CH_3OH afforded 8.2 g (98% yield) of **12** as a white microcrystalline solid. R_f 0.67 (15% EtOAc / 85% Hex); mp 37-39°C; ^1H NMR (400 MHz, $CDCl_3$) δ 10.11 (s, 1H), 9.28 (t, J = 5.6 Hz, 1H), 7.43–

7.32 (m, 5H), 5.46 (s, 2H), 3.87 (m, 2H), 3.49 (q, J = 5.6, 2H), 1.70-1.58 (m, 4H), 1.55 (s, 9H), 1.34–1.22 (m, 36H), 0.95 (t, J = 6.8 Hz, 6H); ^{13}C NMR (100 MHz, $CDCl_3$) δ 187.55, 171.53, 162.87, 161.72, 153.79, 136.48, 128.57, 128.18, 128.01, 94.25, 81.67, 68.14, 47.84, 40.85, 31.97, 29.74, 29.10, 29.69, 29.67, 29.65, 29.54, 29.44, 29.41, 28.97, 28.23, 27.12, 22.73, 14.15; FTIR (microscopic technique) 3292, 3090, 2981, 2920, 2852, 1718, 1640, 1579, 1518, 1216, 1073 cm^{-1}; HRMS (ESI) for $C_{41}H_{69}N_4O_4$ ($M+H^+$) calcd 681.5241 found 681.5249. Anal. Calcd for $C_{41}H_{68}N_4O_4$: C, 72.36; H, 10.09; N, 8.23. Found: C, 72.39; H, 10.15; N, 8.23.

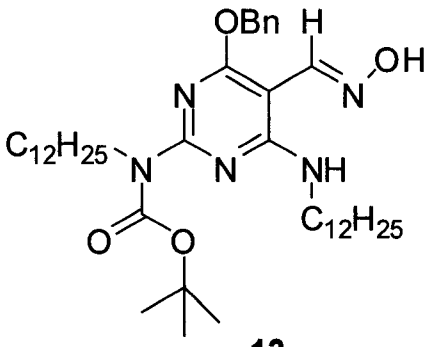

13

Synthesis of **13**.

Pyridine (120 mL) followed by $NH_2OH{\cdot}HCl$ (5.10 g, 73.4mmol) was added to a stirred solution of **12** (20.0 g, 29.4 mmol) at room temperature and stirred for 24 h. Pyridine was removed by distillation under reduced pressure. The product was then dissolved in 600 ml, 1:1 EtOAc / hexanes mixture and the solution was washed with saturated aq. $NaHCO_3$ solution followed by dH_2O and saturated brine. It was dried over anhydrous Na_2SO_4 and concentrated under reduced pressure (rotovap) to give the crude product. Re-precipitation in CH_3OH afforded **13** (19.4 g, 95% yield) as a

white solid. R_f 0.37 (15% EtOAc / 85% Hexanes); mp 54-56°C; ^{1}H NMR (400 MHz, $CDCl_3$) δ 8.55 (s, 1H), 7.85 (t, J = 6.0 Hz, 1H), 7.43–7.30 (m, 5H), 6.84 (s, 1H), 5.40 (s, 2H), 3.82 (m, 2H), 3.51 (q, J = 7.6 Hz, 2H), 1.69 - 1.58 (m, 4H), 1.53 (s, 9H), 1.34–1.24 (m, 36H), 0.89 (t, J = 7.0 Hz, 6H); ^{13}C NMR (100 MHz, $CDCl_3$) δ 167.34, 160.96, 159.23, 154.17, 146.86, 136.98, 128.49, 128.01, 127.97, 87.13, 80.89, 67.98, 47.90, 41.27, 31.98, 29.84, 29.75, 29.74, 29.71, 29.56, 29.48, 29.41, 29.03, 28.36, 27.20, 27.12, 22.74, 14.15; FTIR (microscopic technique) 3311, 3034, 2953, 2910, 2848, 1697, 1567, 1524, 1500, 1206, 1078 cm^{-1}; HRMS (ESI) for $C_{41}H_{70}N_5O_4$ ($M+H^+$) calcd 695.5422 found 695.5426. Anal. Calcd for $C_{41}H_{69}N_5O_4$: C, 70.89; H, 10.03; N, 10.09. Found: C, 70.91; H, 10.25; N, 10.33.

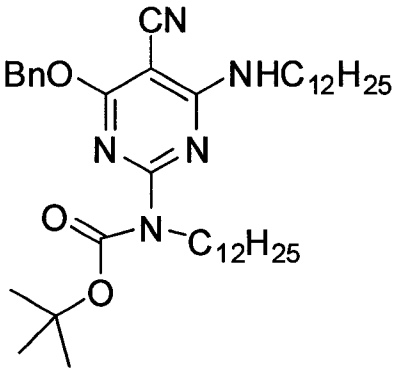

14

Synthesis of **14**.

2,4,6-trichloro[1,3,5]triazine (0.27g, 1.44mmol) was added to DMF (1.5 mL), maintained at 25°C. After the formation of a white solid, the reaction was monitored by TLC (10 minutes) until complete disappearance of TCT. **13** (0.50g, 0.72mmol) in DMF (10 mL) was added followed quickly by adding Et_3N (2.5 mL). The yellow suspension immediately turned deep brown, and the mixture was allowed to stir at r.t.

overnight. Saturated aq. $NaHCO_3$ (5 mL) was added and the mixture was extracted with DCM (4 × 20 mL). The combined organic fractions were washed with H_20 (15 mL), brine (20 mL) then dried over Na_2SO_4. The solvent was evaporated and the resulting crude product was precipitated in hot methanol to give **14** (0.45 g, 92% yield) as white solid. R_f 0.72 (15% EtOAc / 85% Hexanes); mp 77°C; ^1H NMR (400 MHz, $CDCl_3$) δ 7.45–7.28 (m, 5H), 5.46 (s, 2H), 5.35 (t, J = 4 Hz, 1H), 3.84 (m, 2H), 3.49 (q, J = 7.2 Hz, 1H), 1.70–1.58 (m, 4H), 1.54 (s, 9H), 1.36–1.24 (m, 36H), 0.89 (t, J = 7.2 Hz, 6H); ^{13}C NMR (100 MHz, $CDCl_3$) δ 170.29, 164.19, 160.65, 153.44, 136.04, 128.47, 128.11, 127.88, 115.08, 81.73, 68.67, 68.25, 47.81, 41.55, 31.81, 29.58, 29.55, 29.53, 29.50, 29.47, 29.40, 29.25, 28.78, 28.06, 26.92, 26.79, 22.58, 13.99; FTIR (microscopic) 3303, 3176, 2915, 2849, 2221, 1751, 11706, 1610, 1587, 1214, 1125 cm^{-1}. HRMS (ESI) for $C_{41}H_{68}N_5O_3$ ($M+H^+$) calcd. 678.5322 found 678.5329. Anal. Calcd. for $C_{41}H_{67}N_5O_3$: C, 72.68; H, 9.99; N, 10.34. Found: C, 72.65; H, 9.96; N, 10.21.

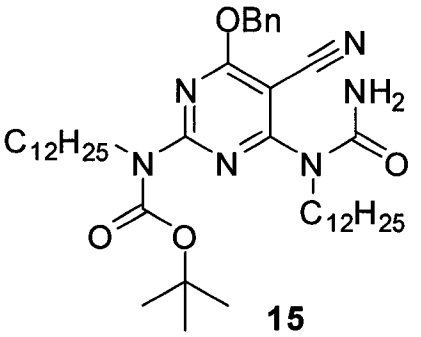

15

Synthesis of **15**.

To a solution of **14** (2.8 g, 4.1 mmol) and DIPEA (5 mL) in DCM (40 mL), N-(chlorocarbonyl) isocyanate (1.98 mL, 24.6 mmol) was added at 0°C under N_2 atmosphere. After stirring for 1 h at 0°C, the mixture was allowed to warm to room temperature and was stirred for an additional 24 h. The reaction mixture was cooled to 0°C and quenched slowly with saturated aq. $NaHCO_3$ (20 mL). The product was extracted with CH_2Cl_2 (300 mL) and the extract was washed with distilled H_2O (3 × 50 mL), and saturated brine (100 mL) and dried over anhydrous Na_2SO_4. After evaporation of the solvent under reduced pressure (rotovap), the product was re-precipitated in CH_3OH to give **15** (2.8 g, 94% yield) as a white solid. R_f 0.68 (30% EtOAc / 70% Hexanes); mp 77-79 °C; ^{1}H NMR (400 MHz, $CDCl_3$) δ 7.44–7.32 (m, 5H), 5.51 (s, 2H), 4.19 (m, 2H), 3.89 (m, 2H), 1.73–1.58 (m, 2H), 1.54 (s, 9H), 1.30–1.24 (m, 36H), 0.98-0.86 (m, 6H); ^{13}C NMR (100 MHz, $CDCl_3$) δ 172.30, 163.71, 158.20, 155.30, 152.15, 135.19, 128.58, 128.28, 127.19, 113.85, 83.08, 69.41, 47.80, 46.80, 31.81, 31.79, 29.55, 29.53, 29.52, 29.50, 29.48, 29.29, 29.24, 29.22, 27.91, 26.91, 22.58, 22.57, 14.01, 13.99; FTIR (microscopic technique) 3399, 3283, 3037,

2953, 2921, 2851, 2219, 1744, 1725, 1677, 1577, 1525, 1084 cm^{-1}; HRMS (ESI) for $C_{42}H_{69}N_6O_4$ ($M+H^+$) calcd 721.5375 found 721.5371. Anal. Calcd for $C_{42}H_{68}N_6O_4$: C, 70.01; H, 9.53; N, 11.67. Found: C, 69.97; H, 9.56; N, 11.46.

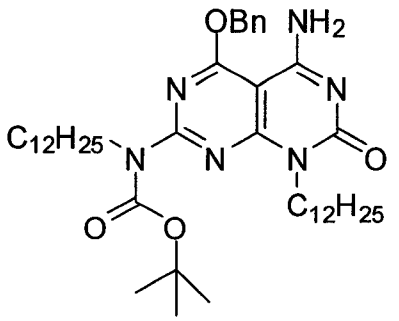

16

Synthesis of **16**.

A solution of **15** (2.00 g, 2.78 mmol) in CH_2Cl_2 (10 mL) and NH_3 in CH_3OH (7.0 N, 50 mL) was stirred under N_2 atmosphere at room temperature for 5 h. Solvents were removed under reduced pressure (rotovap) and the crude product was re-precipitated in CH_3OH to give **16** (2 g, 100% yield). R_f 0.25 (1:1 EtOAc/Hexanes); mp 158-160°C; ^1H NMR (400 MHz, $CDCl_3$) δ 7.44–7.39 (m, 5H), 6.92 (s, 1H), 6.52 (br s, 1H), 5.58 (s, 2H), 4.17 (m, 2H), 3.93 (m, 2H), 1.72-1.62 (m, 4H), 1.57 (s, 9H), 1.34–1.22 (m, 36H), 0.88 (t, J = 7.2 Hz, 6H); ^{13}C NMR (100 MHz, $CDCl_3$) δ 166.42, 160.71, 160.69, 160.68, 156.07, 153.06, 135.03, 129.00, 128.98, 128.65, 85.91,82.31, 70.07, 48.12, 42.94, 31.97, 29.74, 29.70, 29.57, 29.41, 29.40, 28.93, 28.20, 28.16, 27.24, 27.15, 22.73, 14.15; FTIR (microscopic technique) 3462, 2954, 2915, 2872, 2848, 1752, 1669, 1588, 1494, 1205, 1121 cm^{-1}; HRMS (ESI) for $C_{42}H_{69}N_6O_4$

(M+H$^+$) calcd 721.5375 found 721.5376. Anal. Calcd for $C_{42}H_{68}N_6O_4$: C, 70.10; H, 9.53; N, 11.67. Found: C, 69.53; H, 9.42; N, 11.58.

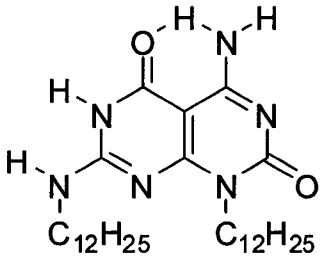

7

Synthesis of **7**.

A solution of **16** (1.10 g, 15.3 mmol) and HCl in dioxane (4.0 M, 18 mL) was refluxed for 24 h. The precipitate formed was filtered, washed with CH_3OH and dried on a filter paper to give **7** (1.1 g, 100% yield) as a white solid. ^{1}H NMR (400 MHz, DMSO-d_6, 100°C) δ 11.80 (br s, 1H), 9.08 (br s, 1H), 8.34 (br s, 1H), 8.16 (br s, 1H), 4.04 (t, J = 6 Hz, 2H), 3.43 (q, J = 5.2 Hz, 2H), 1.67-1.59 (m, 4H), 1.33-1.28 (m, 36H), 0.88 (t, J = 5.4 Hz, 6H); ^{13}C NMR (125.7 MHz, TFA-d_1) δ 165.87, 162.88, 157.83, 156.86, 151.81, 84.83, 56.52, 46.49, 44.91, 33.84, 31.51, 31.25, 30.80, 29.34, 28.73, 24.39, 14.62; FTIR (microscopic technique) 3322, 3174, 2954, 2847, 1715, 1667, 1612, 1544 cm^{-1}; HRMS (ESI) for $C_{30}H_{55}N_6O_2$ (M+H$^+$) calcd 531.4381 found 531.4383. Anal. Calcd for $C_{30}H_{55}ClN_6O_2$: C, 63.56; H, 9.79; N, 14.83. Found: C, 63.20; H, 9.63; N, 14.71.

2.8. References

1. Xiangbing, Z.; Goran, U.; Yongsong, L.; Virgil, P.; Andrea, E. D.; James, K. H. *Nature* **2004**, *428*, 157.
2. (a) Hartgerink, J. D.; Beniash, E.; Stupp, S. I. *Science* **2001**, *294*, 1684. (b) Gronwald, O.; Shinkai, S. *Chem.-Eur. J.* **2001**, *7*, 4329. (c) Shimizu, T. *Macromol. Rapid commun.* **2002**, *23*, 311. (d) Fuhrhop, J.-H.; Heifrich, W. *Chem. Rev.* **1993**, *93*, 1565. (e) Nakashima, N.; Asakuma, S.; Kunitake, T. *J. Am Chem. Soc.* **1985**, *107*, 509.
3. Curatolo, W. *Biochim. Biophys. Acta* **1987**, *906*, 111 & 137.
4. Kunitake, T.; Okahata, Y. *J. Am. Chem. Soc.* **1980**, *102*, 549.
5. (a) Antonietti, M.; Forster, S. *Adv. Mater.* **2003**, *15*, 1323. (b) Lazzari, M.; Lopez-Quintela, M. *Adv. Mater.* **2003**, *15*, 1583.
6. (a) Yu, K.; Eisenberg, A. *Macromolecules* **1998**, *31*, 3509. (b) Jenekhe, S. A.; Chen, X. L. *Science* **1999**, *283*, 372.
7. (a) Raez, J.; Manners, I.; Winnik, M. A. *J. Am. Chem. Soc.* **2002**, *124*, 10381. (b) Li, Z.-C.; Liang, Y.-Z.; Li, F.-M. *Chem. Commun.* **1999**, 1557.
8. (a) Berl, V.; Schmutz, M.; Krische, M. J.; Khoury, R. G.; Lehn, J.-M. *Chem. Eur. J.* **2002**, *8*, 1227. (b) Aizenberg, J.; Black, A. J.; Whitesides, G. M. *Nature* **1999**, *398*, 495. (c) Kuether, J.; Seshadri, R.; Knoll, W.; Tremel, W. *J. Mater. Chem.* **1998**, *8*, 641.
9. Fenniri, H.; Deng, B.-L.; Ribbe, A. E. *J. Am. Chem. Soc.* **2002**, *124*, 11064.
10. Giampaolo, G.; Luca, L. D.; Porcheddu, A. *J. Org. Chem.* **2002**, *67*, 6272.
11. Marsh, A.; Silvestri, M.; Lehn, J.-M. *Chem. Commun.* **1996**, 1527.

12. Jorgensen, W. L.; Maxwell, D. S.; Tirado–Rives, J. *J. Am. Chem. Soc.* **1996**, *118*, 11225.

13. Pranata, J.; Jorgensen, W. L. *Tetrahedron* **1991**, *41*, 2491.

14. (a) Fenniri, H.; Mathivanan, P.; Vidale, K. L.; Sherman, D. M.; Hallenga, K.; Wood, K. V.; Stowell, J. G. *J. Am. Chem. Soc.* **2001**, *123*, 3854. (b) Fenniri, H.; Deng, B.–L.; Ribbe, A. E.; Hallenga, K.; Jacob, J.; Thiyagarajan, P. *Proc. Natl. Acad. Sci. USA* **2002**, *99*, 6487. (c) Chin, D. N.; Simanek, E. E.; Li, X.; Wazeer, M. I. M.; Whitesides, G. M. *J. Org. Chem.* **1997**, *62*, 1891.

15. (a) Kovalenko, A. Three–dimensional RISM theory for molecular liquids and solid–liquid interfaces, in: *Molecular Theory of Solvation*, Hirata, F. (ed.) Series: *Understanding Chemical Reactivity*, Mezey, P.G. (ed.) Kluwer Academic Publishers, Dordrecht, **2003**, *24*, 169. (b) Kovalenko, A.; Hirata, F. *J. Chem. Phys.* **1999**, *110*, 10095. (c) Kovalenko, A.; Hirata, F. *J. Chem. Phys.* **2000**, *112*, 10391.

16. (a) Moralez, J.G.; Raez, J.; Yamazaki, T.; Motkuri, R.K.; Kovalenko, A.; Fenniri, H. *J. Am. Chem. Soc.*, **2005**, *127*, 8307. (b) Johnson, R.S.; Yamazaki, T.; Kovalenko, A.; Fenniri, H. *J. Am. Chem. Soc.*, **2007**, *129*, 5735.

17. Jorgensen, W. L.; Madura, J. D.; Swenson, C. J. *J. Am. Chem. Soc.* **1984**, *106*, 6638.

18. Jorgensen, W. L., *J. Phys. Chem.* **1986**, *90*, 1276.

19. Dietz, W.; Heinzinger, K. *Ber. Bunsenges. Phys. Chem.* **1985**, *89*, 968.

CHAPTER 3

SYNTHESIS AND HIERARCHICAL SELF-ASSEMBLY STUDIES OF SELF-COMPLEMENTARY MOTIFS

3.1. Introduction

Fenniri and co-workers have designed different hexameric RNTs with predefined dimensions.[1] Lehn's G^C base had been modified with different functionalities and their self-assembly have resulted in different arrays of RNTs as reported by Fenniri and co-workers (Figure 3.1).[1,2]

At the same time that Lehn and co-workers reported the synthesis of the G^C base moiety, Mascal and co-workers reported a shorter synthetic route for synthesizing similar G^C bases.[3] Their short synthetic route resulted in the replacement of the non-bonding N-atom in the G-ring of Lehn's G^C base with a sp^2 C-atom (Figure 3.1). They obtained X-ray structure of the self-complementary G^C base, which confirmed that six G^C bases associated in a precise ADD-DAA H-bonding pattern to form a hexameric rosette (Figure 3.2). The X-ray structure did not provide enough information as to whether the rosettes are capable of stacking to form RNTs. We thus designed novel G^C bases modeled after Mascal's G^C precursor and studied their self-assembling properties in solution by scanning electron microscopy (SEM), transmission electron microscopy (TEM), tapping mode atomic force microscopy (TM-AFM), ultraviolet-visible spectroscopy (UV-visible), dynamic light scattering (DLS) and molecular modeling.

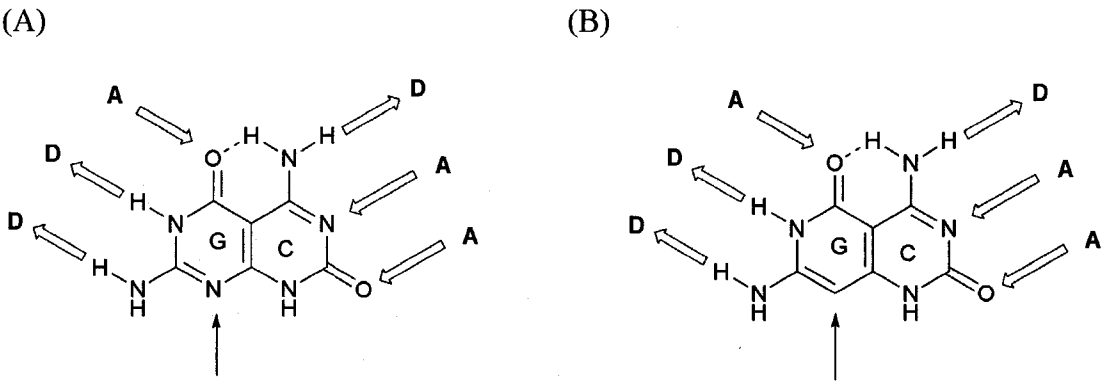

Figure 3.1. (A) Fenniri /Lehn's G^C motif (B) Mascal's G^C motif. Thick arrows showed similarity in their intermolecular H-bond patterns (ADD-DAA) while the thin arrows showed the only difference between the two motifs.

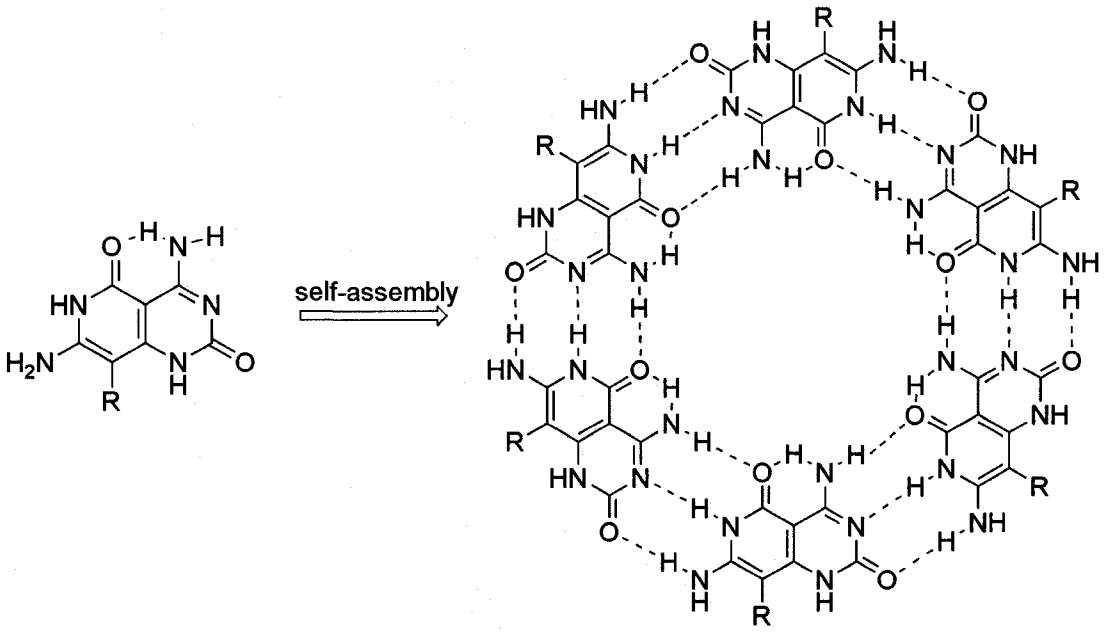

Figure 3.2. Hexameric Rosette formed by self-complementary G^C base.[1-3]

3.2. Systems Design

Three G^C bases were synthesized with G^C heterocyclic head modeled after Mascal's G^C motif (Figure 3.3). G^C base **22** was first synthesized to investigate whether Mascal's type G^C motifs were capable of forming RNTs in solution. It indeed formed RNTs in aqueous solution. The results obtained made us synthesize G^C base **23**, hoping that the allyl functional group would increase its solubility and also make its outer surface more hydrophobic. The self-assembly properties of G^C **22** and **23**, as well as their fast rate of RNTs bundling in water necessitated the synthesis of G^C base **24**, whose aldehyde function group got hydrated in water thereby making its outer surface hydrophilic in water. G^C base **24**, showed the slowest assembly in water. This synthetic strategy was very helpful in studying the driving force for RNTs bundling in aqueous and polar solvents. The synthesis and microscopic studies as well as other studies carried out on the three motifs in solutions are discussed throughout this chapter.

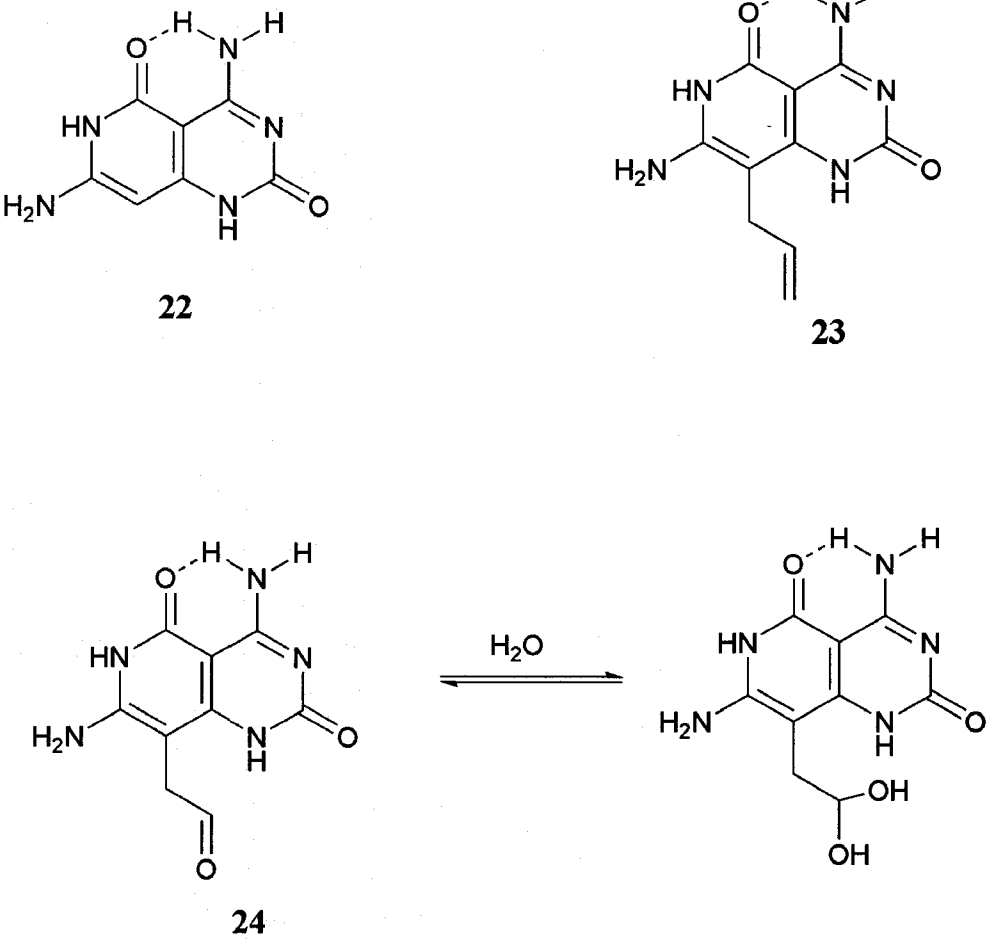

Figure 3.3. Self-complementary G^C bases **22-24**.

3.3. Synthesis of G^C Base **22**: Results and Discussions

The synthesis of **22** (Scheme 3.1) began with the cyclization of the commercially available 2-aminoprop-1-ene-1,1,3-tricarbonitrile,[4] **25**, with sodium methoxide to give **26** in 88% yield and its regioisomer in less than 10% yield (Scheme 3.2). No cyclization occurred when position 3 of the tricarbonitrile had two alkyl substituents. For this reason and the conditions under which the cyclization took place, we proposed two possible mechanisms for the base cyclization as illustrated in Scheme 3.2. Attempts at Boc protecting the more reactive amino group at position 6 under various conditions with di-*tert*-butyl dicarbonate, only led to the tetra-Boc product, **27**. Unfortunately, treatment of **27** with 10% trifluoroacetic acid, partially deprotected the amino group at position 4 and fully deprotected the one at position 6, furnishing **28** in 50% yield. The structure of **28** was confirmed by X-ray crystallography (Figure 3.4). Acetylation of **26** with acetic anhydride provided **29** in moderate 52% yield and the unreacted starting material was removed with 10% citric acid or 2.5% HCl wash (Scheme 3.3). Annulation of **29** with *N*-(chlorocarbonyl) isocyanate followed by basic work-up afforded the desired bicycle product, **30**, in 85% yield. Finally, deprotection of **30**, with HBr/acetic acid followed by basic work up gave the desired G^C base, **22**, in 75% yield. Overall, G^C base **22** was obtained in four steps without column chromatography in a 29% overall yield.

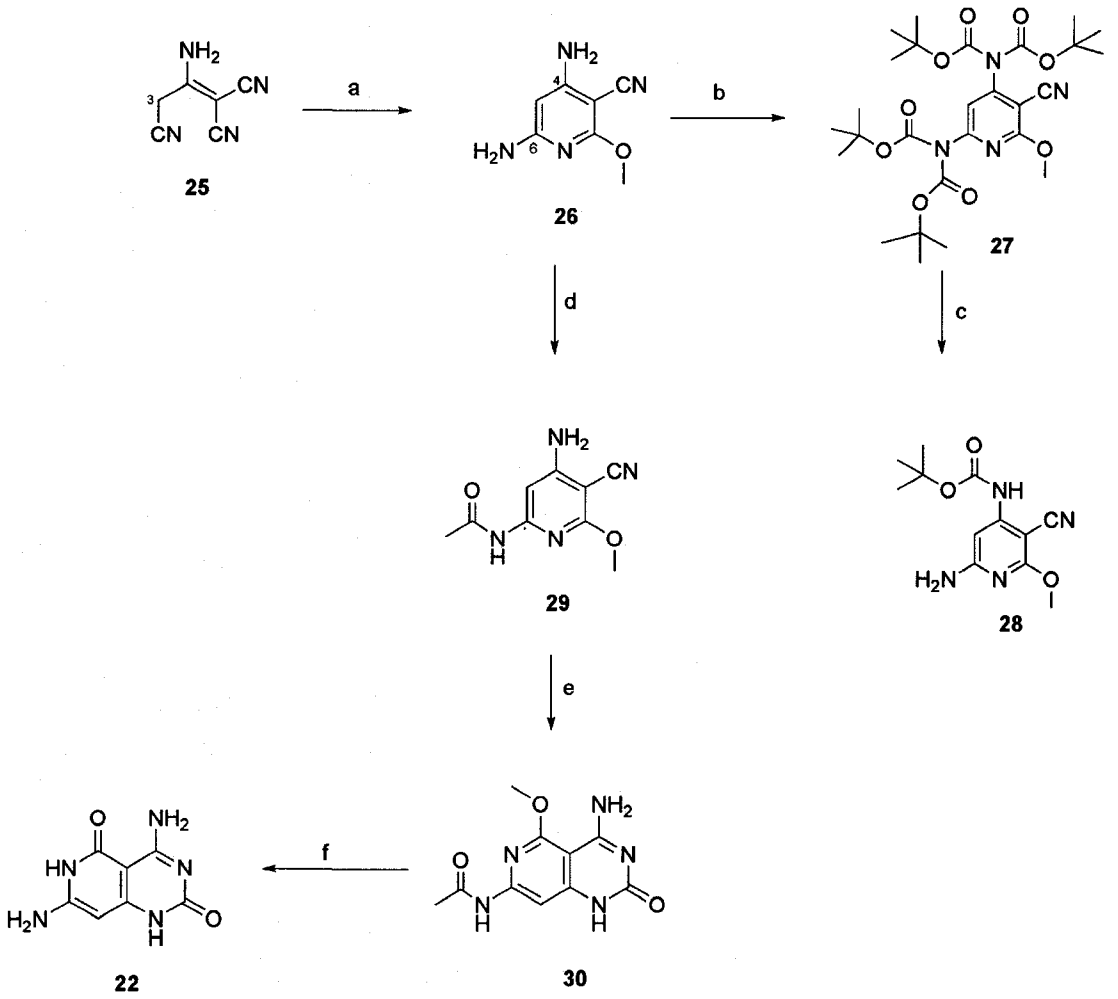

Scheme 3.1. Synthesis of **22**. Reagents and conditions: (a) NaOMe, MeOH, 65-70°C, 72 h; (b) Boc_2O, DMAP, Et_3N, THF, rt, 24 h; (c) 10% TFA/ DCM, 20 h; (d) Ac_2O, DMAP, Et_3N, THF, rt, 48 h; (e) ClCONCO, CH_2Cl_2, 4 h then 7N NH_3, MeOH, 6 d; (f) 33% HBr-AcOH, reflux, overnight then 7N NH_3, MeOH, 1 h.

Option A

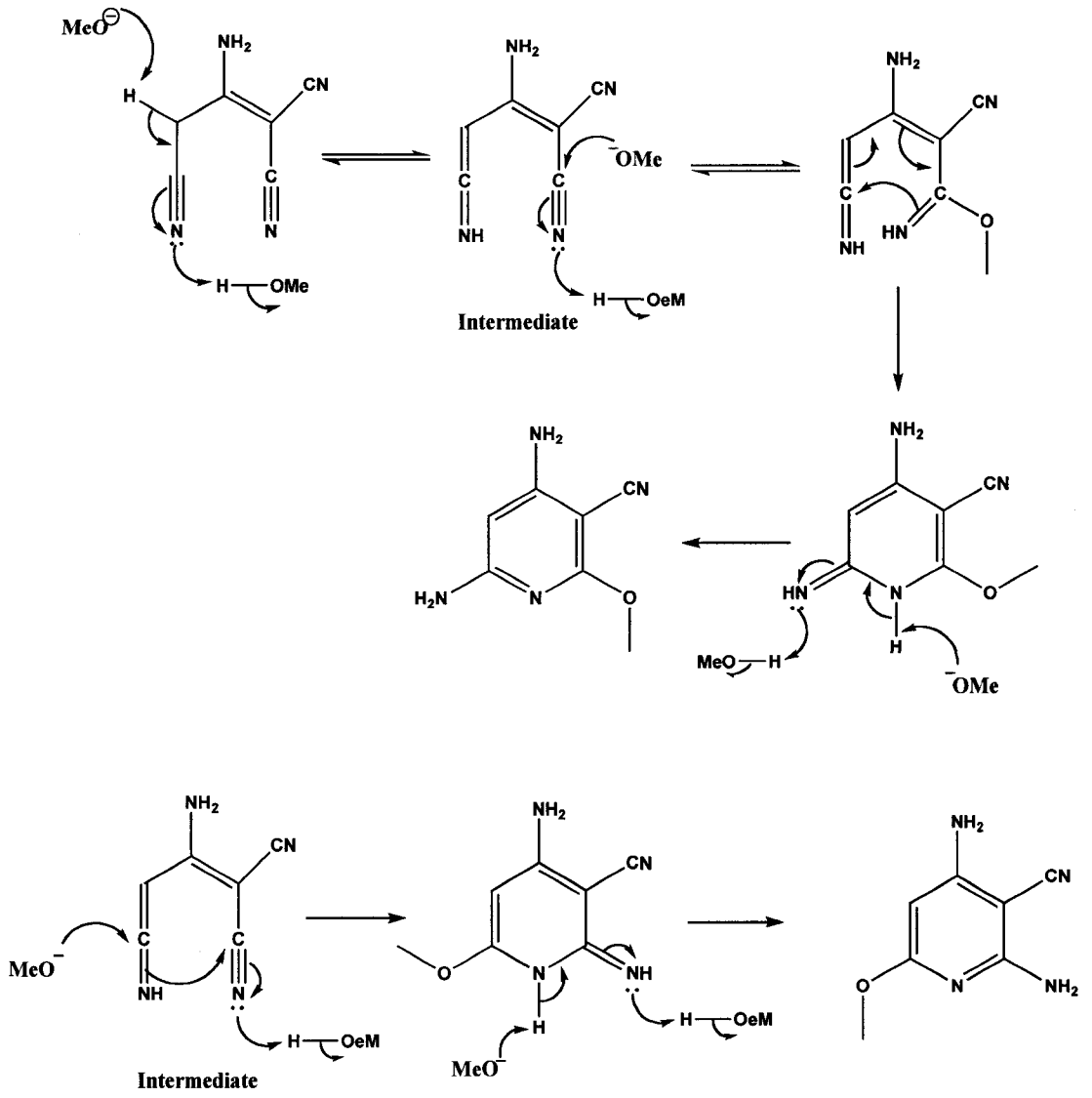

Scheme 3.2a. Proposed mechanism of the base cyclization of **25**.

Option B

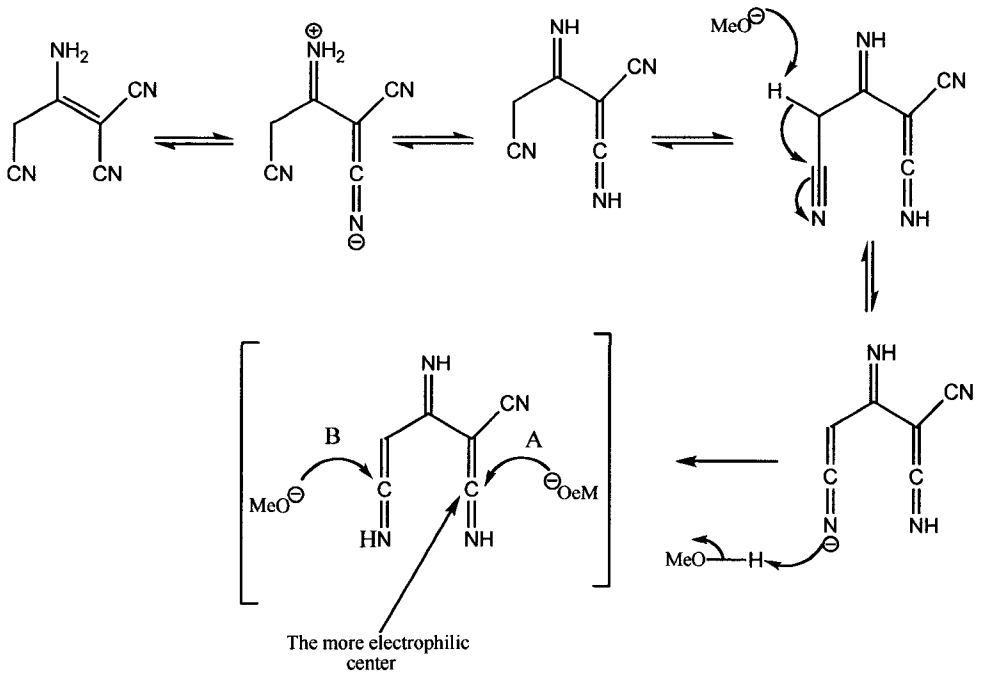

Path A

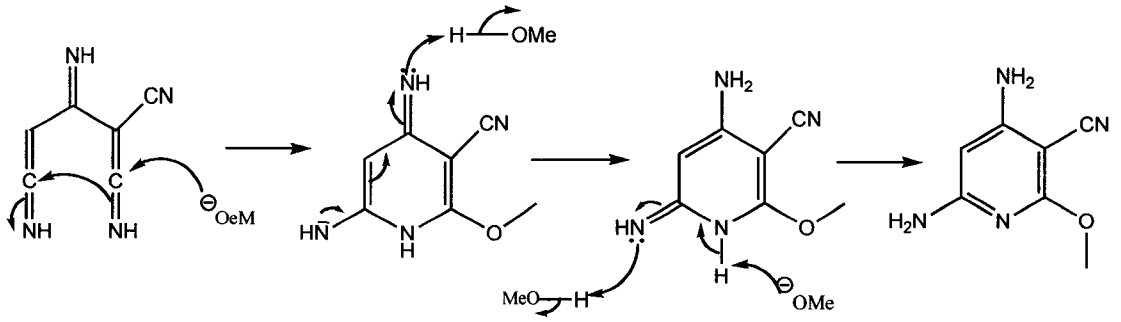

Path B

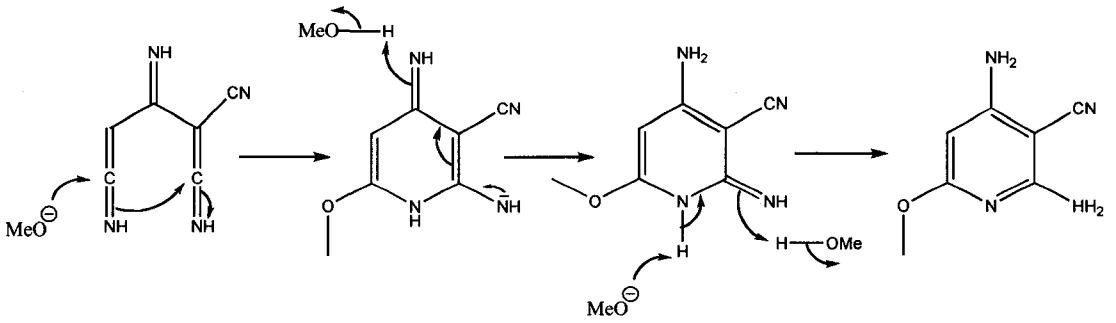

Scheme 3.2b. Proposed mechanism of the base cyclization of **25**.

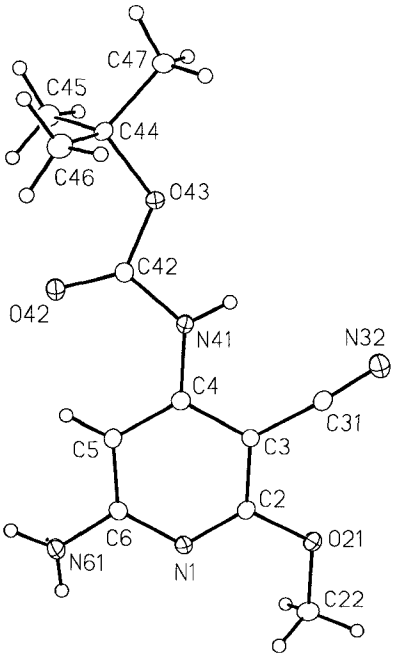

Figure 3.4. ORTEP view of **28**.

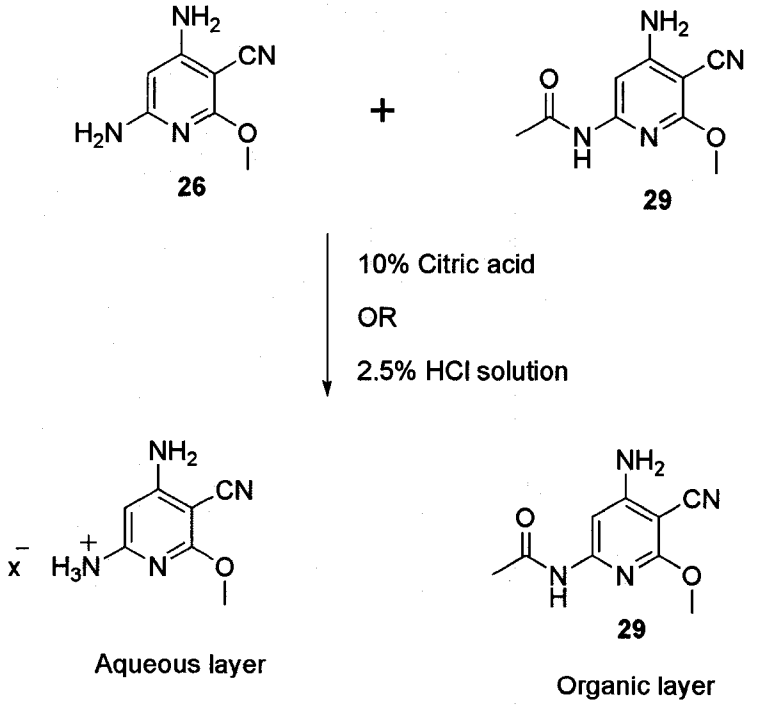

Scheme 3.3. Acid separation of **26** and **29**.

3.4. Synthesis of G^C Base **23**: Results and Discussions

The synthesis of **23** began with the treatment of **25** with allylbromide to give **31** in 80% yield (Scheme 3.4). Cyclization of **31** with sodium methoxide gave **32** in 41% yield and its regioisomer **33** in 57%. Boc-protection of the more reactive amino group at position 6 with di-*tert*-butyl dicarbonate and lithium hexamethyldisilazide gave di-Boc **34** in 45% yield. The structures of **33** and **34** were confirmed by X-ray crystallography (Figure 3.5). Annulation of **34** with *N*-(chlorocarbonyl) isocyanate gave the expected urea intermediate, which did not cyclize upon treatment with base. However, the treatment of **34** with sodium methoxide in methanol gave **35** in 100%. We proposed two possible mechanisms both having the same intermediate step for the base induced partial deprotection (Scheme 3.5). The annulation of **35** with *N*-(chlorocarbonyl) isocyanate followed by basic workup provided bicycle **36** in 92% yield. Finally, treatment of **36** with trimethylsilyl iodide, successfully cleaved the Boc protecting group and the aromatic methyl ether to give allyl functionalized G^C base **23** in 88% yield. G^C base **23** was thus synthesized in 6-steps in 12% overall yield.

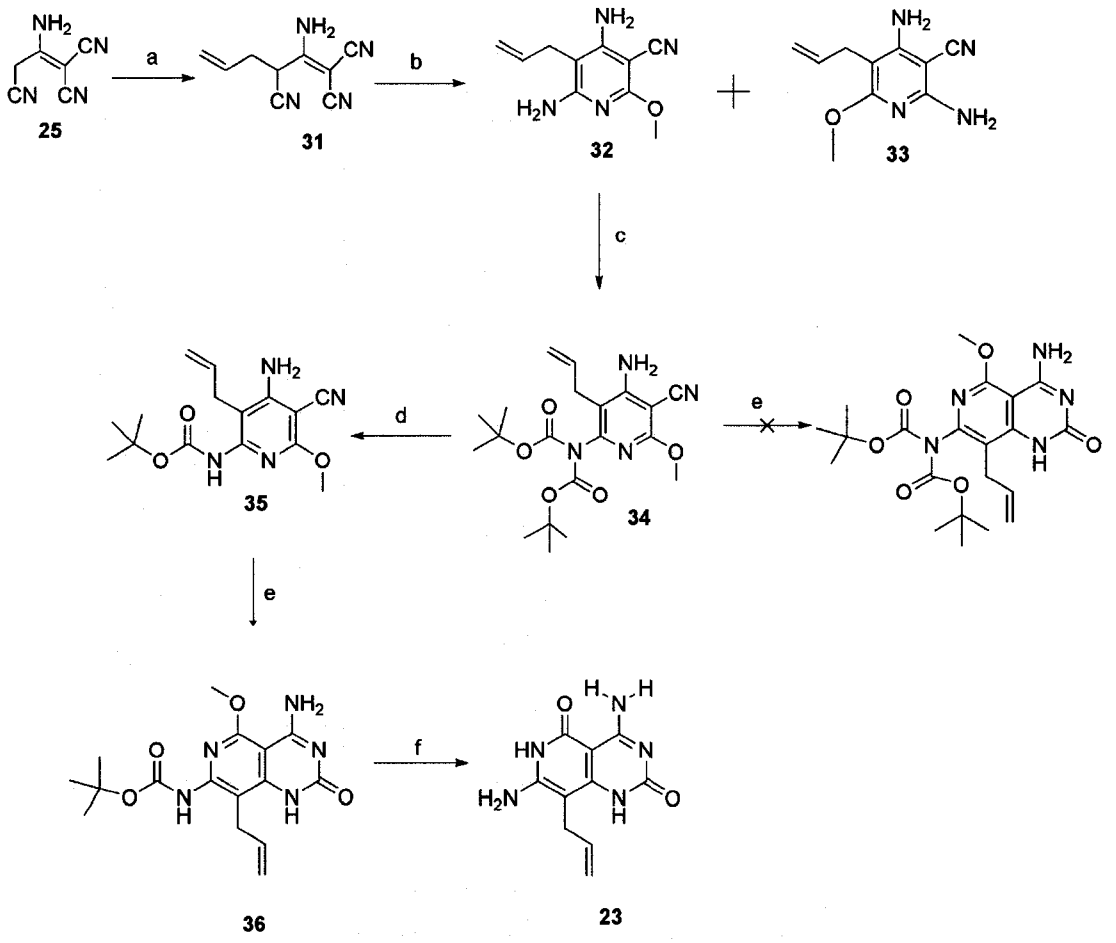

Scheme 3.4. Synthesis of **23**. Reagents and conditions: (a) Allylbromide, DIPEA, DME, rt, 24 h; (b) NaOMe, MeOH, reflux, 48 h; (c) Boc_2O, LHMDS, THF, -78°C-rt, 2 h; (d) NaOMe, rt, 3 d; (e) ClCONCO, CH_2Cl_2, rt, 3 h then NaOMe, 2 d; (f) Me_3SiCl, NaI, MeCN, 100 h overnight.

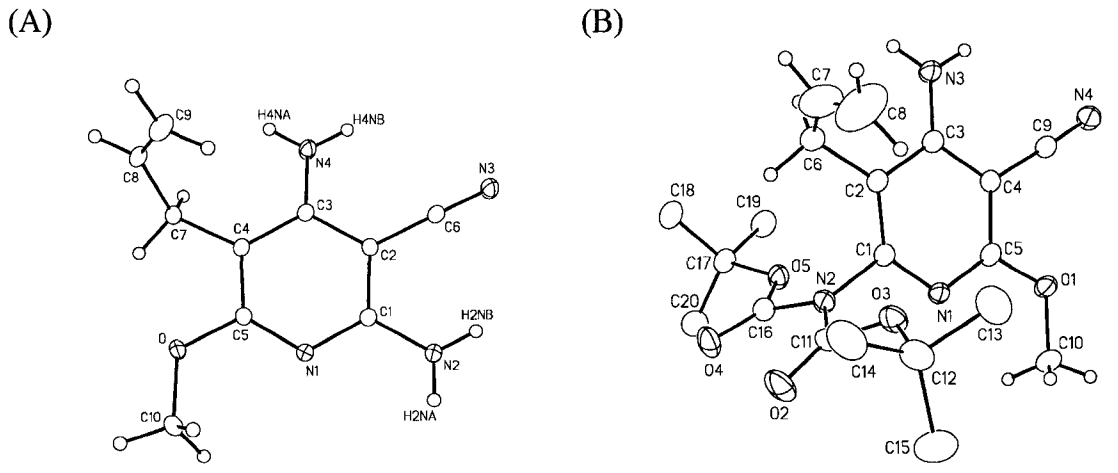

Figure 3.5. ORTEP views of (A) **33** and (B) **34**.

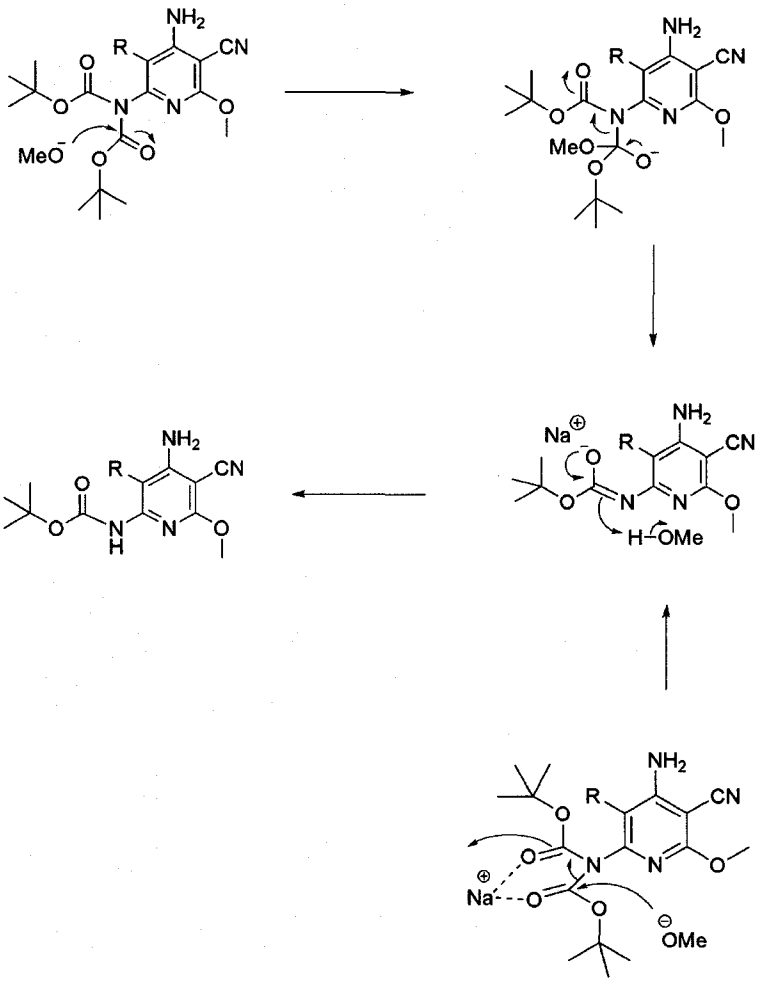

Scheme 3.5. Proposed mechanism for the conversion of di-Boc **34** to mono-Boc **35**.

3.5. Synthesis of G^C Base **24**: Results and Discussions

Compound **24** was synthesized from **36**. Boc protection of **36** with di-*tert*-butyl dicarbonate gave **37** in 80% yield (Scheme 3.6). The reactions of **37** with catalytic osmium tetroxide and N-methyl morpholine-N-oxide, followed by oxidative cleavage with sodium periodate afforded **38** in 85% yield. The simultaneous demasking of both the amino and latent carbonyl function with trimethylsilyl iodide proceeded smoothly to give target **24** in 98% yield. Overall, **24** was thus prepared in 4 steps from **36** in 67% yield.

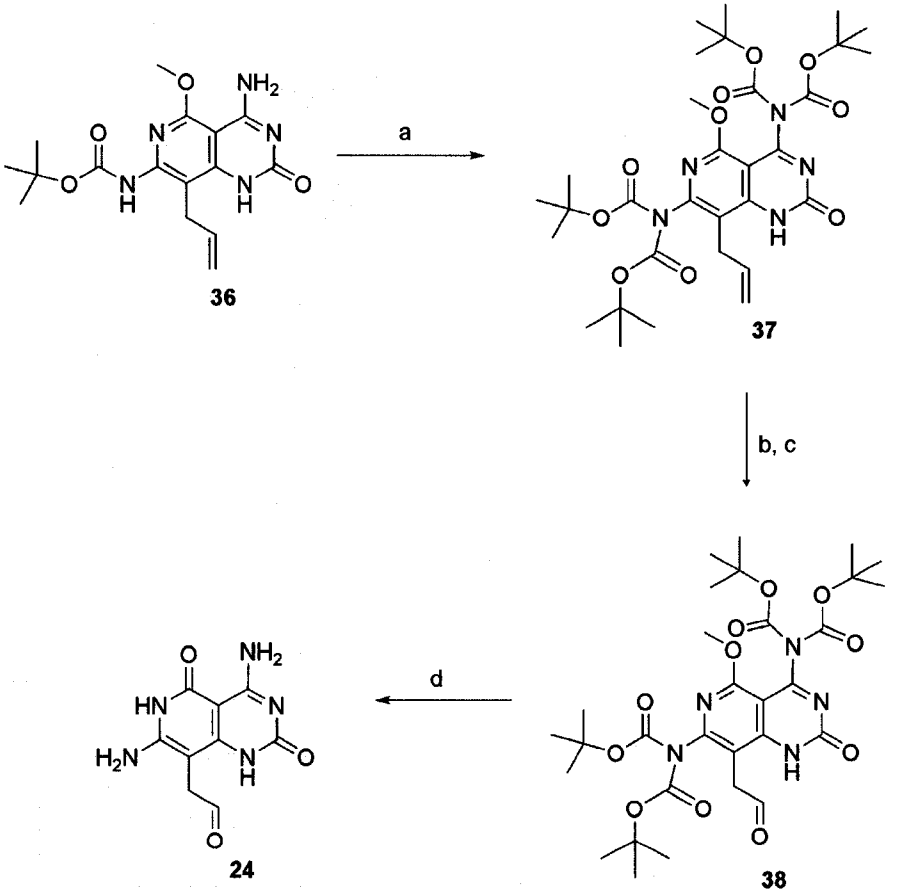

Scheme 3.6. Synthesis of **24**. Reagents and conditions: (a) Boc_2O, DMAP, Et_3N, THF, rt, 24 h, 80%; (b) OsO_4, NMO, acetone/ H_2O, rt; 2 d; (c) $NaIO_4$, DCE/H_2O, rt, 24 h, 85%; (d) Me_3SiCl, NaI, MeCN, 100 h, overnight, 98%.

3.6. Microscopic Characterization of the G^C Motifs -SEM, AFM, TEM.

3.6.1. G^C Base **22:** In Water

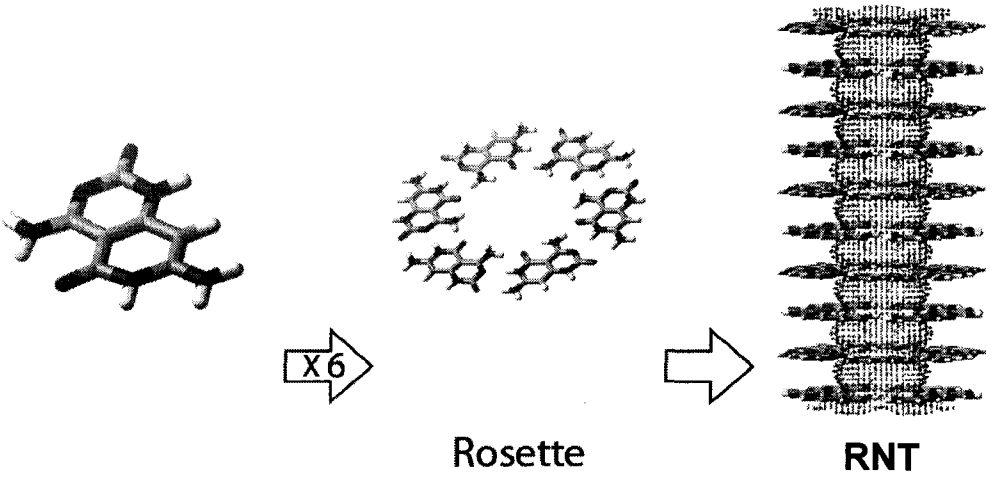

Figure 3.6. Hierarchical self-assembly of G^C base **22** into rosette and RNT in water.

G^C base **22** was found to be soluble in a wide spectrum of organic solvents at low concentration. However, RNTs (Figure 3.6) and bundles of tubes were exclusively observed in aqueous solutions for concentration range of 0.05 to 0.4 g/L (solubility limit). Time dependent SEM studies were carried out on the assembled sample in the aqueous solution (8.58×10^{-4} M) from 20 minutes to 21 days. A rapid assembly was observed within an hour. It was observed that the tubes began to align from an hour to two days in solution, after which no single tube was visible (Figure 3.7). The tubes then aggregated into huge bundles and no observable change in the morphology of the aggregate was seen after seven days in solution.

TEM samples were prepared from an aqueous solution of **22** (8.58×10^{-4} M) and negatively stained with uranyl acetate (Figure 3.8). In agreement with the calculated

average diameter of 2.2 nm by molecular modeling, the diameter of a single RNT measured from TEM images was found to be 2.2 ± 0.2 nm. This diameter value is consistent with the height profiles obtained from TM-AFM images of single RNT, which give slightly compressed diameters of 2.0 ± 0.2 nm.[5]

TM-AFM micrographs also showed the tubes in uniformly align orientation (Figure 3.9) within the first three hours, which agreed with the SEM observation. Heights measured in bundles comprised of 2 – 6 RNTs and showed an increase in the height of single RNT to 2.2 ± 0.2 nm.

We suspect two possible driving forces for the bundling process. First is the formation of relatively strong inter-RNT hydrogen bonds. More specifically, each of the six G^C modules in a rosette is capable of forming two inter-rosette hydrogen bonds. Thus, each rosette can form up to 12 inter-rosette hydrogen bonds in addition to 18 intra-rosette hydrogen bonds (Figure 3.10). An alternative explanation for the bundling is the outer surface of the RNTs are sufficiently hydrophobic making the RNTs come together avoiding the hydrophilic water molecule

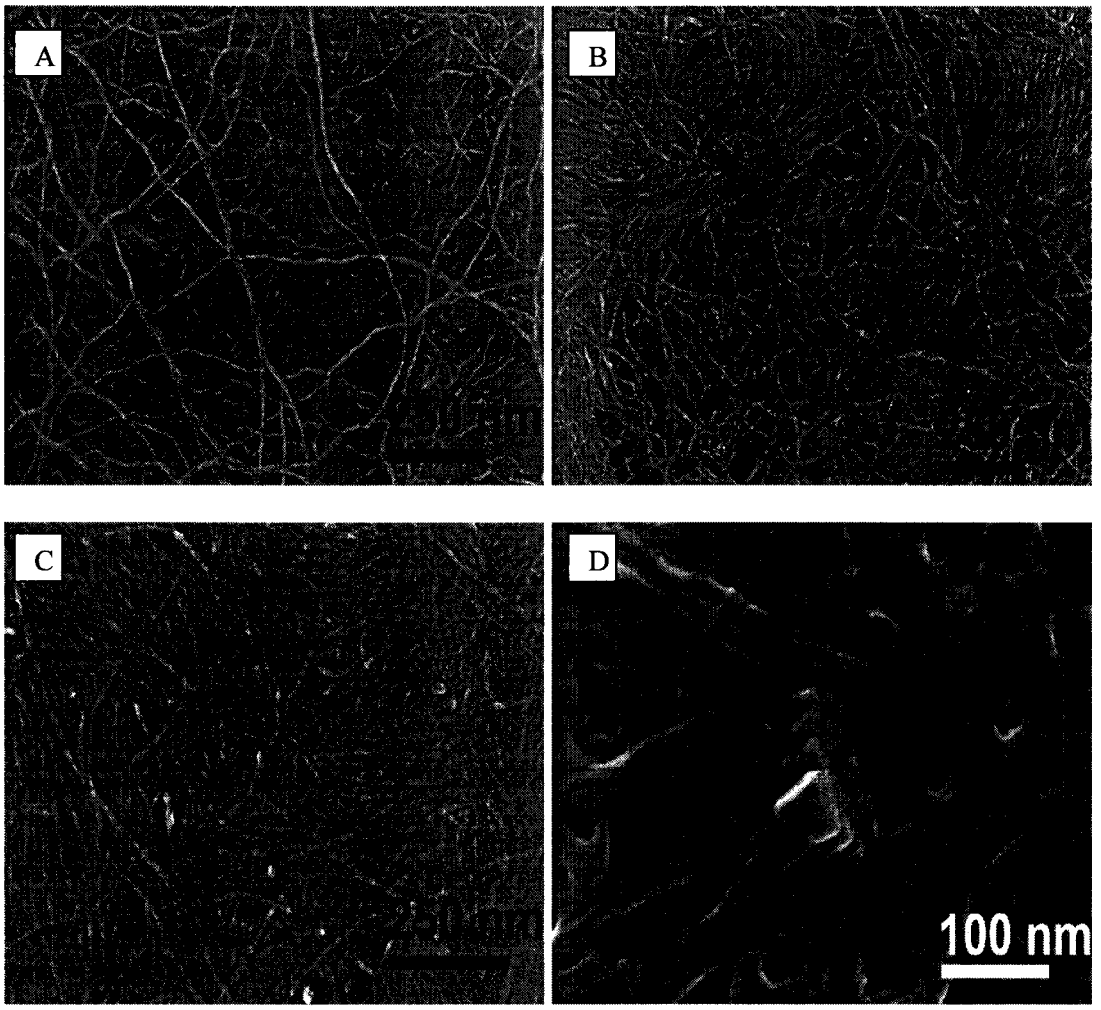

Figure 3.7. Time dependent SEM studies of **22** in water (8.58×10^{-4} M) (A) 28 minutes (B) 1 h (C) 2 d (D) 7 d The samples were drop cast on carbon grids at indicated time intervals from stock solution.

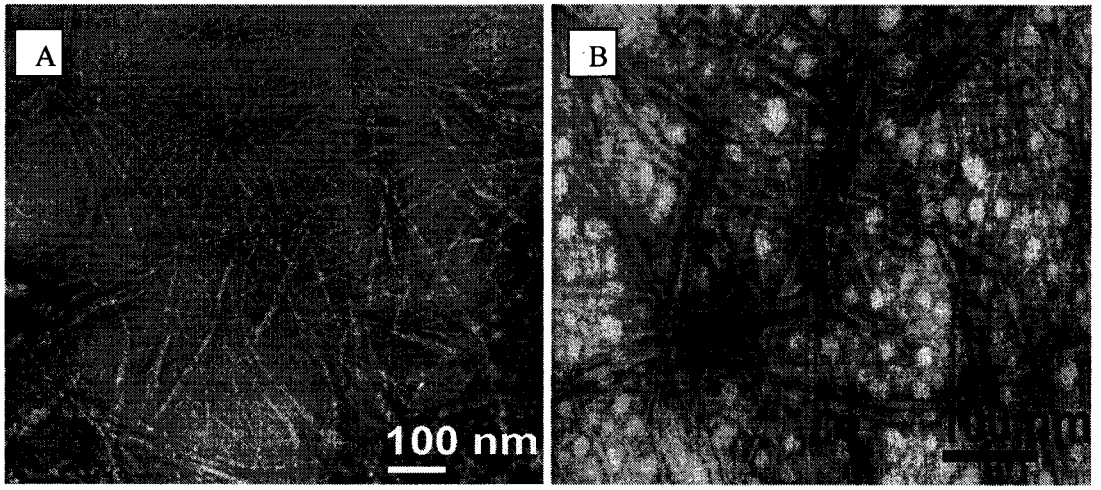

Figure 3.8. TEM micrographs of negatively stained assembly obtained from **22** in water (8.58×10^{-4} M) at 2 h (A) low magnification (B) high magnification. The sample was drop cast on carbon grid.

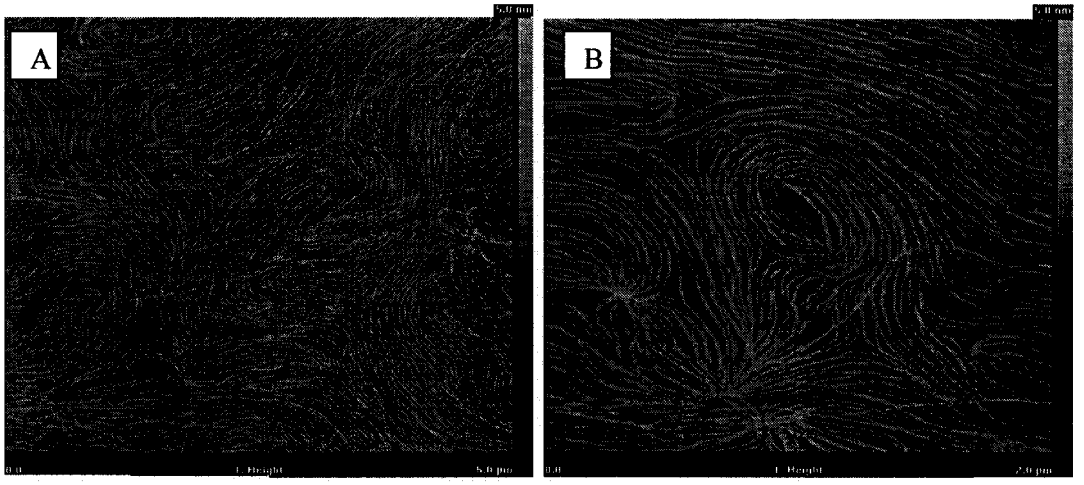

Figure 3.9. TM-AFM micrographs obtained from **22** in water (8.58×10^{-4} M) at 3 h (A) low magnification (B) high magnification. The sample was spin cast on mica.

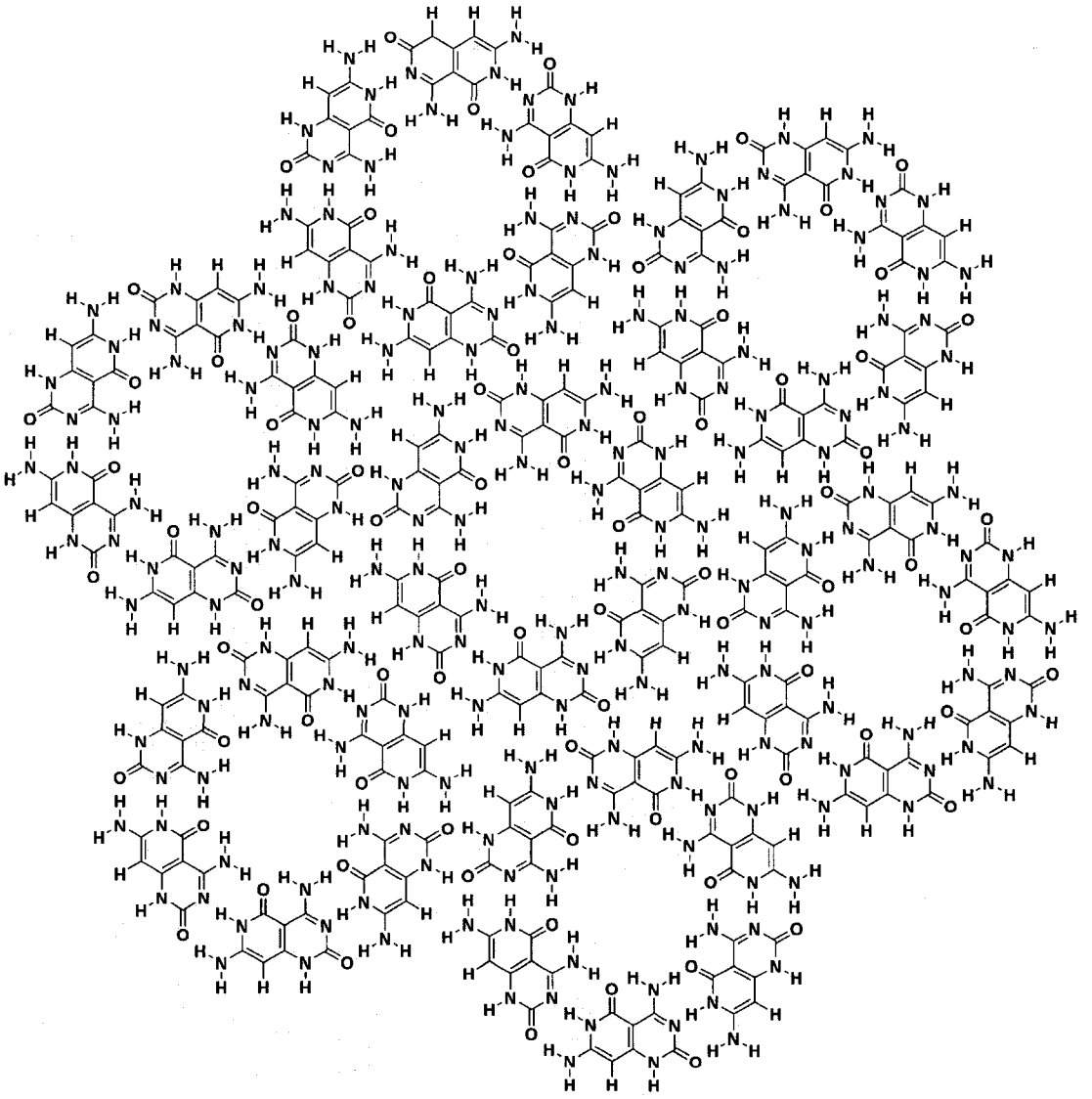

Figure 3.10. Proposed inter-rosette hydrogen bonds formation, which results in tubes bundling.

To distinguish between these two possibilities, compounds **23** and **24** were self-assembled in water. The allyl group in **23** made the outer surfaces of its self-assembled RNTs more hydrophobic and when the aldehyde group in **24** was hydrated by water molecules the outer surfaces of its RNTs became hydrophilic. This opposite tuning of **23** and **24** impacted the morphologies of their RNTs in water.

3.6.2. G^C Base **23**: Hydrophobic Tail in Water

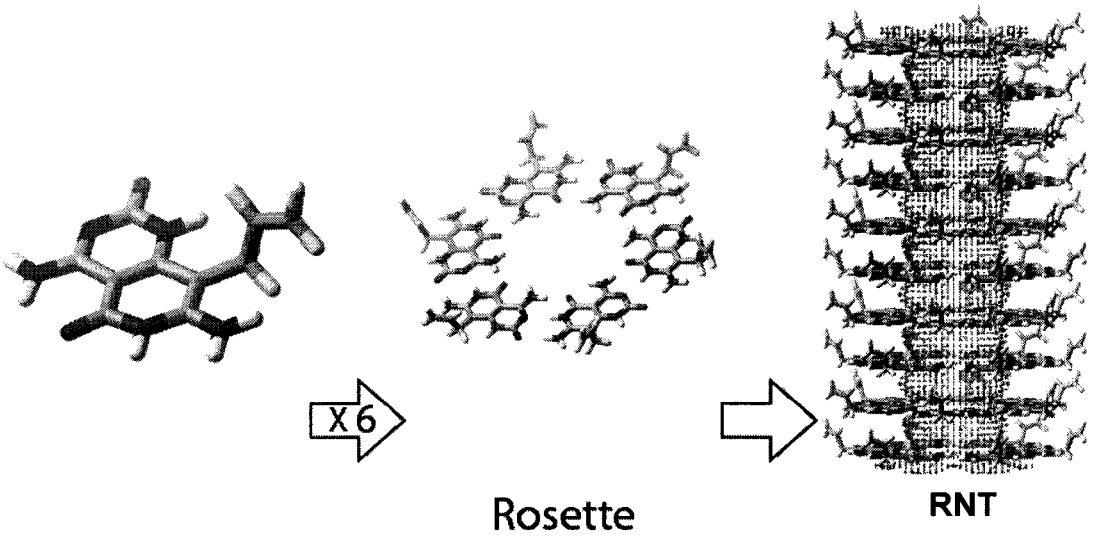

Figure 3.11. Hierarchical self-assembly of G^C base **23** into rosette and RNT in water.

G^C base **23** which bears the hydrophobic tail, self-assembled in water and gave different morphologies depending on time (Figure 3.11). It solubility range (0.05 to 0.7 g/L) is greater than that of **22**. When its aqueous solution (8.58×10^{-4}M) was monitored over the same time period as **22** by SEM, single RNTs were only observed within thirty minutes to an hour. Helical bundles were seen within an hour to 24 hours.[6] Long and well aligned nanorods[7] were observed at three days in solution and the rods appeared to have channels. After this time period, the uniformity of the rods was lost and a new level of complex aggregation emerged. Some of the aggregate was observed to be standing perpendicular to the carbon grid (Figure 3.12).[8] The observed self-assembly and bundling of tubes of **23** was faster than **22**. Intermolecular H-bonding, hydrophobic interaction and van der Waals interactions could all be responsible for these observations.

The diameter of a single RNT measured from TEM (negatively stained with uranyl acetate) in water was found to be 2.85 ± 0.07 nm, which is in good agreement with the 2.81 nm obtained by molecular modeling (Figure 3.13).

The measured diameter of single RNT from AFM gave a value of 2.60 ± 0.2 nm. TM-AFM was also used to monitor the self-assembly process of **23** in aqueous solution and the result obtained also agreed with the SEM result (Figure 3.14).

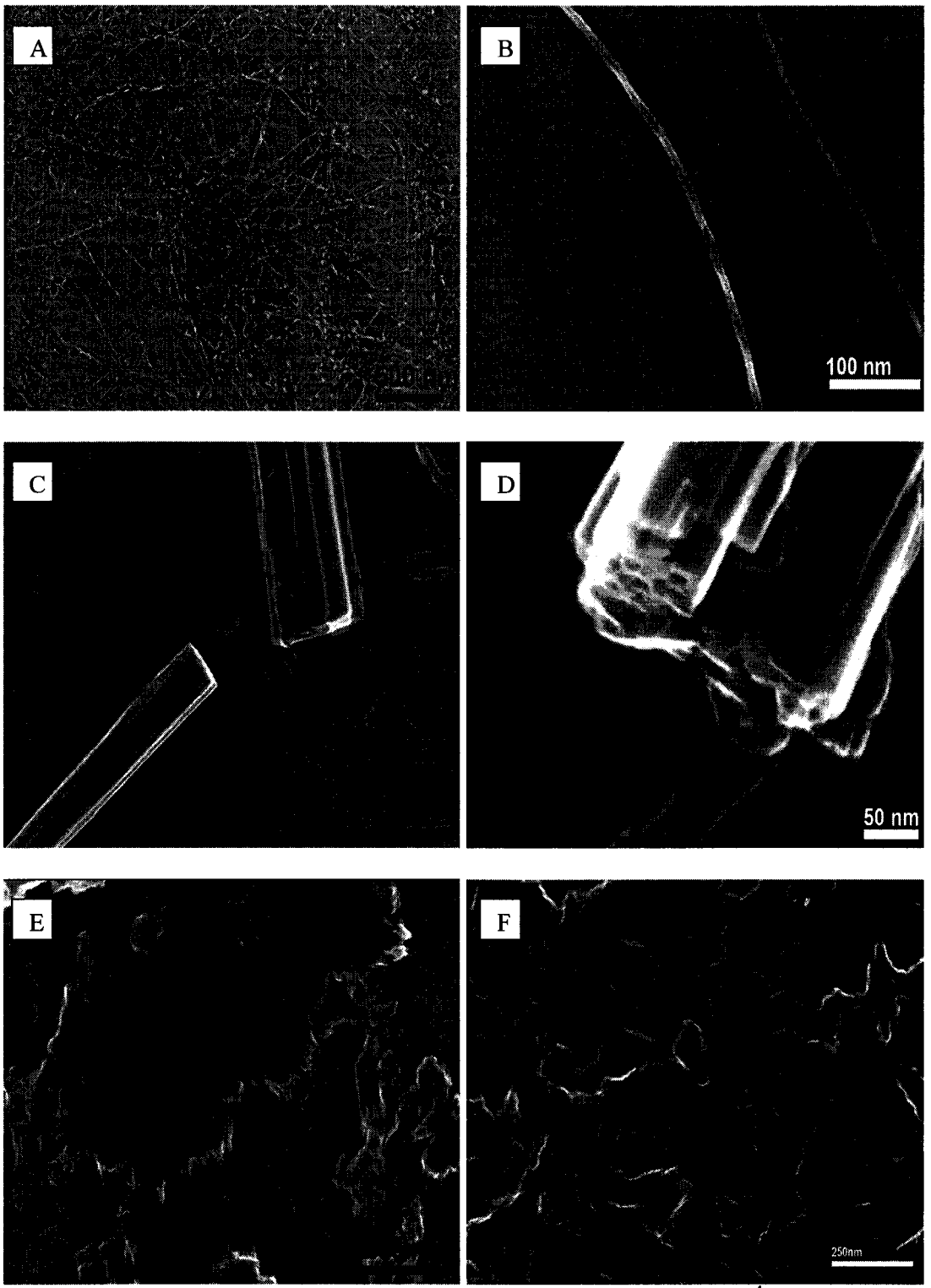

Figure 3.12. Time dependent SEM studies of **23** in water (8.58×10^{-4} M) (A) 1 h (B) 1 d (C) 3 d, low magnification (D) 3 d, high magnification (E) 5 d (F) 7 d. The samples were drop cast on carbon grids at indicated time intervals from stock solution.

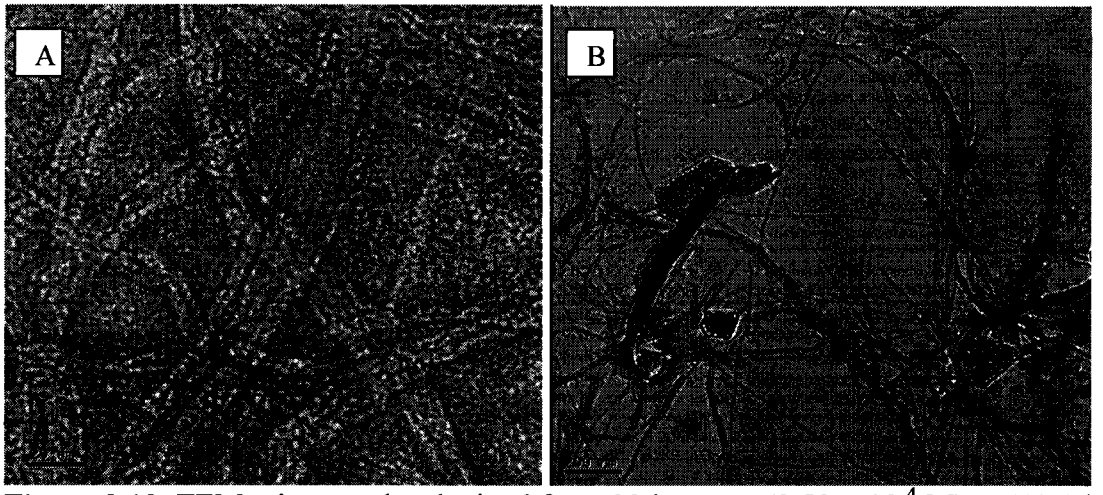

Figure 3.13. TEM micrographs obtained from **23** in water (8.58×10^{-4} M) at (A) 1 h, negatively stained assembly (B) 1 d (unstained). The samples were drop cast on carbon grids at indicated time intervals from stock solution.

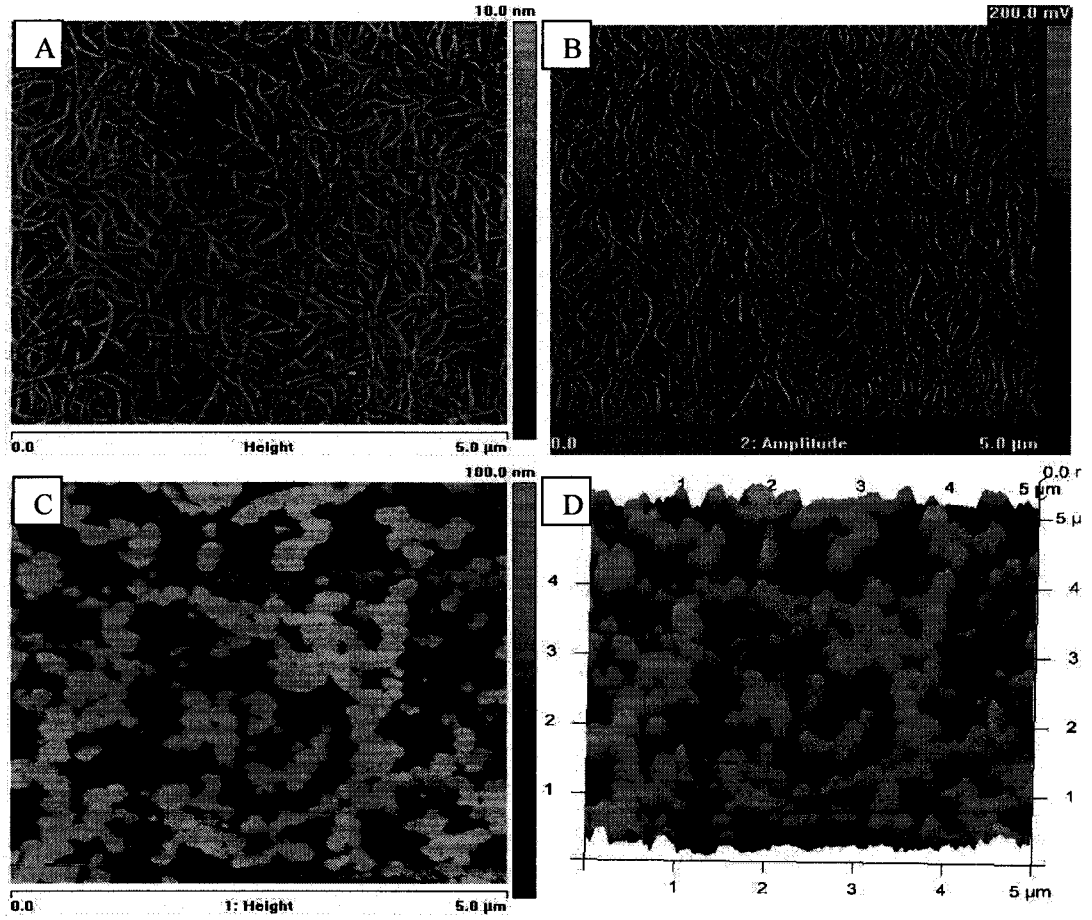

Figure 3.14. Time dependent TM-AFM studies of **23** in water (8.58×10^{-4} M) (A) 1 h (B) 1 h (C) 5 d (D) 3-D view of C. The samples were spin cast on mica at indicated time intervals from stock solution.

3.6.3. G^C Base **24**: Hydration Site in Water

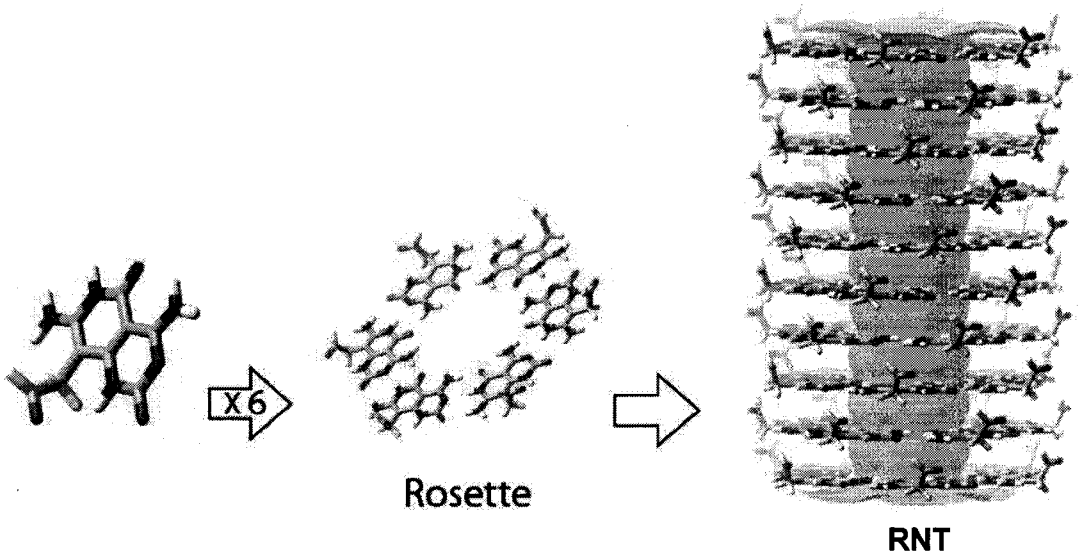

Figure 3.15. Hierarchical self-assembly of G^C base **24** into rosette and RNT in water.

24, is soluble up to 1 g/L in water and formed RNT (Figure 3.15). Aqueous solutions of **24** (8.58×10^{-4} M), monitored by SEM (Figure 3.16), TEM (Figure 3.17) and TM-AFM (Figure 3.18) all showed well dispersed single RNTs within the first three days of self-assembly. Although bundles of tubes were observed at seven days, there were still observable single RNTs (Figure 3.16). There were no signs of nanorods or complex aggregates of bundles up to the monitored 21 days and there was no significant change in the morphology or level of bundling of tubes after seven days. The rate of assembly and aggregation of **24** in water appeared to be the slowest out of the three motifs.

The diameters of a single RNT measured from TM-AFM and TEM (negatively stained with uranyl acetate) in water were found to be 2.60 ± 0.20 and 2.71 ± 0.09 nm respectively, which also agree with the 2.7 nm obtained by molecular modeling.

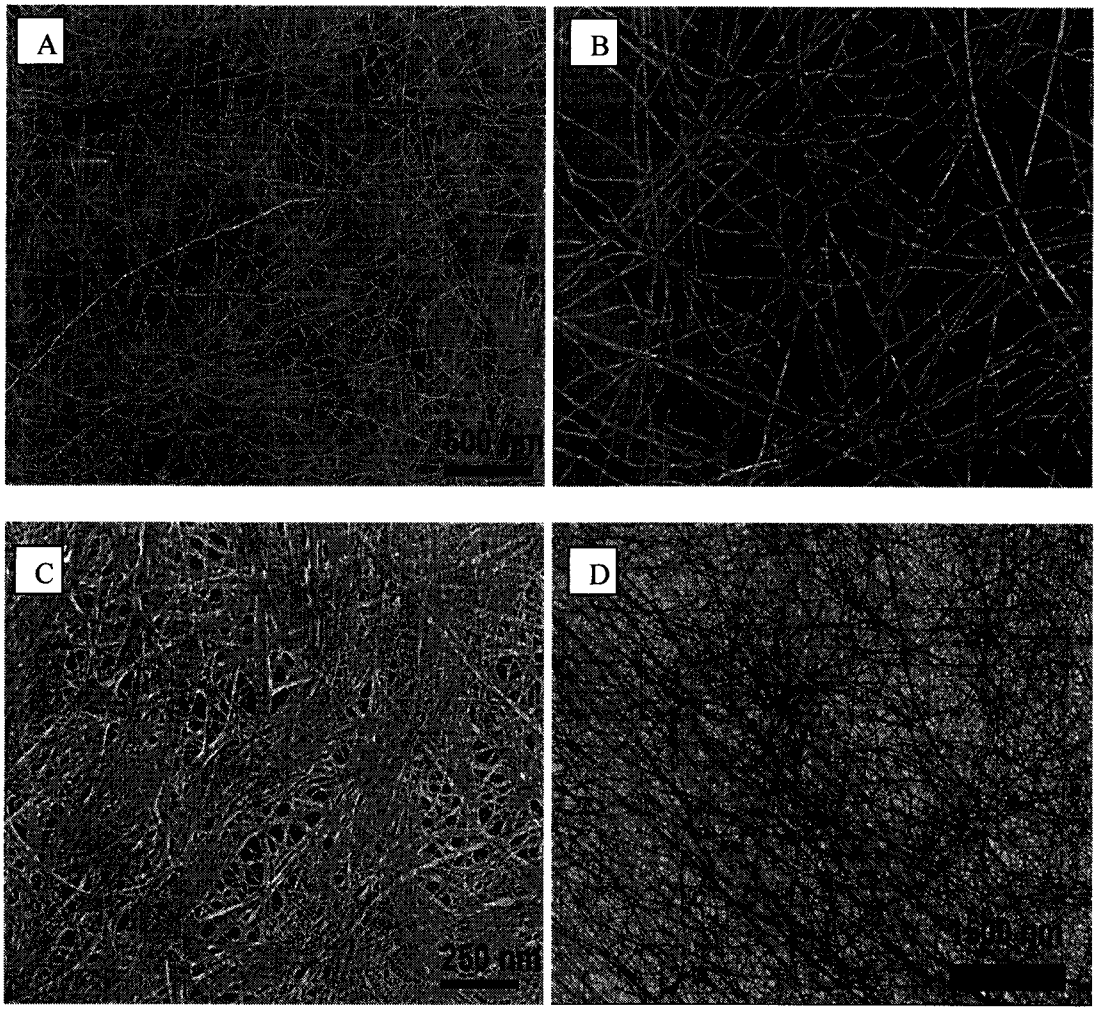

Figure 3.16. Time dependent SEM studies of **24** in water (8.58×10^{-4} M) (A) 1 d, low magnification (B) 1 d, high magnification (C) 7 d (D) 7 d, Transmission mode. The samples were drop cast on carbon grids at indicated time intervals from stock solution.

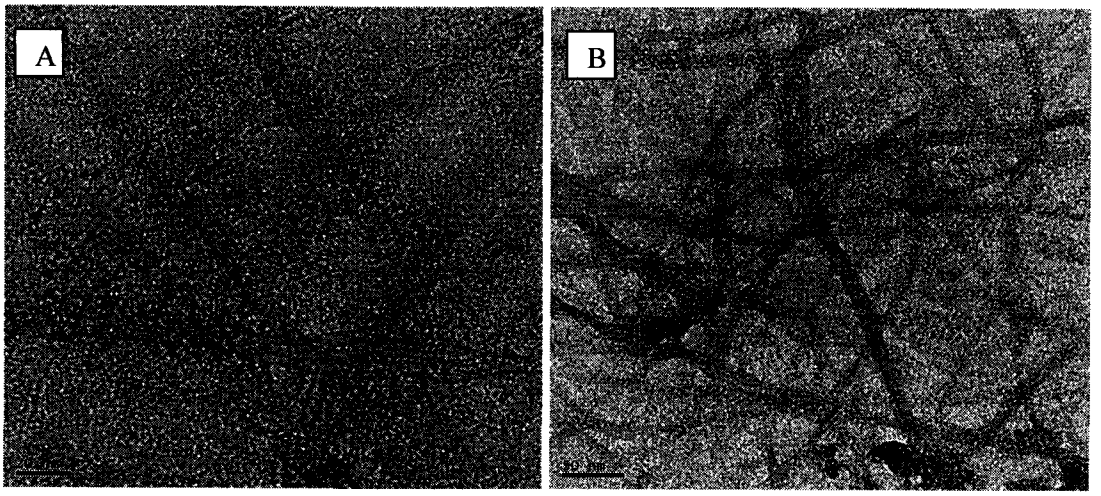

Figure 3.17. TEM micrographs of negatively stained assembly obtained from **24** in water (8.58×10^{-4} M) at (A) 1 d, high magnification (B) 1 d, low magnification. The sample was drop cast on carbon grid.

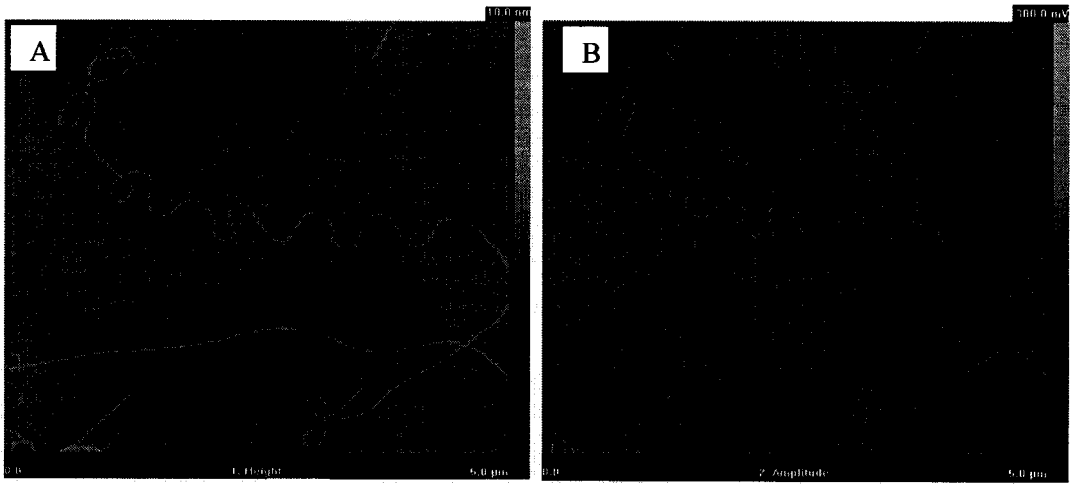

Figure 3.18. TM-AFM micrographs of **24** in H_2O (8.58×10^{-4} M) at 1 d (A and B). The sample was spin cast on mica.

3.7. UV-Visible Studies of G^C Bases **22-24** in Water

Aqueous stock solutions of G^C bases **22-24** at concentrations of 6.7×10^{-4} M were diluted ten fold to UV-Vis concentration 6.7×10^{-5} M at various time intervals (5 minutes to seven days) and their UV-Vis spectra were obtained. A sharp hypochromic effect was observed over the first 3 hours for **22**, which slows down after 7 days. A sharper hypochromic effect was observed within an hour of assembly of **23** and showed gradual drop after 3 hours. No significant hypochromic drop was observed for **24** until after a day, with only a slight change between a day and seven days (Figure 3.19). These hypochromic effects suggest π-π stacking interactions between rosettes $\mathbf{22}_6$, $\mathbf{23}_6$ and $\mathbf{24}_6$ to form RNTs.[9] G^C base **24** was expected to be more stabilized by water molecules (solvation), which should decrease its rate of assembly and aggregation relative to **22** and **23**. This UV-Vis result is consistent with the microscopies (SEM, TEM and TM-AFM) experimental results.

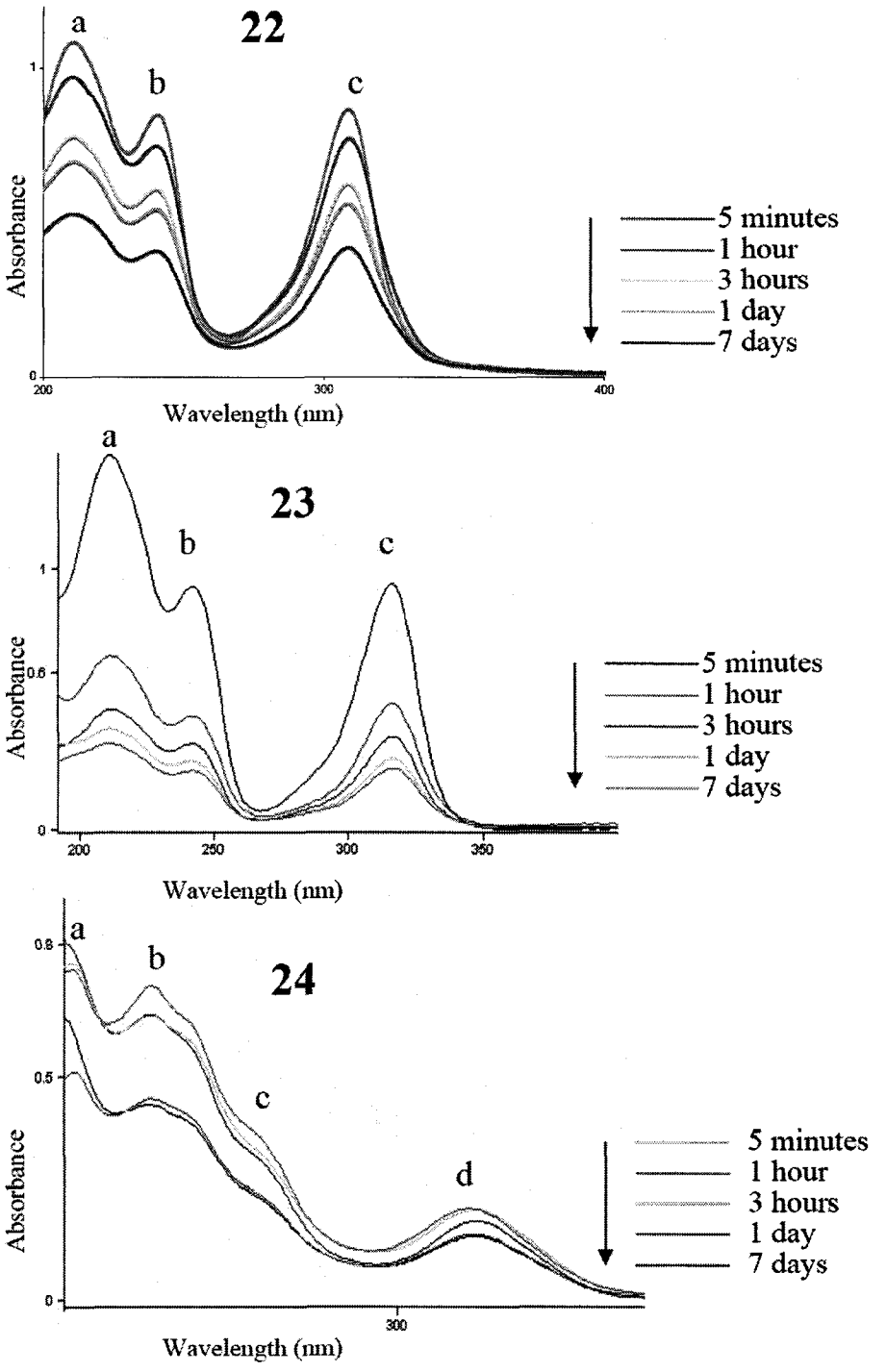

Figure 3.19. Time dependent UV-Vis. spectra of aqueous solution (6.7×10^{-5} M) at 20°C of G^C bases **22**, λ^{a}_{max}= 210 nm, λ^{b}_{max}= 241 nm, λ^{c}_{max}= 309 nm; **23**, λ^{a}_{max} = 211 nm, λ^{b}_{max}= 241 nm, λ^{c}_{max}= 316 nm; and **24**, λ^{a}_{max}= 193 nm, λ^{b}_{max} 220 nm, λ^{c}_{max}= 255, λ^{d}_{max}= 326 nm.

3.8. Dynamic Light Scattering (DLS) Studies of G^C Bases **22-24** in Water

Additional evidence for fast self-assembly of **22-24** was obtained from dynamic light scattering (DLS). 6.7×10^{-4} M aqueous solutions of **22-24** were monitored over time by DLS. A rapid increase in the size of the aggregates beyond the instrument's detection limit (~10 μm) occurred over 20 minutes for **22** and **23**, supporting fast self-assembly. As shown in Figure 3.20, **22** and **23** reached their maximum count within two hours while it took **24** more than four hours to reach the maximum count. This again is consistent with the SEM, TEM, TM-AFM and UV-Vis observations.

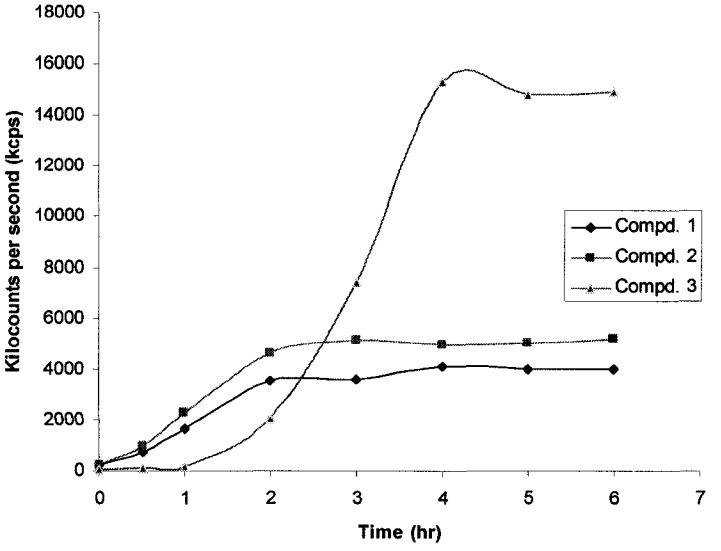

Figure 3.20. DLS plot showing the rate of aggregations of **22-24** in water.

3.9. Driving Force for Tube Bundling

The self-assembly of the three motifs were compared at the same concentration in water and studied over 21 days period. Only **24,** which outer surface could be hydrated by water molecules the most, showed the presence of single RNT over the longest period of time (up to seven days). G^C base **22** showed single RNT up to three hours and **23**, showed single RNT only up to an hour before bundle of tubes and rods were seen.

Since all of the three motifs were capable of forming the same number of inter-rosette hydrogen bonds in solution and the major difference between them was the ease of solvation of their outer surfaces. We then conclude that hydrophobic interaction plays a very important role in the observed tubes bundling and the subsequent rods formation by **22** and **23** in aqueous solution (Figure 3.21).[10] These experimental results suggested that if the outer surfaces of RNTs are capable of both hydrophobic interactions and inter-rosettes hydrogen bond interactions in solution, both interactions with other forces like van der Waals force would increase the rate of aggregations and complexity to give nanorods and other three dimensional structures in solution.

The use of both interactions (hydrophobic and inter-rosette hydrogen bond) in the design of motifs that self-assembly into RNTs would make the construction of ever sophisticated architectures in nanotechnology possible.

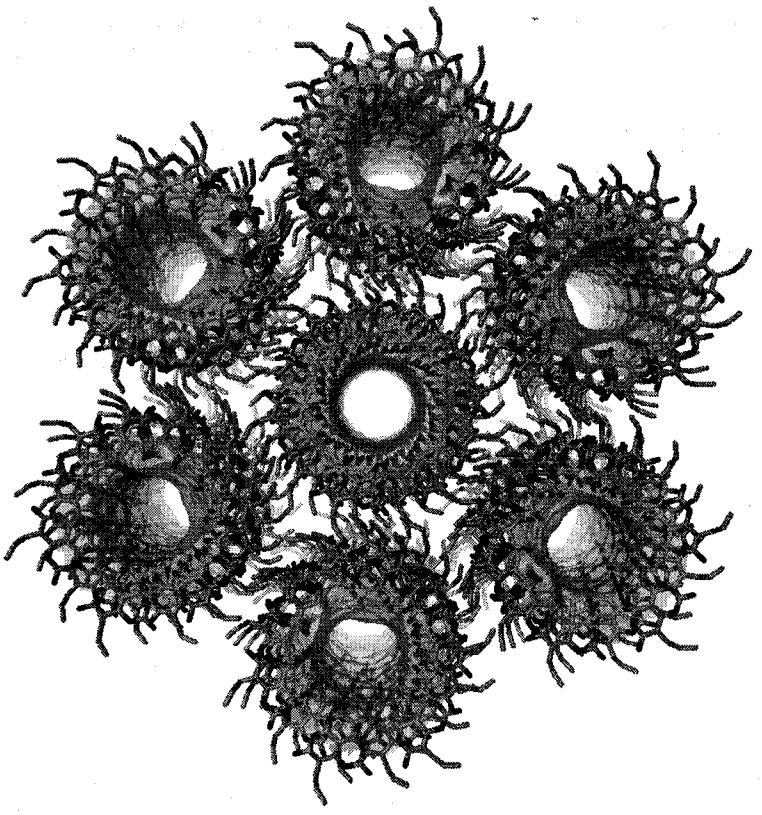

Figure 3.21. Hydrophobic interactions between the RNTs of **23**.

3.10. Self-Assembly of G^C Base **23** in Methanol and Acetonitrile

Out of the three motifs that were studied, only **23** self-assembled in other solutions aside from aqueous solution. This again could be due to its highest hydrophobic outer surface. It self-assembled in both methanol and acetonitrile, which are polar protic solvents. Single RNTs were observed by SEM within a day of self-assembling in methanol and long bundles were observed at above 5 days (Figure 3.22).

Both short and long nanorods were observed after two days of assembly in acetonitrile (Figure 3.23). No other morphology was observed in acetonitrile at all concentrations studied (0.05 to 0.7 g/L).

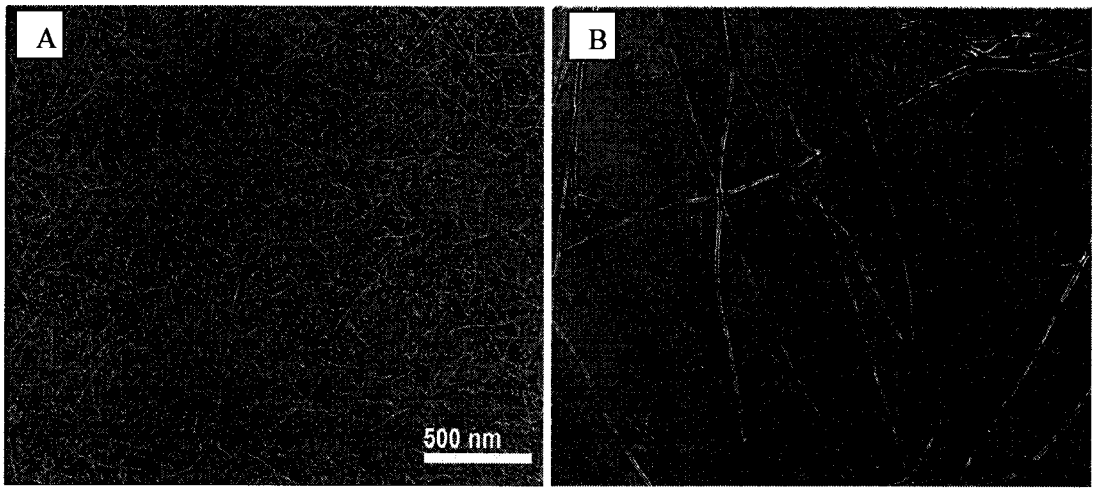

Figure 3.22. SEM micrographs obtained from the assembly of **23** in methanol at (A) 1 d (B) 5 d. The samples were drop cast on carbon grids at indicated time intervals from stock solution.

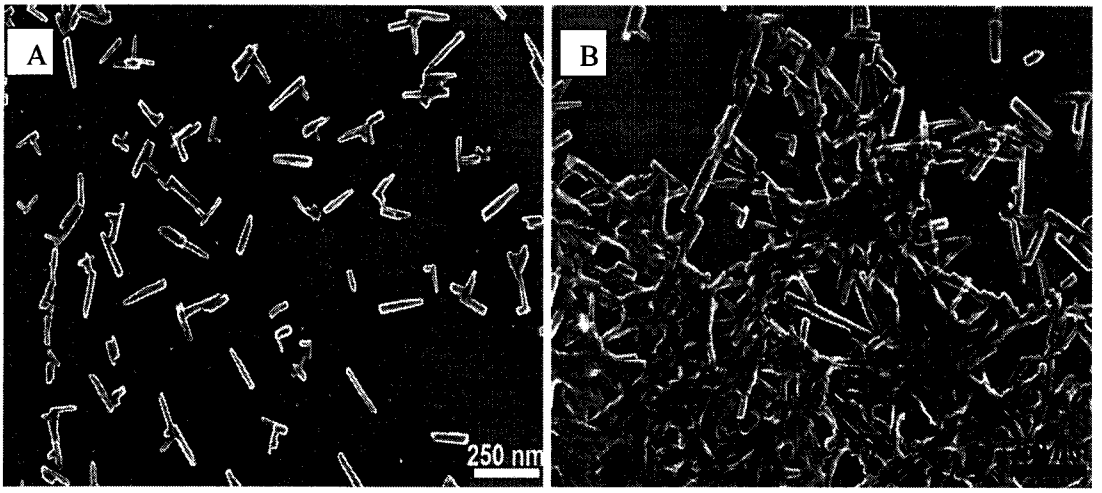

Figure 3.23. SEM micrographs obtained from two days assembly of **23** in acetonitrile showing (A) short nanorods (B) long and short nanorods. The sample was dropcast on carbon grid.

3.11. Molecular Modeling and Association Free Energies

Molecular modeling of the three motifs were performed to estimate their theoretical diameters in water and to check whether theory (solvation and association free energies) support the observed self-assembly of the motifs as shown by SEM, TEM, TM-AFM, UV-Vis and DLS experiments.

The estimated outer diameter of the most stable rosette conformations of G^C base **22**, **23** and **24** in water were 2.22, 2.81 and 2.7 nm respectively (Figure 3.24). Since **22**, was the first to be synthesized and self-assembled, we were compelled to compare the stability of its RNT with similar module using Lehn's precursor, **39** (Figure 3.25). The rosette stacks of **22** and **39** in water were constructed and their internal energies, solvation free energies and association free energies (Kcal/mol) were calculated. The difference between the association free energy of **22** and **39** showed that **22** would form tube more efficiently than **39**.

(A)

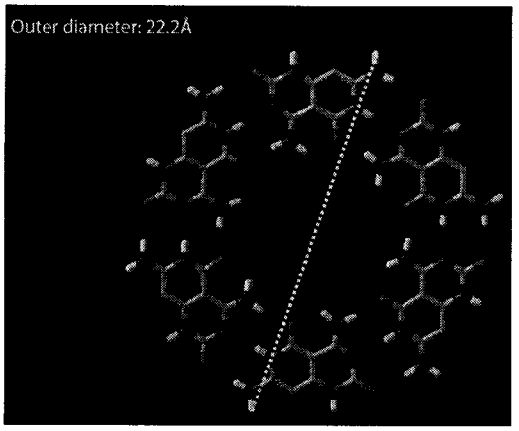

(B)

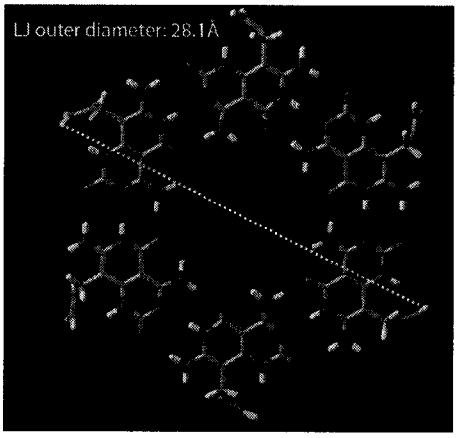

(C)

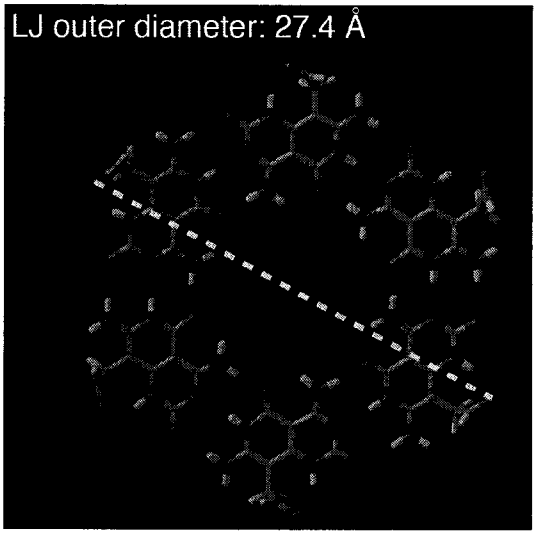

Figure 3.24. Molecular modeling estimation of the outer diameters of the rosette of (A) **22,** 2.22 nm (B) **23,** 2.81 nm (C) **24,** 2.74 nm

(A)

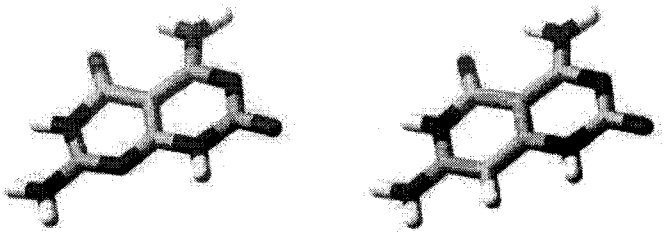

39 22

(B)

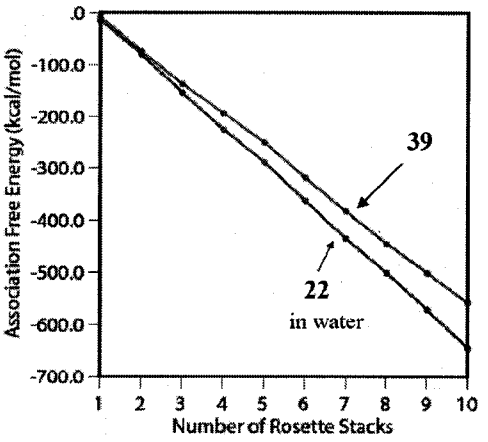

Figure 3.25. (A) MacroModel of **39** and **22**; (B) Association free energies of **39** and **22** in water.

Eight initial conformations of RNTs were generated each with stacking distance of 3.7 A° for **23** and **24** respectively based on the modeling study of similar motif with n-propane side chain. Association free energies of stacking for the most stable RNT conformation of **23** in water and methanol were negative, which suggested that **23** will form RNTs in both solvents (Figure 3.26). Similarly, the association free energies of stacking for the most stable RNT conformation of **24** in water was negative (Figure. 3.27). SEM, TEM and AFM results support these calculations.

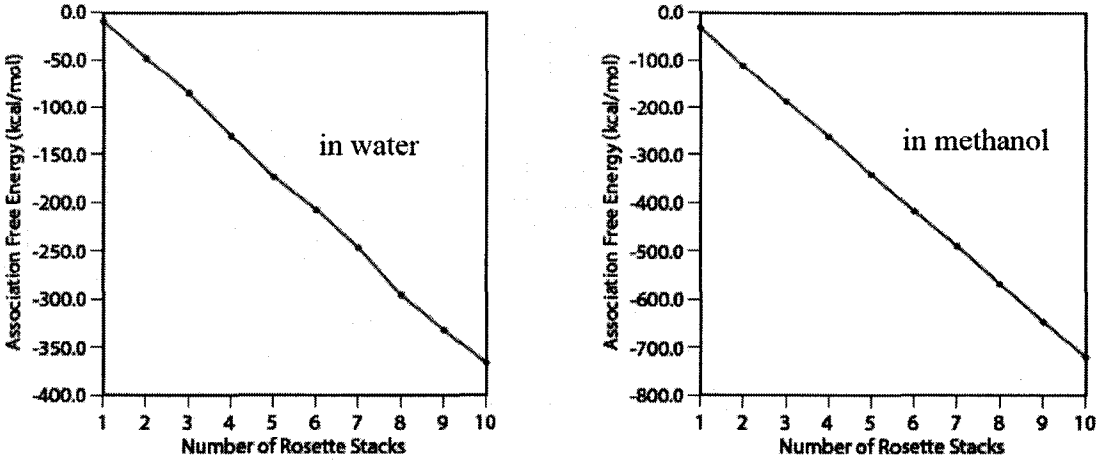

Figure 3.26. Association free energies of **23** in water and in methanol respectively.

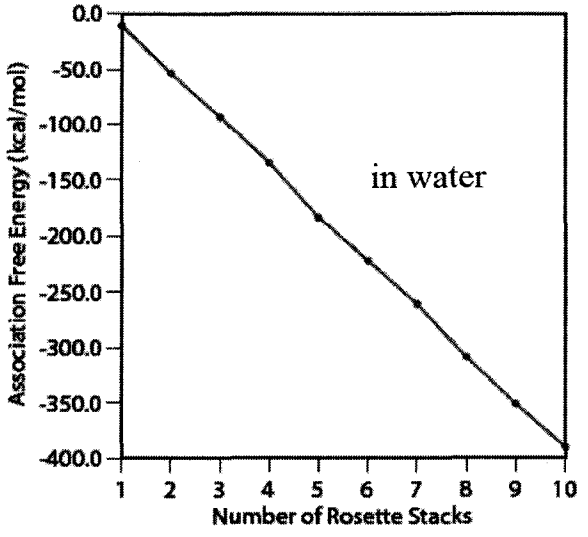

Figure 3.27. Association free energies of **24** in water.

3.12. Preliminary Studies of the Three G^C Motifs

3.12.1. Acid-Mediated G^C Base Sheets Formation in Solution.

The pH of the three motifs was obtained to be between 8.10- 8.50 in water using electronic pH meter. We were interested in knowing what would happen to the self-assembly process if the pH of the G^C base was reduced to below 3.00 by adding acid to their aqueous solutions. Addition of one equivalent of 33% hydrobromic in acetic acid to **22** resulted in the protonation of one its ring nitrogens which takes part in intermolecular hydrogen bonding as revealed by low temperature ^{1}H NMR studies (Figure 3.28) in DMF. The protons were assigned using cyclonoe ^{1}H NMR experiments. The protonation changed the hydrogen bonding pattern of the G^C base from ADD-DAA to ADD-DDA. As expected the protonated **22** did not form RNT when self-assembled in water (above one day) instead it formed layers of sheets as shown by SEM (Figure 3.29). The same experiment was done using two equivalents of Hydrochloric acid for **23** and **24** and both showed similar laminar structures when studied by SEM after a day of assembly in solution. As illustrated in Figure 3.30, the protonated G^C base could also be self-complementary held together by four intermolecular hydrogen bonds to form tape. Tapes would then pack into sheet with their long axes parallel and the stacking of the sheet would form the three-dimensional laminar structures observed by SEM.

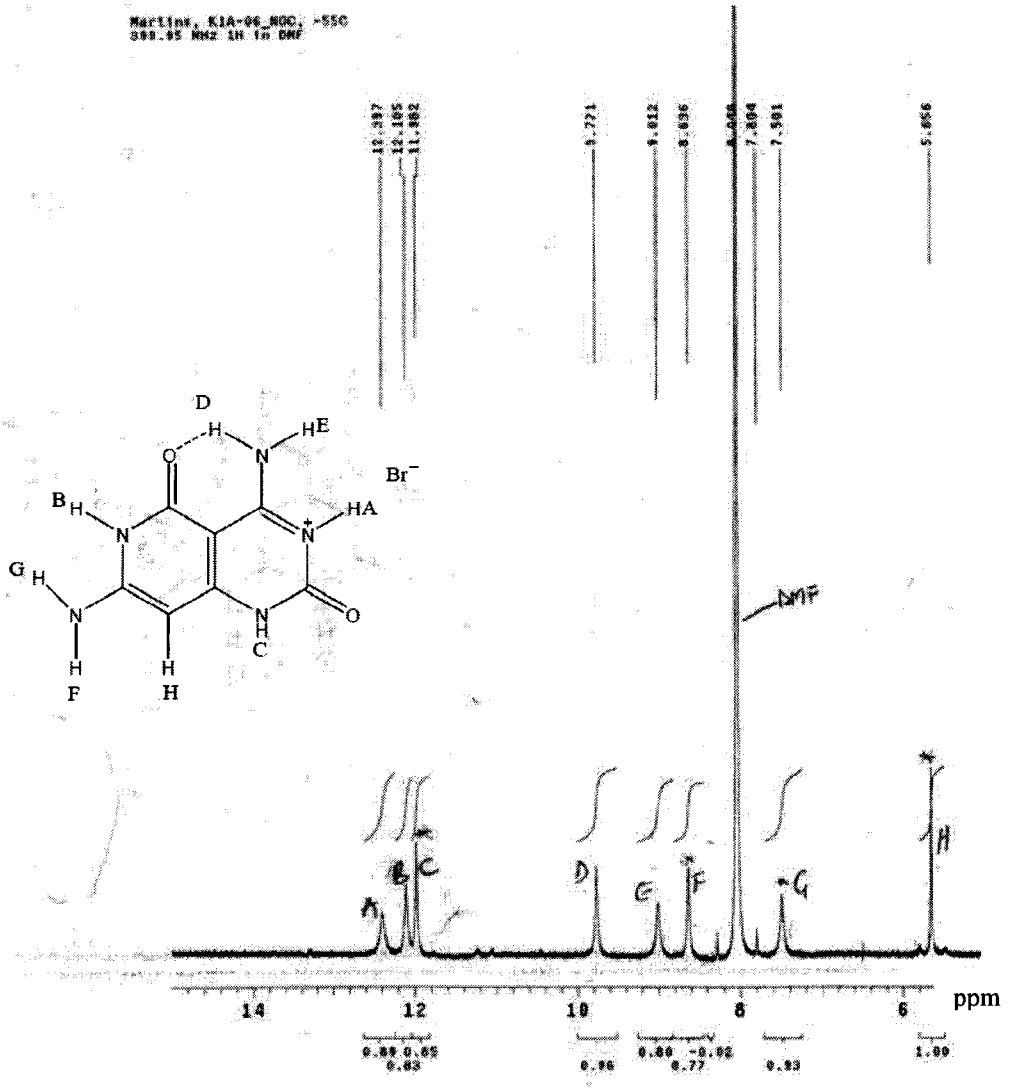

Figure 3.28. ^{1}HNMR of protonated **22** in DMF at -55°C

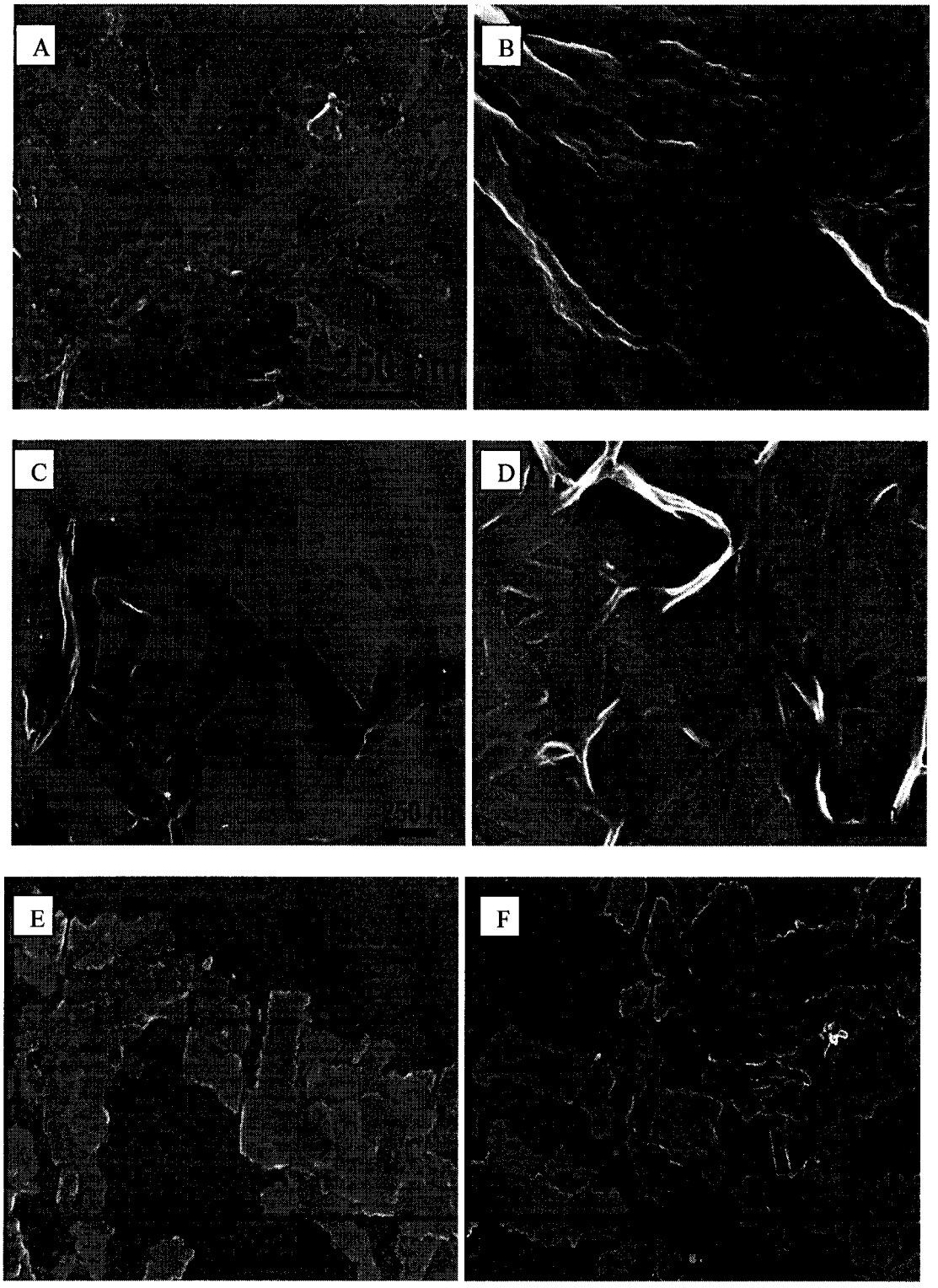

Figure 3.29. SEM micrographs of protonated **22** (A, B), **23** (C, D) and **24** (E, F). The samples were drop cast on carbon grids after 1 day in all cases.

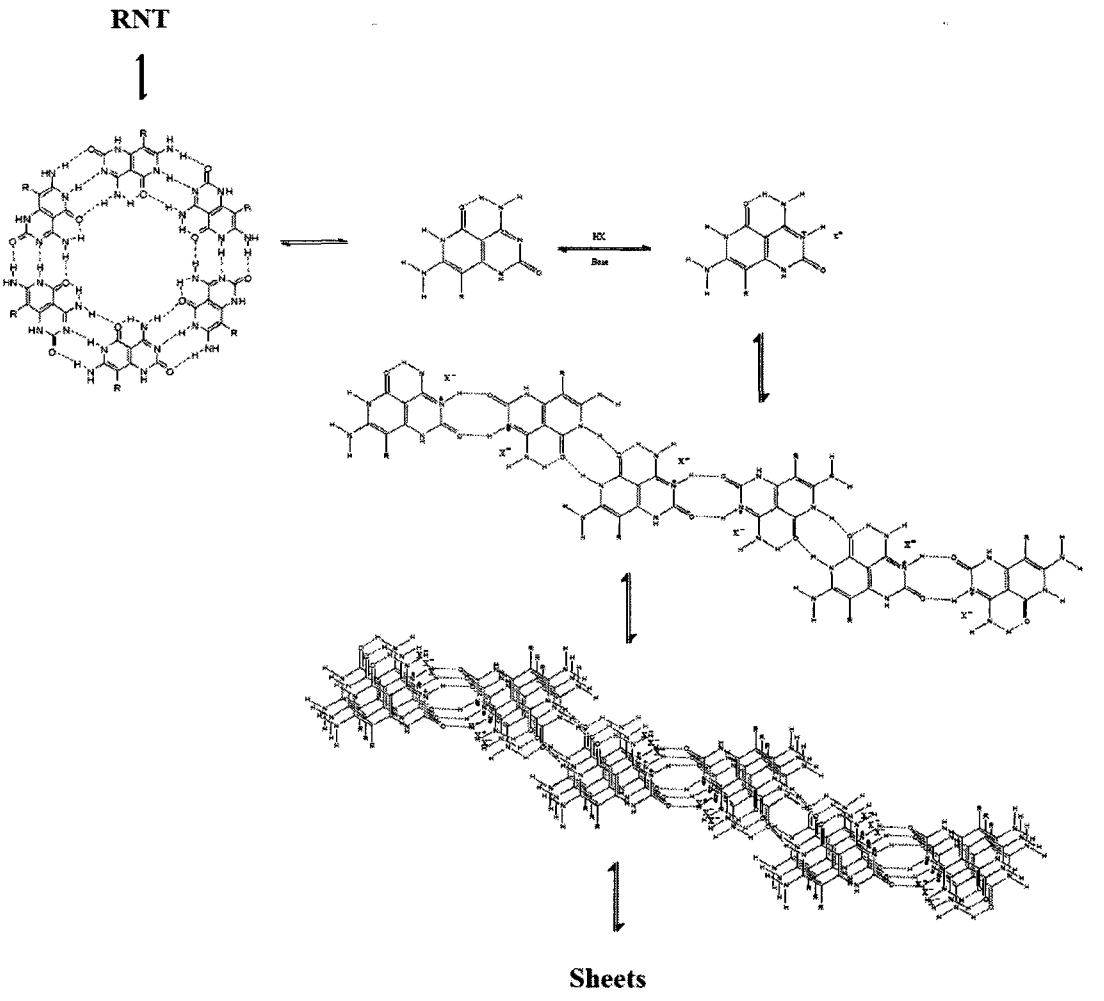

Figure 3.30. Proposed mechanism of acid-mediated G^C base sheets formation.

3.12. 2. Rosette Nanotube Templated Synthesis of Silver Nanowires

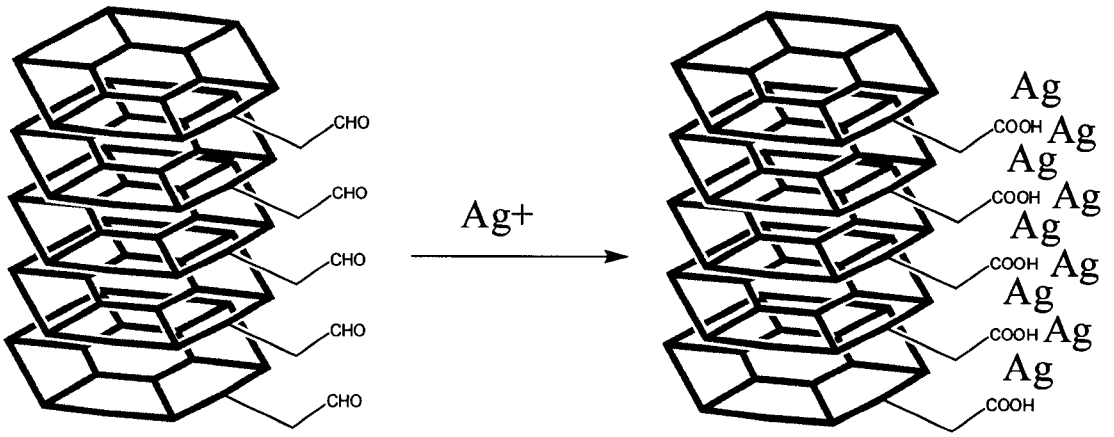

Figure 3.31. Tollen's qualitative test on self-assembled **24**.

DNA metallization procedures were developed in order to increase the conductivity of subsequent DNA nanostructures, thereby enabling their use as molecular wires. We reasoned that it may be possible to program selective metallization process to occur on the RNTs of **24** in aqueous since its morphology is stable in solution. Silver metallization was chosen because **24** has aldehyde group, which can be oxidized to carboxylic acid using Tollen's reaction (Figure 3.31). $AgNO_3$ was added to an aqueous solution of self-assembled **24** to oxidize the aldehyde to carboxylic acid group. Ag(1) was reduced to Ag(0) to complete the oxidation process, which was then deposited on the resulting carboxylic acid groups. The use of $Ag(NH_3)_2OH$ solution (Tollen's reagent) was found to disrupt the self-assembly of **24**. The effectiveness of the silver deposition process by $AgNO_3$ was revealed by SEM (Figure 3.32). Ag(0) neatly deposited on the outside wall of the RNTs where the

oxidation reaction had occurred. There was no isolation of the silver metal from the RNTs. **24**, can thus serve as a template for supramolecular nanowire in solution.

This is a preliminary investigation and further study should be carried out on the silver deposition method. All attempts to deposit silica on the RNTs tubes of G^C bases **22-24** were unsuccessful.

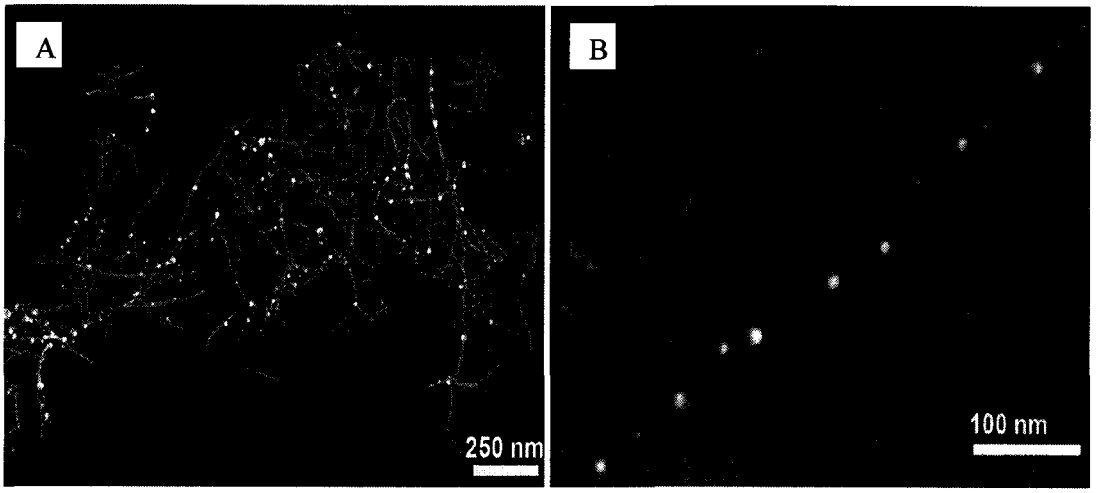

Figure 3.32. SEM micrographs of silver deposition on the RNT of **24** (A) low resolution image showing RNT with Ag(0) deposition (B) high resolution image showing Ag(0) on RNT. The sample was drop cast on carbon grid.

100 μL of 57 μM aqueous solution of $AgNO_3$ was added to 1.00 mL of 0.57 μM aqueous solution of **24**. The solution was heated to boiling and allowed to cool to room temperature for an hour. After that it was drop cast on 600 mesh carbon coated copper grid, dried in vacuum and imaged and the above images were obtained.

3.13. Hydrogen Bond Mediated Tape and Sheet Formation in Solid-State

The X-ray crystallographic studies showed that nitrile **33**, self-assembled into three-dimensional solid structure mediated by hydrogen bonds and π-π stacking interactions.[11,12] **33**, are held through two pairs of NH...N intermolecular bonds (Figure 3.33). The NH...H bond lengths are described in Table 3.1. The continuous alternating sequence of the molecule resulted in W-tape (Figure 3.34), which then packed into sheet with their long axes parallel. The stacking of the sheet gave the 3-D solid structure. It was observed that the opposite face of the pyridyl ring is blocked by the allyl group of an adjacent molecule related by the crystallographic inversion center (1/2, 1/2, 1/2) (i.e. the closest contact distance is 2.82 Å, between C6 and the hydrogen H9B generated by the symmetry operation (1–x, 1–y, 1–z)). The distance between planes of nearest neighbour "stacked rings" is 3.50 Å (D_{plane}) and the distance between centroids of nearest neighbour 'stacked' rings is 3.54 Å (D_{cent}) resulting in an offset angle of 8.62° between stacks rings (Figure 3.35).

The view of two tapes with their long axes parallel (Figure 3.34B) suggest that if designed properly with the right hydrogen bond information, an analogue of **33**, could form hexameric rosette (Figure 3.36).

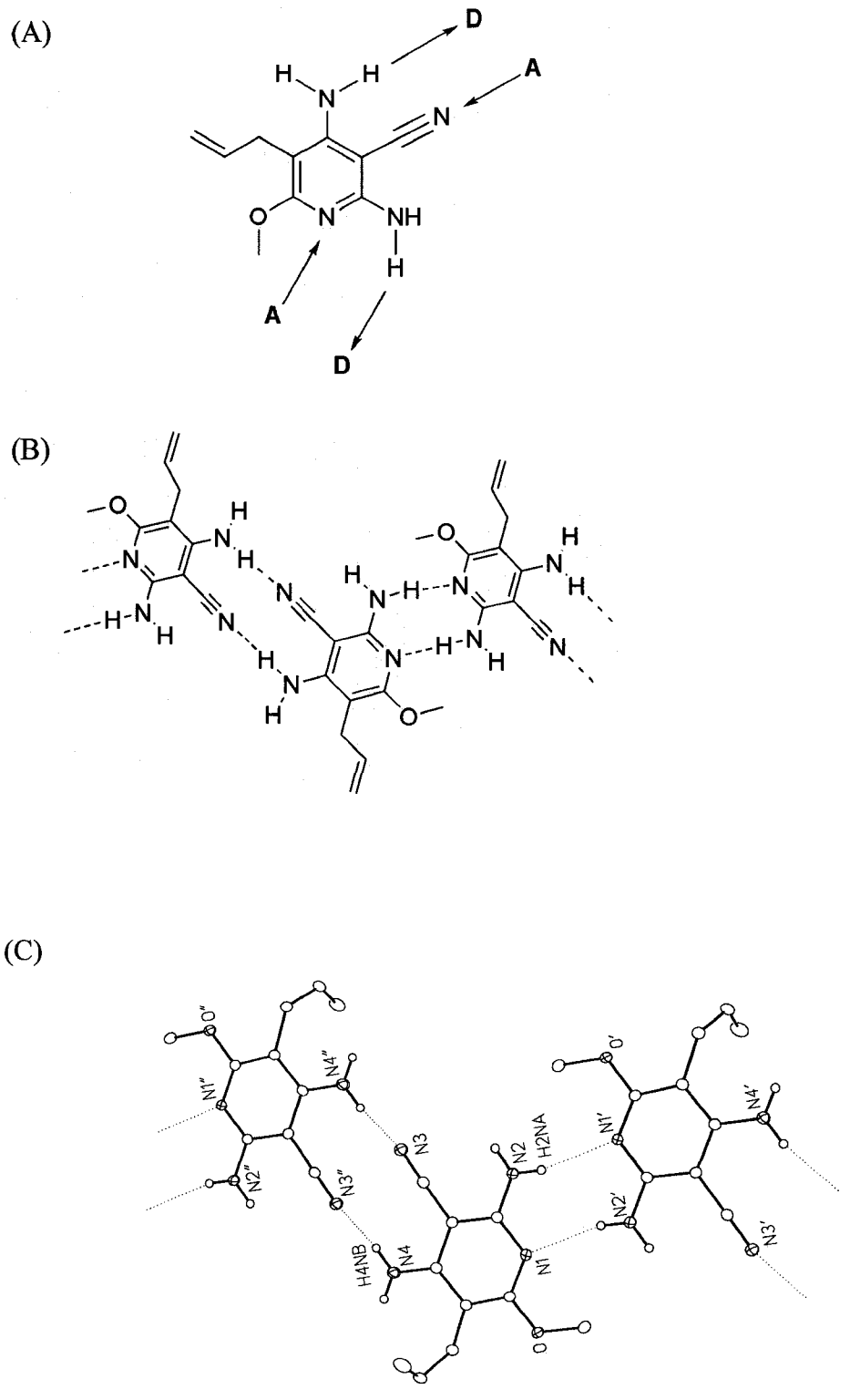

Figure 3.33. (A and B) Self-complementary hydrogen bond pattern of **33**, (C) ORTEP view of hydrogen bonds mediated tape formation.

(A)

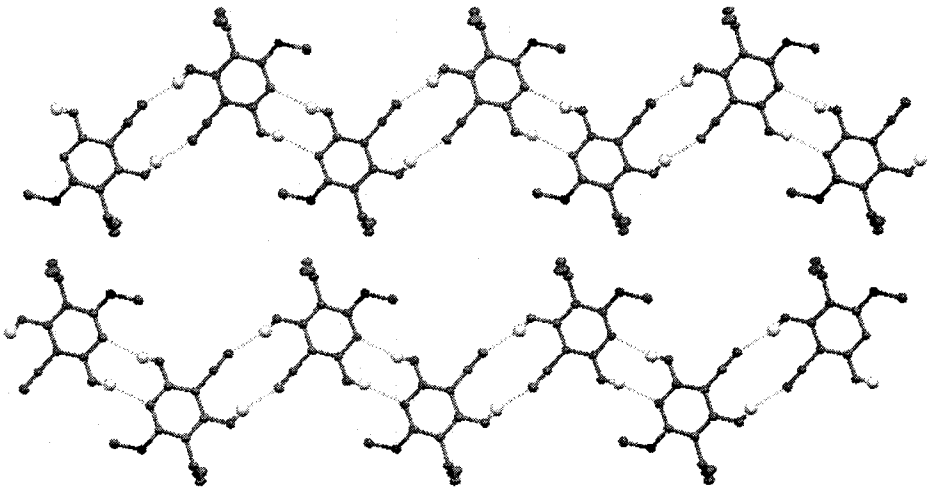

(B)

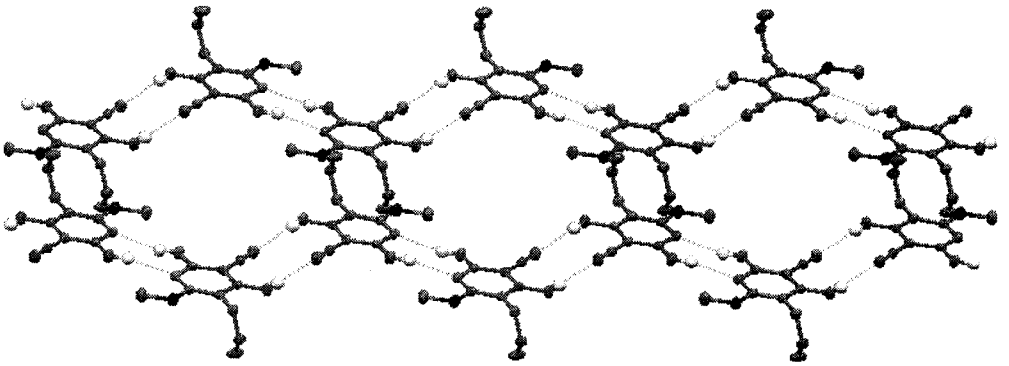

(C)

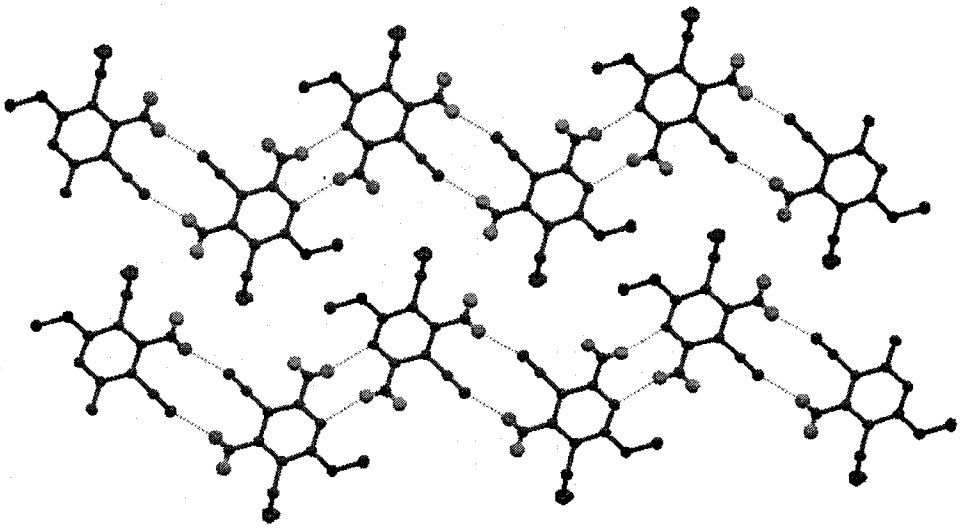

(D)

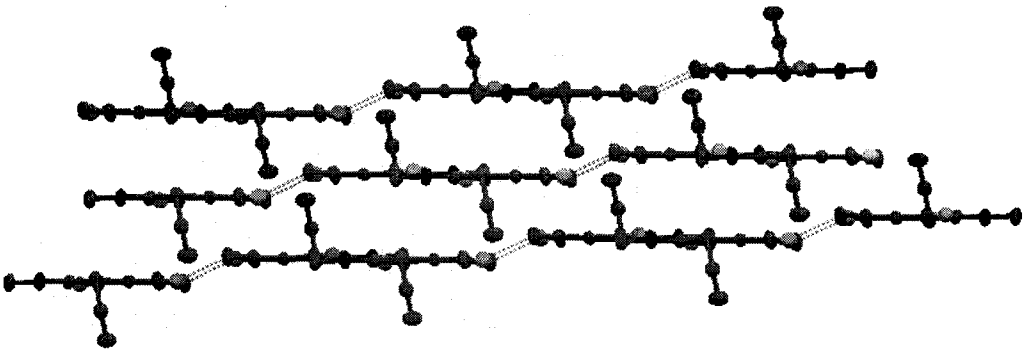

Figure 3.34. Crystal structures of **33**. (A and B) top views of two tapes in the same plane with their long axes parallel to form sheet (C) top view of the stacking of the sheet into 3-D solid (D) side view of the stacked 3-D solid structure.

Table 3.1. Hydrogen-Bonded Interactions of **33**.

D–H···A	D–H (Å)	H···A (Å)	D···A (Å)	∠D–H···A (deg)	Note
N2–H2NA···N1[a]	0.88	2.33	3.1875(14)	163.9	[a]At 1–x, $\bar{y}$, $\bar{z}$
N4–H4NB···N3[b]	0.88	2.28	3.0650(14)	148.3	[b]At $\bar{x}$, 1–y, $\bar{z}$

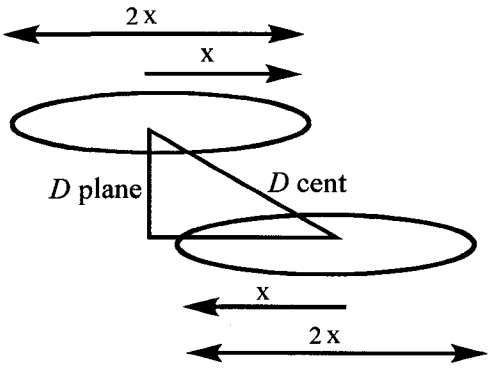

Offset angle = $\cos^{-1}[D_{plane}/D_{cent}]$

Figure 3.35. Illustration of offset angle calculation in stacked rings.

(A)

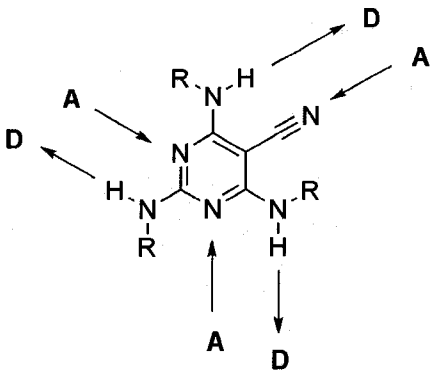

(B)

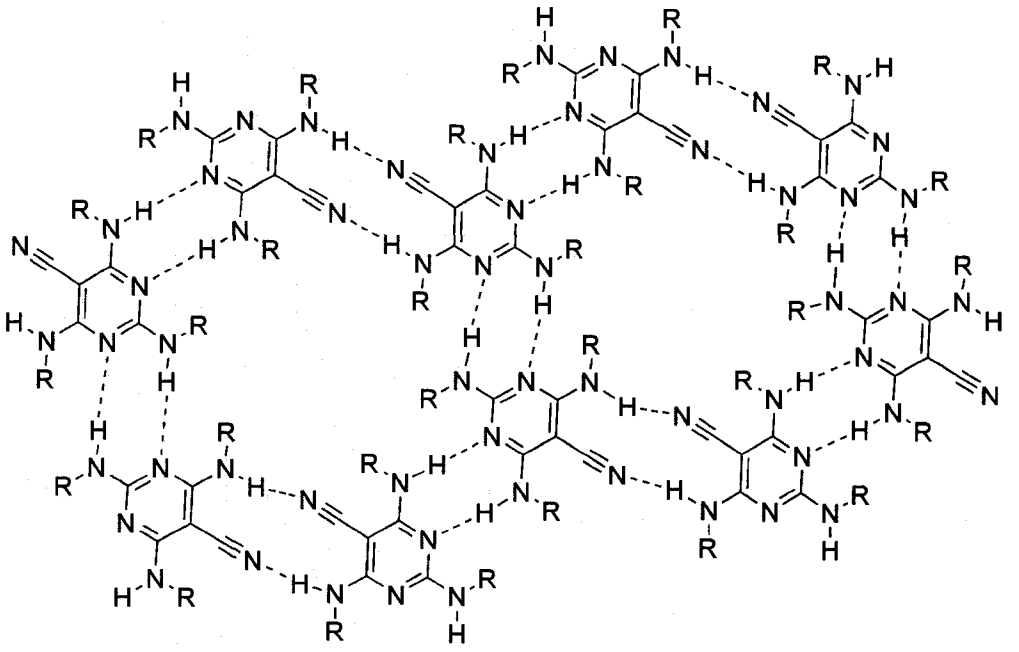

Figure 3.36. Proposed self-complementary motif that could form hexameric rosette based on Figure 3. 34B.

3.14. Conclusion

We have demonstrated that (1) G^C bases **22-24** modeled after Mascal's G^C base precursors self-assembled, forming tubes in solution, (2) the presence of sp^2 carbon in the G-ring of the G^C motifs do not prevent self-assembly, (3) the morphologies of the tubes in solution can be tuned synthetically by putting a hydrophobic or hydrophilic tail on the G^C base, (4) hydrophobic interaction is the driving force for the bundling of RNTs.

We have also shown that with pH control, the RNTs can be opened to form sheets or laminar structures. A novel self-complementary compound forming supramolecular tape and sheet was also synthesized and fully characterized by X-ray crystallography in solid state.

Preliminary investigation has shown that aldehyde functionalized RNT can serve as a good template for silver metal deposition, which in turn can serve as a nanowire. A comprehensive study should be carried out on the silver templated nanowire, which includes the optimization and conductivity measurement.

I recommend that different analogs and functionalization of these G^C base motifs should be designed. The use of G^C base motifs that required short synthetic steps to design have provided us with plenty of time for studying their self-assembly and to seek applications for them. I hope researchers working on the self-assembly of RNTs will study all the different morphologies shown by G^C bases **22-24** separately and research their relevance to the future of nanotechnology and supramolecular chemistry.

3.15. Experimental Details

3.15.1. Physical Studies

1. AFM imaging. RNT samples were prepared by dissolving the compounds in appropriate solvent, heating the sample to the boiling point, then allowing the solution to cool to room temperature. Samples for AFM imaging were prepared in a Class 10000 Clean Room by casting a 25 μL drop on 10×10 mm^2 freshly peeled Mica grade V-4 (SPI supplies) substrates on a Cookson G3-8 Desk-Top Precision Spin Coating System. AFM measurements were performed in tapping mode (TM–AFM) at a scan rate of 2 Hz per line using a Digital Instruments/Veeco Instruments MultiMode Nanoscope IV equipped with an E scanner. Silicon cantilevers (MikroMasch USA, Inc.) with spring constants of 40 N/m were used.

2. TEM/SEM imaging. Samples for transmission electron microscopy (TEM) and scanning electron microscopy (SEM) were prepared by placing a carbon–coated 400–mesh copper grid on a droplet of RNT (G^C bases **22-24**) for 25 s, blotting excess sample, then staining by placing the grid on a droplet of uranyl acetate (2% in water) of for 20 s. The grid was then blotted and dried at 100°C under reduced pressure prior to imaging. TEM imaging was performed on a JEOL 2010 microscope operating at 200 kV. SEM images were obtained without negative staining, at 5 kV accelerating voltage and a working distance of 3.0 mm on a high resolution Hitachi S–4800 cold field emission SEM.

3. DLS measurements. Dynamic Light Scattering (DLS) experiments were performed on a Malvern Zetasizer Nano S working at a 90° scattering angle at 25°C. The instrument is equipped with a 40 mW He–Ne laser (λ = 633 nm) and an

avalanche photodiode detector. Size distributions were calculated using an inverse Laplace transform algorithm, and the hydrodynamic radii were calculated using the Stokes–Einstein equation. All samples were filtered through 0.2 μm nonsterile PVFD membranes (Whatman filters) prior to measurement.

3.15.2. Synthetic Procedures

2-aminoprop-1-ene-1,1,3-tricarbonitrile, N-(chlorocarbonyl)isocyanate, 7N NH_3 in methanol and acetic anhydride were obtained from Aldrich. Methanol and dichloromethane were dried with solvent purification system. N-(chlorocarbonyl) isocyanate and acetic anhydride were freshly distilled before use. Thin layer chromatography (TLC) was performed on UV_{254} pre-coated TLC plates. Proton and carbon nuclear magnetic resonance (^1H NMR) spectra were recorded on 100 to 600 MHz spectrometers. Melting points were recorded on a Büchi capillary melting point apparatus (model B–545). Mass spectrometric analysis was performed by positive mode electrospray ionization on either a Micromass ZabSpec Hybride Sector-TOF or a PerSeptive Biosystems Mariner Biospectrometry Workstation (Mass Spectrometry Laboratory at the Department of Chemistry, University of Alberta).

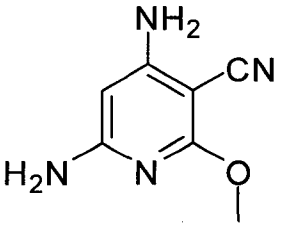

26

Synthesis of **26**.

Compound **25** (10.0 g, 75.7 mmol) was added to a solution of sodium methoxide prepared from sodium metal (15.7 g, 681.1 mmol) and methanol (350 mL). The resulting suspension was refluxed for 72 h. The solvent was evaporated under reduced pressure. Distilled H_2O (400 mL) was added to the residue and cooled in an ice-bath for 4 h. The precipitate formed was filtered under vacuum, washed with H_2O (50 mL). 10% citric acid (~ 400 mL) was used to wash the residue while maintaining the pH between 1-1.5. The undissolved precipitate was washed with H_2O (100 mL) and dried under vacuum overnight. The crude product was recrystallized in dichloromethane to give **26** (10.8 g, 87.0%). mp 179-180°C; R*f* = 0.36 (2% CH_3OH: DCM); ^{1}H NMR (400 MHz, DMSO-d_6) δ 3.75 (s, 3H), 5.31 (s, 1H), 6.16 (s, 2H), 6.22 (s, 2H); ^{13}C NMR (100 MHz, DMSO-d_6) δ 52.9, 67.5, 82.5, 116.7, 158.4, 160.2, 165.7; IR (microscopic) 1553.0, 1638.6, 1656.2, 2200.3, 2962.3, 3244.4, 3339.3, 3402.4, 3433.6, 3511.5 cm^{-1}; HRMS (ESI) calcd for $C_7H_9N_4O$ (M+1) *m/z* 165.0771, found 165.0772.

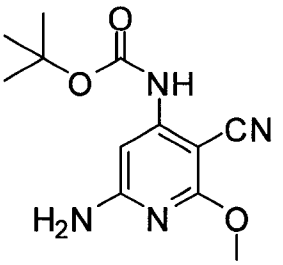

28

Synthesis of **28**.

DMAP (3.0 g, 24.4 mmol) and Et_3N were added to a solution of **26** (1.0 g, 6.0 mmol) in THF at r.t. followed by Di-*tert*-butyl dicarbonate (8.7 g, 30.5 mmol). After stirring the solution for 24 h, it was concentrated under reduced pressured and the residue dissolved in EtOAc followed by 10% citric acid wash (3 × 15 mL). The organic solvent was washed with saturated aq. $NaHCO_3$, followed by H_2O and then concentration. TFA (0.3 mL, 3.0 mmol) was added to the product in DCM (10 mL) at r.t and then stirred for 22 h before evaporating the solvents under reduced pressure. Diffraction quality single crystal of **28** (0.8 g, 50%) was obtained upon recrystallization in $CHCl_3$ and hexane. X-ray crystallography confirmed the structure (Figure 3.4). R*f* = 0.4 (30% EA: Hexane); ^{1}H NMR (400 MHz, DMSO-d_6) δ 1.39 (s, 9H), 5.29 (s, 1H); ^{13}C NMR (100 MHz, DMSO-d_6) δ 27.5, 114.6, 54.1, 80.1, 149.2, 81.5, 71.3, 159.8, 164.1, 166.2. MS(ESI) $C_{12}H_{17}N_4O_3$ (M+1)/*z* 265.2.

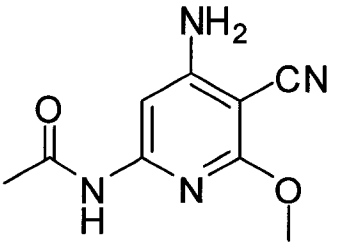

29

Synthesis of **29**.

Triethylamine (13.6 mL, 97.5 mmol) and DMAP (1.5 g, 12.2 mmol) was added to a solution of **26** (4.0 g, 24.4 mmol) in dry THF (170 mL). The reaction mixture was stirred under argon at rt for 5 minutes before adding freshly distilled Ac_2O (6.9 mL, 73.1 mmol). The solution was further stirred for 48 h under argon at r.t. The reaction was quenched with saturated aq. $NaHCO_3$ (10 mL) and the solvent was evaporated under reduced pressure. The resulting oily residue was dissolved in DCM (150.0 mL) and washed with H_2O (15 mL), 10% citric acid (3× 20 mL), H_2O (10 mL), 2.5% HCl (4× 20 mL), saturated aq. $NaHCO_3$ (2× 15 mL), H_2O (2× 15 ml), brine (15 mL) and dried over Na_2SO_4 before evaporating the solvent. The crude compound was recrystallized in DCM and hexane to give **29** (2.1 g, 52%). mp 232-234°C; R*f* = 0.36 (2% CH_3OH: DCM); ^1H NMR (400 MHz, DMSO-d_6) δ 2.17 (s, 3H), 3.95 (s, 3H), 7.00 (s, 2H), 7.29 (s, 1H), 10.22 (s, 1H); ^{13}C NMR (100 MHz, DMSO-d_6) δ 23.9, 53.4, 72.4, 90.9, 114.9, 151.4, 159.8, 164.2, 169.3; IR (microscopic) 1582.2, 1617.9, 1651.0, 1693.8, 2205.1, 2960.3, 3217.5, 3326.7, 3440.4 cm^{-1}; HRMS (ESI) calcd for $C_9H_{10}N_4O_2Na$ (M+Na) *m/z* 229.0696, found 229.0694.

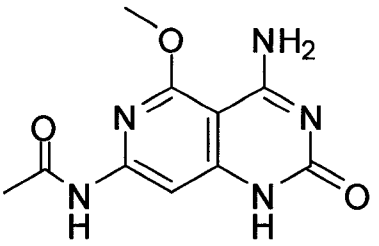

30

Synthesis of **30**.

N-(chlorocarbonyl) isocyanate (2.3 mL, 28.9 mmol) was added to a solution of **29** (1.5 g, 7.2 mmol) in dry DCM (70 mL). The solution was stirred at r.t. for 4 h under argon. Saturated aq. $NaHCO_3$ (20 mL) was then added and the resulting precipitate was vacuum filtered and washed with H_2O and CH_3OH and then dried. The residue was dissolved in 7N NH_3 in methanol and stirred at r.t. under inert argon for 6 days. The solvent was evaporated under reduced pressure. The product was then precipitated in CH_3OH to give **30** (1.3 g, 85%). ^1H NMR (300 MHz, DMSO-d_6) δ 2.14 (s, 3H), 4.03 (s, 3H), 7.46 (s, 1H), 7.51 (s, 1H), 7.90 (s, 1H), 10.41 (s, 1H), 10.88 (s, 1H); ^{13}C NMR (100 MHz, DMSO-d_6) δ 24.1, 53.9, 89.0, 90.8, 150.9, 153.1, 155.3, 159.5, 161.7, 169.4; IR (microscopic) 1523.7, 1611.1, 1702.8, 3010.9, 3418.1 cm^{-1}; HRMS (ESI) calcd for $C_{10}H_{12}N_5O_3$ (M+H) *m/z* 250.0935, found 250.0937.

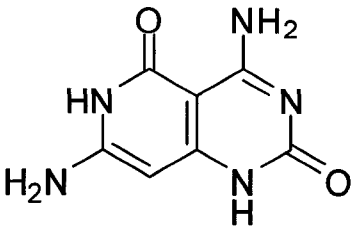

22

Synthesis of **22**.

A solution of **30** (0.5 g, 2.4 mmol) in 33% HBr-HOAc (40.0 mL) was refluxed overnight and then carefully poured into a mixture of saturated aq $NaHCO_3$ (300.0 mL) and ethyl acetate (50.0 mL). The resulting precipitate was filtered and washed with H_2O (× 3) followed by ethyl acetate (× 3) and then dried. 7N NH_3 in methanol was added to the dry residue and stirred at rt for 1 h. The solvent was evaporated and CH_3OH (20.0 ml) was added to the crude solid, filtered and washed with H_2O (50.0 mL). The solid was then precipitated in 95% ethanol to give **22** (0.4 g, 75.0%). ^1H NMR (400 MHz, DMSO-d_6) δ 5.37 (s, 1H), 7.46 (br, 2H), 8.18 (s, 1H), 9.33 (s, 1H), 11.44 (s, 1H), 11.58 (s, 1H); ^{13}C NMR (100 MHz, DMSO-d_6) 76.7, 82.5, 147.9, 152.4, 155.9, 157.3, 161.2; IR (microscopic) 1455.2, 1593.9, 2927.6, 3126.4, 3313.1, 3744.0 cm^{-1}; HRMS (ESI) calcd for $C_7H_8N_5O_2$ (M+H) *m/z* 194.0673, found 194.06743; calcd for $C_{14}H_{15}N_{10}O_4$ (2M+H) *m/z* 387.1272, found 387.1271; calcd for $C_{21}H_{22}N_{15}O_6$ (3M+H) *m/z* 580.1872, found 580.1875.

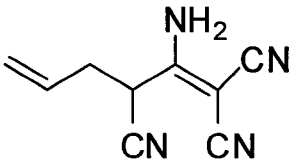

31

Synthesis of **31**.

DIPEA (52.7 mL, 303 mmol) was added to a solution of 2-amino-1,1,3-tricyanopropene **25** (20.0 g, 151 mmol) in DME (350 mL) and then stirred at r.t. for 30 min. Allylbromide (14.1 mL, 167 mmol) was subsequently added and the mixture was stirred at r.t. for an additional 24 h. The precipitated ammonium salt was filtered off and washed with 50 mL of DME. The solvent was evaporated and the brown oily residue was dissolved in 300 mL of DCM then washed with 0.5M HCl (3 × 20 mL), followed by 30 mL of saturated aq. $NaHCO_3$ (2 × 30 mL) and with brine (30 mL). The acid wash was extracted with 30.0 mL of DCM and the combined organic extract was dried over anhydrous Na_2SO_4 and filtered. The solvent was evaporated to give yellow crude solid. Automated flash chromatography (combiflash) with maximum 70% EtOAc (separate bottles of EtOAc and hexane) was used to purify the product, which gave **31** (20.8g, 80.0%). R*f* = 0.46 (1:1 EtOAc: Hexane); ^{1}H NMR (400MHz; DMSO-d_6) δ 2.47-2.76 (2H, m), 4.07 (1H, t, *J* = 8Hz), 5.17-5.22 (2H, m), 5.65-5.75 (1H, m), 8.91 (1H, s), 8.96 (1H, s); ^{13}C NMR (100MHz, DMSO-d_6) δ 34.36, 34.38, 49.83, 114.11, 115.02, 116.34, 119.79, 131.57, 167.03; FTIR (microscopic) 1644.9, 1673.0, 2165.4, 2217.7, 2260.1, 2940.2, 2985.5, 3199.1, 3349.0 cm^{-1}; Anal. Calcd for

$C_9H_8N_4$: C, 62.78; H, 4.68; N, 32.54. Found C, 62.78, H, 4.68, N, 32.54; HRMS (EI) calcd for $C_9H_8N_4$ (M+H) *m/z* 172.0749, found 172.0753.

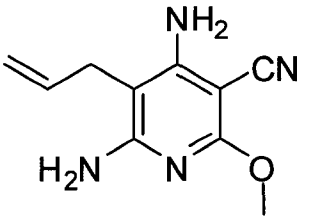

32

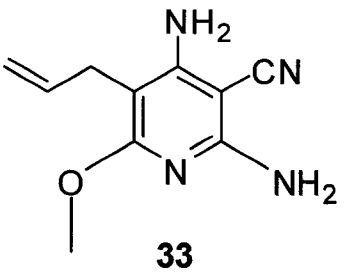

33

Synthesis of **32** and **33**.

A solution of **31** (7.1 g, 41 mmol) in dry CH_3OH (200 mL) was treated with powdered sodium methoxide (22.3 g, 414 mmol) and the mixture was refluxed for 48 h. The solution was then cooled and was solvent evaporated. Distilled water (250 mL) was added and the product was extracted with of DCM (3 × 80 mL). The combined organic extracts were evaporated and the product was then purified by automated flash chromatography (combiflash) with maximum of 70% EtOAc (separate bottles of EtOAc and hexane) to provide **32** as yellow solid (3.5 g, 41%) and **33** as a white solid (4.9 g, 59.0%).

32: R*f* = 0.37 (1:1 EtOAc: Hexane); ^{1}H NMR (400MHz; DMSO-d_6) δ 3.07-3.08 (2H, m), 3.76 (3H, s), 4.89-4.92 (1H, m), 5.01-5.05 (1H, m), 5.65-5.88 (1H, m), 5.88 (2H, s), 6.06 (2H, s); ^{13}C NMR (100MHz, DMSO-d_6) δ 26.9, 52.8, 68.19, 90.2, 114.3, 116.9, 134.7, 155.6, 157.9, 163.7; FTIR (microscopic) 1587.2, 1630.9, 2195.3, 2211.8, 2922.7, 2955.4, 2982.6, 2996.0, 3008.4, 3249.6, 3348.3, 3377.2, 3459.9,

3482.6 cm^{-1}; HRMS (ESI) calcd for $C_{10}H_{13}N_4O$ (M+1) *m/z* 205.10839, found 205.10831.

33: R*f* = 0.52 (1:1 EtOAc: Hexane); ^1H NMR (400MHz; DMSO-d_6) δ 3.05-3.08 (2H, m), 3.72 (3H, s), 4.85-4.96 (2H, m), 5.66-5.76 (1H, m), 5.91 (2H, s), 6.16 (2H, s); ^{13}C NMR (100MHz, DMSO-d_6) δ 26.2, 53.1, 68.7, 90.7, 113.9, 117.1, 135.7, 155.7, 158.9, 163.0; FTIR (microscopic) 1577.7, 1634.2, 2200.2, 2959.2, 2978.4, 3008.4, 3052.9, 3089.5, 3243.3, 3359.3, 3465.7, 3490.4 cm^{-1}; HRMS (ESI) calcd for $C_{10}H_{13}N_4O$ (M+1) *m/z* 205.10839, found 205.10831.

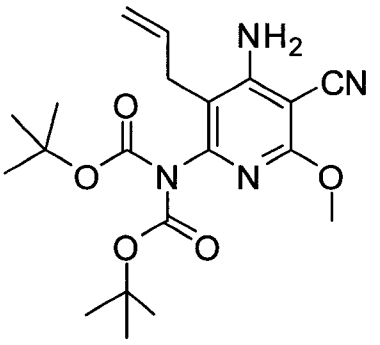

34

Synthesis of **34**.

Di-*tert*-butyl dicarbonate (11.7 g, 53.8 mmol) was added to a solution of **32** (5.5 g, 26.9 mmol) in dry THF (200 mL) at -78°C. After stirring for 15 minutes, a solution of lithium hexamethyldisilazide in THF (1.0 M, 53.8 mL, 53.8 mmol) was added. The reaction was warmed to room temperature over 1 h and then stirred for an additional 1 h. The solvent was evaporated and the residue was dissolved in DCM and then washed twice with 100 mL of H_2O. The organic layer was dried and purified by

automated flash chromatography (combiflash) with maximium of 30% EtOAc (separate bottles of EtOAc and hexane) to give **34** (4.9 g, 45%). **34**, was recrystallized in a mixture of dichloromethane and hexane and its X-ray structure was obtained. R*f* = 0.58 (1:1 EtOAc: Hexane); ^{1}H NMR (400MHz; DMSO-d_6) δ 1.34 (18 H, s), 3.07-3.09 (2H, m), 4.96-5.01 (2H, m), 5.64-5.71(1H, m), 6.89 (2H, s); ^{13}C NMR (100MHz, DMSO-d_6) δ 27.4, 28.5, 53.8, 76.6, 82.3, 110.2, 114.6, 115.9, 133.2, 150.02, 150.06, 158.2, 162.8; FTIR (microscopic) 1570.2, 1661.6, 1705.1, 1784.0, 2217.8, 2937.5, 2980.6, 3089.7, 3270.2, 3367.7, 3367.7, 3425.6 cm^{-1}; HRMS (ESI) calcd for $C_{20}H_{28}N_4O_5Na$ (M+Na) *m/z* 427.19519, found 427.19511

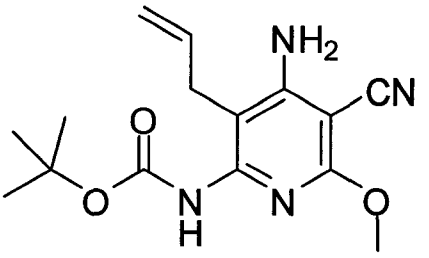

35

Synthesis of **35**.

34, was dissolved in dry methanol (120 mL) and then treated with powdered sodium methoxide (4.8 g, 89 mmol). After stirring at room temperature for 3 d, the solvent was evaporated and distilled water (150 mL) was added to the residue. A yellow precipitate formed which was extracted with chloroform (3 × 50 mL). The combined organic extracts were washed brine (20 mL) then dried over anhydrous Na_2SO_4 before evaporating the solvent. The product was purified by automated flash chromatography (combiflash) with maximium of 40% EtOAc (separate bottles of

EtOAc and hexane) to give **35** (1.7 g, 100%). R*f* = 0.55 (1:1 EtOAc: Hexane); ^{1}H NMR (400MHz; DMSO-d_6) δ 1.41 (9H, s), 3.2 (2H, d, J = 6.4), 3.81 (3H, s), 4.92-4.99 (2H, m), 5.65-5.75 (1H, m), 6.60 (1H, s), 8.84 (1H, s); ^{13}C NMR (100MHz, DMSO-d_6) δ 27.9, 28.0, 53.4, 74.9, 78.9, 105.8, 115.1, 134.7, 149.7, 152.8, 157.9, 162.4; FTIR (microscopic) 1506.8, 1578.0, 1638.3, 1713.3, 2214.3, 2950.7, 2983.6, 3083.2, 3247.7, 3307.5, 3361.0, 3484.8; HRMS (ESI) calcd for $C_{15}H_{20}N_4O_3Na$ (M+Na) *m/z* 327.14276, found 327.14267.

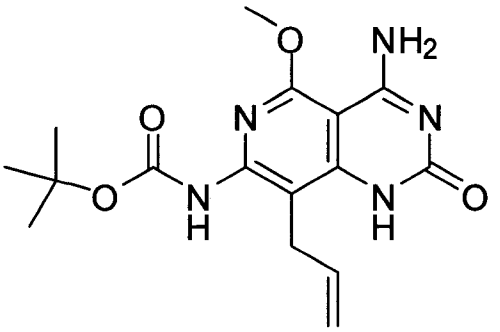

36

Synthesis of **36**.

Freshly distilled N-(chlorocarbonyl) isocyanate (0.8 mL, 7.2 mmol) was added to a solution of **35** (0.6 g, 1.8 mmol) in dry dichloromethane (30 mL) and was stirred at r.t. for 3 h. The reaction mixture was cooled to 0°C slowly treated with 20 mL saturated aq. $NaHCO_3$. The layers were separated and the white cloudy organic fraction was washed with brine (20 mL) and then concentrated. The white residue was dissolved in dry CH_3OH and sodium methoxide (2.0 g, 37 mmol). After stirring at r.t. for 24 h the solvent was evaporated under reduced pressure and the 100.0 mL

of water was added to the residue. The resulting white precipitate was collected by filtration and washed with 50 mL of water and then dried under house vacuum overnight to give **36** (0.6 g, 92%) as a pure white solid. ^{1}H NMR (400MHz; DMSO-d_6) δ 1.43 (9H, s), 3.44 (2H, d, J = 4.8), 3.95 (3H, s), 4.88-4.94 (2H, m), 5.69-5.77 (1H, m), 7.67 (1H, s), 8.10 (1H, br s), 9.0 (1H, br s), 9.9 (1H, br s); ^{13}C NMR (100MHz, DMSO-d_6) δ 27.2, 28.0, 53.9, 79.2, 90.4, 114.9, 135.1, 149.3, 152.8, 157.8, 158.1, 162.4; FTIR (microscopic) 1590.4, 1617.9, 1651.1, 1746.2, 2975.6, 3159.8, 3454.8 cm^{-1}; HRMS (ESI) calcd for $C_{16}H_{22}N_5O_4$ (M+H) *m/z* 348.16663, found 348.16633.

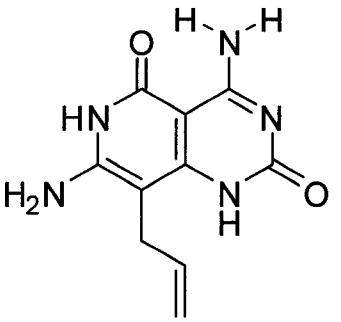

23

Synthesis of **23**.

Chloromethylsilane (0.1 mL, 0.9 mmol) was added to a stirred suspension of **36** (0.05 g, 0.14 mmol) and sodium iodide (0.2 g, 1.4 mmol) in acetonitrile (15 mL), and the mixture was heated at reflux overnight with light excluded. The reaction was then cooled to 0 °C, and treated with saturated aq sodium bicarbonate (10 mL) followed by a sodium thiosulfate solution (25 mL) prepared by dissolving anhydrous sodium thiosulfate (1.0 g) in H_2O (25 mL). The resulting colorless solution with white precipitate was allowed to sit for 5 h before the precipitate was collected by filtration

and washed with H_2O (250 mL). The solid was dried under house vacuum overnight to give **23** as a white pure solid (0.03 g, 88.0%). ^{1}H NMR (600MHz; DMSO-d_6) δ 3.191-3.198 (2H, m), 4.90-4.98 (2H, m), 5.68-5.73 (1H, m), 6.58 (1H, s), 6.59 (1H, s), 7.62 (1H, d, J = 14.4), 8.84 (1H, s), 9.75 (1H, br s), 10.93 (1H, s); ^{13}C NMR (100MHz, DMSO-d_6) δ 24.7, 82.9, 84.9, 114.0, 134.9, 151.7, 152.3, 154.7, 160.3, 163.6; FTIR (microscopic) 1463.8, 1568.7, 2972.3, 3133.7, 3484.7 cm^{-1}; HRMS (ESI) calcd for $C_{10}H_{12}N_5O_2$ (M+H) *m/z* 234.09855, found 234.09871.

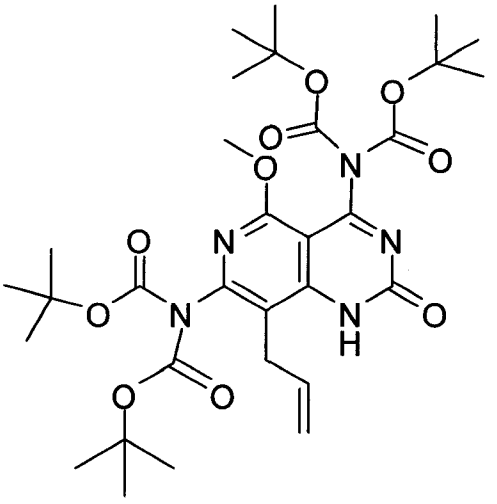

37

Synthesis of **37**.

A solution of **36** (0.1 g, 0.3 mmol), DMAP (0.04 g, 0.29 mmol) and Et_3N (0.3 mL, 2.3 mmol) in THF (40.0 mL) was treated with Boc_2O (0.4 g, 1.7 mmol) was added under N_2 atmosphere. After stirring at rt. for 24 h, the reaction was quenched with H_2O (5 mL) and the solvent was removed under reduced pressure (rotavap). The residue oily product was dissolved in EA (50 mL), washed with dH_2O (10 mL), 10% aqueous citric acid (10 mL × 3), H_2O (10 mL × 2), 5% aqueous $NaHCO_3$ (10 mL), and brine (20 mL), then dried over anhydrous Na_2SO_4. After filtration and

concentration, the residual oily product was purified by gravity silica gel chromatography (5-20% EA/Hex) to yield **37** (0.2 g, 90.0%) as a white solid.

^{1}H NMR (600MHz; DMSO-d_6) δ 1.28 (s, 18H), 1.30 (s, 18 H), 3.42-3.43 (m, 2H), 3.87 (s, 3H), 4.77-4.80 (m, 1H), 4.99-5.01 (m, 1H), 5.79-5.83 (m, 1H), 11.76 (s, 1H); ^{13}C NMR (100MHz, DMSO-d_6) δ 27.1, 27.3, 27.33, 54.7, 82.8, 83.2, 115.7, 133.5, 148.5, 149.5, 157.6, 161.8; HRMS (ESI) calcd for $C_{31}H_{45}N_5O_{10}Na$ (M+Na) *m/z* 670.30586, found 670.30583.

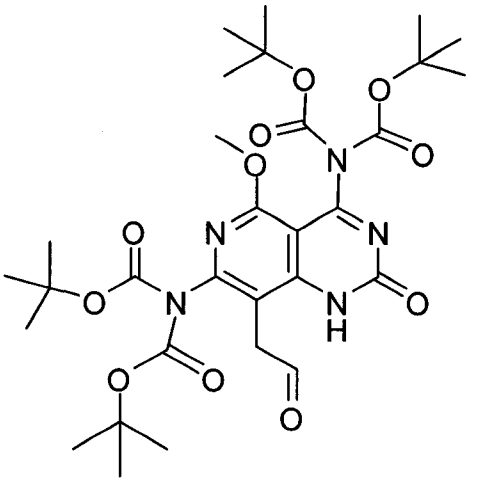

38

Synthesis of **38**.

50% aq. NMO (0.12 mL, 0.59 mmol) was added to a stirred solution of **37** (0.19 g, 0.29 mmol) in acetone/dH_2O (8:1, 20 mL). After stirring for 5 min., OsO_4 (0.1 M solution in t-BuOH, 0.15 mL, 0.02 mmol) was added drop wise. The resulting solution was stirred at r.t. for 2 d then quenched with aq. sodium sulfite until all the excess OsO_4 was destroyed. The white crystalline sodium sulfite was filtered off and then 10.0 mL of H_2O was added to the filtrate. The resulting diol (LCMS/ES M+H^+/*z* = 682.3) was extracted in $CHCl_3$ (50 mL), and the organic layer was washed with

brine (30 mL). The combined organic layer was dried over anhydrous Na_2SO_4, filtered and then evaporated to dryness under reduced pressure (rotavap). The resulting oily product was dissolved in CH_2Cl_2/H_2O (4:1, 20 mL) and treated with $NaIO_4$ (0.15 g, 0.70 mmol). After stirring at rt. for 3 d, the organic layer was separated and then concentrated under reduced pressure (rotavap). Purification by gravity silica gel chromatography (0-60% EA/Hex) yielded yielded **38** (0.16 g, 85.0%). R*f* = 0.73 (60% EA : Hexanes); ^{1}H NMR (500MHz; DMSO-d_6) δ 1.37 (s, 18H), 1.44 (s, 18H), 3.47 (d, *J*= 2 Hz, 1H), 3.89 (s, 3H), 9.37 (t, *J*= 2 Hz, 1H), 9.61 (s, 1H); ^{13}C NMR (125 MHz, DMSO-d_6) δ 27.3, 39.7, 54.4, 83.5, 83.7, 94.2, 147.8, 158.0, 157.4, 190.2; HRMS (ESI) calcd for $C_{30}H_{44}N_5O_{11}$ (M+H) *m/z* 650.30318, found 650.30322.

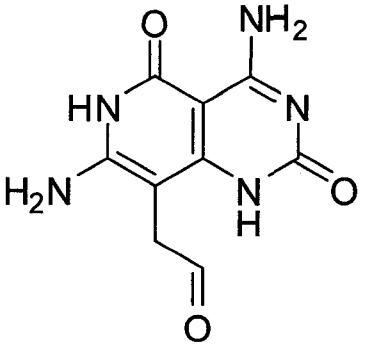

24

Synthesis of **24**.

Chloromethylsilane (0.2 mL, 1.2 mmol) was added to a stirred suspension of **38** (0.08 g, 0.12 mmol) and sodium iodide (0.2 g, 1.2 mmol) in acetonitrile (15 mL), and the mixture was refluxed overnight with light excluded. The reaction was cooled to 0°C, and then treated with a solution of saturated aq. sodium bicarbonate (10 mL) followed by sodium thiosulfate solution (25 mL) prepared by dissolving anhydrous sodium thiosulfate (1.0 g) in H_2O (25 mL). The colorless solution with white precipitate was allowed to sit for 2 h before collecting the precipitate by filtration and washed with H_2O (250 mL). The yellow solid was dried under house vacuum to give **24** as a pure yellow solid (0.03 g, 98.00%). ^{1}H NMR (400MHz; DMSO-d_6) δ 3.30 (br, s, 2H), 6.79 (s, 2H), 7.80 (s, 1H), 9.22 (s, 1H), 11.25 (s, 1H), 11.45 (br, s, 1H), 12.25 (br, s, 1H); ^{13}C NMR (125 MHz, DMSO-d_6) δ 39.5, 96. 5, 101.6, 118.9, 137.9, 148.6, 160.9. MS (ESI) $C_9H_{10}N_5O_3$ (M+H) *m/z* 236. 2

Table 3.2 Crystallographic Experimental Details For **33**.

A. Crystal Data	
formula	$C_{10}H_{12}N_4O$
formula weight	204.24
crystal dimensions (mm)	0.60 x 0.36 x 0.11
crystal system	triclinic
space group	$P\bar{1}$ (No. 2)
unit cell parameters[a]	
a (Å)	6.8698 (8)
b (Å)	9.3787 (11)
c (Å)	9.6440 (11)
α (deg)	107.8121 (15)
β (deg)	108.2296 (15)
γ (deg)	104.2314 (16)
V (Å^3)	520.27 (10)
Z	2
ρ_{calcd} (g cm^{-3})	1.304
μ (mm^{-1})	0.090
B. Data Collection and Refinement Conditions	
diffractometer	Bruker PLATFORM/SMART 1000 CCD[b]
radiation (λ [Å])	graphite-monochromated Mo Kα (0.71073)
temperature (°C)	–80
scan type	ω scans (0.3°) (15 s exposures)
data collection 2θ limit (deg)	55.02
total data collected	4569 ($-8 \le h \le 8$, $-11 \le k \le 12$, $-12 \le l \le 12$)
independent reflections	2357 (R_{int} = 0.0105)
number of observed reflections (*NO*)	2044 [$F_o^2 \ge 2\sigma(F_o^2)$]
structure solution method	direct methods (*SHELXS–97*[c])
refinement method (*SHELXL–97*[d])	full-matrix least-squares on F^2
absorption correction method	Gaussian integration (face-indexed)
range of transmission factors	0.9902–0.9481
data/restraints/parameters	2357 [$F_o^2 \ge -3\sigma(F_o^2)$] / 0 / 136
goodness-of-fit (S)[e]	1.071 [$F_o^2 \ge -3\sigma(F_o^2)$]
final R indices[f]	
R_1 [$F_o^2 \ge 2\sigma(F_o^2)$]	0.0426
wR_2 [$F_o^2 \ge -3\sigma(F_o^2)$]	0.1263

largest difference peak and hole	0.369 and –0.171 e $Å^{-3}$

[a]Obtained from least-squares refinement of 3551 reflections with $4.88° < 2\theta < 55.02°$.

[b]Programs for diffractometer operation, data collection, data reduction and absorption correction were those supplied by Bruker.

[c]Sheldrick, G. M. *Acta Crystallogr.* **1990**, *A46*, 467–473.

[d]Sheldrick, G. M. *SHELXL-97*. Program for crystal structure determination. University of Göttingen, Germany, 1997.

[e]$S = [\Sigma w(F_o^2 - F_c^2)^2/(n - p)]^{1/2}$ (n = number of data; p = number of parameters varied; $w = [\sigma^2(F_o^2) + (0.0823P)^2 + 0.0562P]^{-1}$ where $P = [\text{Max}(F_o^2, 0) + 2F_c^2]/3$).

[f]$R_1 = \Sigma||F_o| - |F_c||/\Sigma|F_o|$; $wR_2 = [\Sigma w(F_o^2 - F_c^2)^2/\Sigma w(F_o^4)]^{1/2}$.

3.16. References

1. (a) Fenniri, H.; Mathiavanan, P.; Vidale, K. L.; Sherman, D. M.; Hallenga, K.; Wood, K. V.; Stowell, J. G. *J. Am. Chem. Soc.* **2001**, *123*, 3854. (b) Fenniri, H.; Deng, B. L.; Ribbe, A. E. *J. Am. Chem. Soc.* **2002**, *124*, 11064. (c) Fenniri, H.; Deng, B. L.; Ribbe, A. E.; Hallenga, K.; Jacob, J.; Thiyagarajan, P. *Proc. Natl. Acad. Sci. U.S.A.* **2002**, *99*, 6487.
2. Marsh, A.; Silvestri, M.; Lehn, J.-M. *Chem. Commun.* **1996**, 1527.
3. (a) Mascal, M.; Hext, N.; Warmuth, R.; Moore, M. H.; Turkenburg, J. P. *Angew. Chem.* **1996**, *35*, 2204. (b) Mascal, M.; Hext, N.; Warmuth, R.; Arnall-Culliford, J. R.; Moore, M. H.; Turkenburg, J. P. *J. Org. Chem.* **1999**, *64*, 8479. (c) Mascal, M.; Farmer, S. C.; Arnall-Culliford, J. R. *J. Org. Chem.* **2006**, *71*, 8146.
4. Junek, H.; Uray, G.; Kotzent, A. *Monatsh. Chem.* **1983**, *114*, 973.
5. (a) Yang, C.-W.; Hwang, I.-S.; Chen, Y. F.; Chang, C. S.; Tsai, D. P. *Nanotechnology* **2007**, *18*, 1. (b) Kasumov, A. Y.; Klinov, D. V.; Roche, P. E.; Gueron, S.; Bouchiat, H. *Appl. Phys. Lett.* **2004**, *84*, 1007.
6. (a) Hartgerink, J. D.; Beniash, E.; Stupp, S.I. *Science* **2001**, *294*, 1684. (b) Fuhrhop, J.-H.; Helfrich, W. *Chem. Rev.* **1993**, *93*, 1565. (c) Jung, J. H.; John, G.; Yoshida, K.; Shimizu, T. *J. Am. Chem. Soc.* **2002**, *124*, 10674.
7. (a) Dujardin, E.; Hsin, L.B.; Wang, C. R. C.; Mann, S.; *Chem commun.* **2001**, *14*, 1264. (b) Wang, H.-L.; Ma, X.-D, Qian, X.-F.; Y, J.; Zhu, Z.-K. *J. Solid State Chem.* **2004**, *177*, 4588. (c) Shi, L.; Gu, Y.; Chen, L.; Yang, Z.; Ma, J.; Qian, Y. *J. Phys. Condens. Matter.* **2004**, *16*, 8459. (d) Xia, Y. N. *Adv. Mater.* **2003**, *15*, 353.

8. (a) Hu, J. T. et al. *Science* **2001**, *292*, 2060. (b) Correa-Duarte, M. A.; Perez-Juste, J.; Sanchez-Iglesias, A.; Giersig, M.; Liz-Marzan, L. M. *Angew. Chem. Int. Ed.* **2005**, *44*, 4375.

9. Cantor, C. R.; Schimmel, P. R. Biophysical Chemistry; *Freeman: New York*, **1980**.

10. (a) Schneider, H.-J; Kramer, R.; Simova, S.; Schneider, U. *J. Am. Chem. Soc.* **1988**, *110*, 6442 (b) Jorgensen, W. L.; Severance, D. L.; *J. Am. Chem. Soc.* **1990**, *112*, 4768.

11. (a) T. Steiner, *J. Chem. Soc. Commun.* **1995**, 1331-1332. (b) R. Taylor, O. Kennard, *Acc. Chem. Res.*, **1984**, *17*, 320. (c) G. R. Desiraju, *Acc. Chem. Res.*, **1991**, *24*, 291. (d) G. C. Pimentel, A. L. McClellan, The Hydrogen Bond; *Freeman, San Francisco*, **1960**. (e) M. Mascal, *Chem. Commun.* **1998**, 303. (f) M. J. Zaworotko, S. Subramaian, *Coord. Chem. Rev.*, **1994**, *137*, 357.

12. (a) C. A. Hunter, *Chem. Soc. Rev.*, **1994**, *23*, 101. (b) C. A. Hunter, J. Singh, J. M. Thornton, *J. Mol. Biol.*, **1991**, *218*, 837 (c) C. A. Hunter, J. K. M. Sanders, *J. Am. Chem. Soc.*, **1990**, *112*, 5525. (d) A. V. Muehldorf, D. Van Engen, J. C. Warner, A. D. Hamilton, *J. Am, Chem. Soc.* **1988**, *110*, 6561.